8-20-2021 9:45 AM

Experimental study and characterization of bubble behaviors in the orifice-induced hydrodynamic cavitation

Haoxuan Zheng, *The University of Western Ontario*

Supervisor: Zheng, Ying, *The University of Western Ontario*
Co-Supervisor: Zhu, Jingxu (Jesse), *The University of Western Ontario*
A thesis submitted in partial fulfillment of the requirements for the Master of Science degree in Chemical and Biochemical Engineering

Abstract

Experimental studies were performed to characterize the development process of orifice-induced cavitation and transitional bubble behaviors. The transition from non-cavitation to fully developed cavitation was carefully studied. Cavitation bubble clouds were observed at orifice, indicating the inception of cavitation. The number of bubbles produced were dramatically increased while the averaged sizes of bubble reduced when cavitation was initiated. Both orifice opening ratio and perimeter can affect the cavitation developing process. A long orifice perimeter promotes the production of fine bubbles. The orifice plates with the smallest opening ratio generated a desired gas-liquid interfacial area at the lowest required pressure. An orifice plate with multiple orifices is recommended in the design of orifice-based cavitation reactor for production of high cavitation intensity.

Keywords

Hydrodynamic Cavitation, Cavitation Inception, Transition Regime, Cavitation Number, Orifice Plate, Bubble Breakup, Flow Regime, Two-Phase Flow, Spectral Analysis

Summary for Lay Audience

Hydrodynamic cavitation was first observed due to the damage it caused in hydraulic machinery. Cavitation process is related to the formation, growth and collapse of bubbles. The collapse of these bubbles was accompanied with significant energy, which caused the damage. However, making good use of the energy released by cavitation can benefit many industrial processes. To date, cavitation phenomena have been applied in many industrial processes such as wastewater treatment, food and beverage industry, and biomedical applications. The bubble behavior regarding the formation and collision in its transition process along with the effects they brought are not yet fully understood. Therefore, this process was studied from multiple perspectives in the present work.

The research was divided into three sections: (1) how does the bubble behavior changes the inception of cavitation process; (2) can the initiation of cavitation be affected by the addition of surfactant; and (3) how does the geometry of cavitation inducer influence the intensity of generated cavitation.

First, experiments were conducted to characterize hydrodynamic cavitation transition process based on the experimental results generated from high-speed camera, pressure transducers and power spectral analysis. Visualization of bubbles and their pressure fluctuations along with the power spectrums generated based on Fast Fourier Transform were analyzed to correlate each other.

Second, investigations were conducted to study the effects of surface tension on the inception of cavitation in the current set up. Five solutions with known surface tension were treated as the working fluid respectively. The bubble clouds and pressure variations generated were recorded and compared.

In the final part of the study, different geometric designs of cavitation inducers were used to illustrate the impact on the intensity of produced cavitation. The data were analyzed based on three criteria: number of bubbles produced, bubble sizes and their interfacial area created. The results showed that an orifice plate with multiple orifices is recommended for production of high cavitation intensity.

Acknowledgments

I would like to acknowledge Dr. Ying Zheng and Dr. Jesse Zhu for their continued support and efforts made throughout the completion of my degree and made this research possible. Their guidance and deep understanding of this field was significantly valuable. I am thankful to Dr. Kamran Siddiqui for providing me with guidance on the visualization technology. I also wish to thank my parents and friends for their support and encourage.

Table of Contents

List of Tables

List of Figures

List of Appendices

Chapter 1

1 Introduction

1.1 Cavitation overview

Cavitation was firstly observed and studied when Reynolds and Parsons examined a failure trial of a British warship in 1885. They suggested that the propeller blade was damaged as a result of implosion of water vapor bubbles and named the phenomenon cavitation. The phenomenon of cavitation is featured by formation, growth, and collapse of bubbles. The collapse of cavitating bubbles was accompanied with a large magnitude of localized energy, which created the damage [1]. However, further understanding of cavitation encouraged researchers to explore possible approaches for making use of the energy released by cavitation. To date, cavitation phenomena have been studied in many industrial processes such as wastewater treatment [2], food and beverage industry [3], biomedical applications [4].

Hydrodynamic cavitation can be generated via reduction in local pressures induced by increasing flow velocities of liquid medium. It is achieved either by passage of liquid through a constriction of a system, such as orifice, venturi etc., or by rotation of an object within a liquid. It features key advantages including easy scale-up, low capital cost and high energy efficiency. An increased research efforts have been observed in hydrodynamic cavitation since 2000 (Figure 1.1). Among the publications, five main different categories were observed, which are theoretical/experimental studies, utilization/production of biomass, wastewater treatment, process intensification/reaction optimization and medical/nanotechnology. The common applications include inactivation of microorganisms, hydrolysis of fatty oils, emulsification, reduction of water contamination [5, 6].

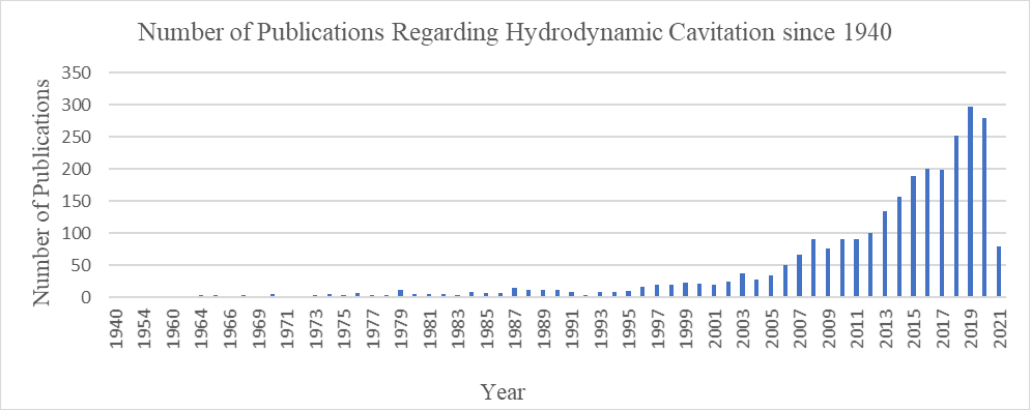

Figure 1.1: Publications regarding hydrodynamic cavitation during the past decades

1.2 Motivation

Hydrodynamic cavitation is of an emerging technology for intensifying various physical and chemical processes in an energy and cost-efficient way. The collapse of cavitating bubbles was always accompanied with a large amount of localized energy, which can be harvested to fortify the mass and heat transfer of a process and to enhance the reaction rates. To effectively use cavitation to intensify a chemical/physical process, the cavitation inception along with the transition from non-cavitation to cavitation flow are of importance. This is a complex subject depending on a wide range of factors including seeding nuclei, fluid velocity and physical properties, and system pressure. It has not yet fully understood.

The complexity of cavitation phenomenon is primarily caused by the interactions between gas and liquid phases, for example, gas bubble interaction, liquid-gas mixing and two-phase flow through a constriction. Previous studies have investigated cavitation flows and the behaviors of cavitation bubbles. Little attention has been given on the transition process of cavitation. Understanding of the transition to cavitation will provide a fundamental basis for the design and process control of a cavitation intensified process. The research presented in the thesis focuses on the transition process and the inception of hydrodynamic cavitation generated via an orifice plate. High-speed camera and pressure transducers were employed to record the pressure fluctuations of the system and bubble behaviors for understanding the gas and liquid interactions.

1.3 Objectives

Though cavitation flow and bubble behaviors have been extensively studied both experimentally and theoretically in open waters [7, 8], only a few studies focused on cavitational reactors and the transitional behavior of cavitation in the literature. Due to its complexity, the transition process of hydrodynamic cavitation has not yet been well understood. However, it serves as a core knowledge in the design of a cavitation-based reactor for process intensification. Therefore, the purpose of the present study is to improve the understanding of the transitional behaviors along with the effects of cavitation inception. The specific objectives of the present experimental research are:

- To characterize the transitional bubble behaviors of hydrodynamic cavitation.
- To understand the effects of liquid flow rates and surface tensions on the cavitation inception.
- To investigate the effects of the design of an orifice plate on the performance of hydrodynamic cavitation

1.4 Thesis structure

This thesis is written in the traditional thesis format provided by the School of Graduate and Postdoctoral Studies (SGPS) at the University of Western Ontario. It consists of six chapters, the summary of which are presented below:

The first chapter gives the introduction to cavitation technology. The objectives and the motivations of the research are explicitly stated. The history of hydrodynamic cavitation and the increased industrial applications of the hydrodynamic cavitation technology were briefly overviewed.

The second chapter provides a comprehensive literature review of the fundamentals of hydrodynamic cavitation and its applications. Cavitation generation mechanism and the development process were introduced. The theoretical background, influencing factors along with the characterization methods for cavitation and its inception process were presented in detail. Two types of hydrodynamic cavitation reactors (Stationary and

rotational) were introduced and compared. Cavitation induced reaction enhancement and relevant industrial applications are briefly discussed in the end.

The third chapter addresses the experimental design and techniques of measurement. It provides details of the experimental apparatus and measurement techniques that were used in this study. The data acquisition techniques and image processing were described in detail.

The fourth chapter contains the characterization of hydrodynamic cavitation transition process from multiple perspectives based on the experiment results. High-speed camera along with pressure transducers are used in order to demonstrate the detailed changes of gas bubbles and system pressure during the transition process. Various analyses including visualization of bubbles, pressure fluctuation and power spectrum analysis were performed to correlate each other.

The fifth chapter investigates the influence of geometric design on the intensity of produced cavitation. Two parameters were selected and a total number of six orifice designs were studied featuring different combinations of orifice perimeters and orifice openings. The results were analyzed and compared to evaluate their individual performance. And the best option is purposed.

The sixth chapter summaries the present work. Conclusions are made based on the results presented in chapters 4 and 5, recommendations for future work were also made.

Chapter 2

2 Literature review

2.1 Hydrodynamic cavitation

The way used to generate cavitation is frequently served to as a criterion to define the types of cavitation. Four main types of cavitation were commonly defined, which are hydrodynamic, acoustic, optic and particle cavitation. The latter two types of cavitation were discovered lately. Optic cavitation is generated by high energy light, such as a laser. When irradiating a liquid medium, the light energy is absorbed and used to heat up the local liquid beyond its boiling temperature so that vapor cavities/bubbles are formed, grew and then collapsed, which is referred to optic cavitation. Elementary particles such as protons, neutrinos and photons can also be used to break down liquid medium to produce cavitation, which is often known as particle cavitation [9]. Both optical and particle cavitation are the consequence of local deposition of energy [10]. They are frequently employed in laboratory environment for fundamental study of cavitation since single cavities or specially required cavities are generated [11]. Acoustic and hydrodynamic cavitation, on the other hand, are first studied and widely applied in both academia and industry due to the ease of operation and generation of required intensities of cavitation conditions. Like the discovery of cavitation in hydraulic systems, acoustic cavitation came to researchers' attention because of incidents of an underwater sound projector in 1920s when unexpected shorter distance of sound transmission and frequent destruction of sound transducers were taken place [12]. Ultrasound with the frequency ranging from 20KHz to 1MHz propagates through liquid medium, generating mechanical vibration and negative local pressures, which result in acoustic cavitation. The chemical effects of acoustic cavitation were quickly recognized by chemists. The research has become so prevalent that "sonochemistry" was dedicated to describing the research concerned with understanding the effect of ultrasound in forming acoustic cavitation in liquids. However, the short wavelength of ultrasound severely limits its transmission distance. This inherent aspect of ultrasound leads to a critical drawback, low scalability, which hinders the application of acoustic cavitation to large-scale commercial operations.

Hydrodynamic cavitation is generated via pressure fluctuations caused by varying flow velocities of liquid medium. The hydrodynamic cavitation bubbles behave in similar patterns to acoustic cavitation bubbles [9]. On the basis of numerical simulation, Moholkar et al. [13] suggested that the intensity of sound waves in the case of acoustic cavitation and the recovery pressure downstream in the case of hydrodynamic cavitation are similar to each other; the frequency of ultrasound and the pressure recovery rate are analogous to each other as well. However, acoustic cavitation tends to generate highly intense cavity collapse while hydrodynamic cavitation can create a large quantity of cavities with relatively low intensity [14]. With similar cavitational outcomes to acoustic cavitation, hydrodynamic cavitation features key advantages including high scalability, cost-effective operations along with high efficiency. Therefore, hydrodynamic cavitation is a promising alternative to acoustic cavitation [9]. It has been applied in various commercial settings for process intensification [15].

The collapse of cavitating bubbles was always accompanied with a large magnitude of localized energy in terms of extremely high local temperatures and pressures [16]. The localized energy generated from the collision of cavitation bubble leads to a significant structural and mechanical change. As millions of microscopic bubbles can be produced during the cavitation process, they generate powerful shockwaves that can turn process material into microscopic sizes when bubbles collapse.

Vapor-filled cavities collapse adiabatically to create extreme heat and localized hot spots. Therefore, each cavity can be treated as a microreactor during the collapse phase since both the temperature and pressure will reach the highest peak, and the entrapped organic molecules will thermally be decomposed into smaller molecules within this region. Though this region's temperature is extremely high, the region itself is so tiny that the heat dissipates rapidly, therefore bulk of the liquid is kept at normal temperature.

At the same time, due to the oscillation of cavities and its subsequent collapse, high shear microjet and turbulence is created in the interface region. The turbulence and mixing allow the particles to distribute uniformly and interact with each other sufficiently which leads to the formation of fine emulsions. The surface area available is then greatly

increased thus enhancing the reaction rates. Therefore, the speed of reaction at the bubble-liquid interface is higher than that in the bulk liquid region. Furthermore, emulsions created by cavitation are typically more stable and it requires hardly any surfactant to maintain the stability. This is extremely helpful especially in the field of phase transfer reactions [17].

2.2 Cavitation and cavitation number

Cavitation bubbles (cavities) generally appear as local pressure is decreased below liquid vapor pressure. To achieve a pressure reduction in a flow system, Bernoulli's principle provides the guideline. Variations of liquid velocity and pressure distribution in the flow field are described in Equation 2.1. A constriction is frequently used in the passage of a fluid to increase the fluid velocity that, in turn, results in the pressure reduction at the constriction. Venturi tubes and spray nozzles are familiar examples.

$$p_1 + \frac{1}{2}\rho v_1^2 = p_2 + \frac{1}{2}\rho v_2^2 \tag{2.1}$$

Where P_1 and P_2 denotes the pressures at two points in a flowing system, $v1$ and $v2$ are their corresponding fluid velocity, as shown in Figure 2.1. Liquid velocity in the tube increases at the expense of pressure. At the throat, the liquid reaches its highest velocity ($v2$) where the pressure (P_2) is dropped to its lowest value.

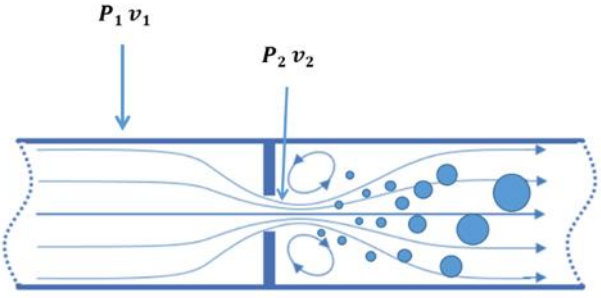

Figure 2.1: Graphic illustration of Hydrodynamic cavitation

Vapor bubbles are formed when the local pressure drops below the saturation pressure at the given temperature [18]. If P_2 becomes lower than the vapor pressure of the liquid, vapor bubbles may appear. At a point in the downstream of the constriction, a sudden pressure recovery occurred simultaneously with collapse of the bubbles where a significant amount of energy is released [1]. The lower the throat pressure is, the more severe the cavitation reaches and the more energy discharges. It is crucial to predict the inception of cavitation since it plays an important role not only in the explanation of the cavitation physics but also helps to study the flow patterns during the hydrodynamic cavitation process and to design cavitation devices.

2.2.1 Cavitation inception

Cavitation inception defines the initiation of cavitation phenomenon. Either to avoid the formation of cavitation or to make good use of cavitation, the cavitation inception is a key parameter in predicting the hydrodynamics of a liquid flow. It is a complex subject depending on a wide range of factors including seeding nuclei, fluid velocity, physical properties, and system pressure. Though extensive research efforts have been made, it is still far from completely understood at the present time. Thoma [19] was the first who suggested an index of cavitation (σ) to describe cavitation.

$$\sigma = \frac{p_s - p_v}{\Delta p} \tag{2.2}$$

Where: p_s is the suction pressure of pump, p_v the vapor pressure of liquid corresponding to its temperature and Δp the pressure rise obtained from suction to discharge at the best efficiency point of pump.

This parameter was first suggested for use with pumps but had the disadvantage that variations in parameter occur from pump to pump. In investigation of an open liquid flowing over a submerged object, Plesset [20] proposed cavitation

parameter, K, to qualitatively correlate flow patterns. When K was small, cavitating flow pattern could be established.

$$K = \frac{p_o - p_v}{\frac{1}{2}\rho v_o^2} \tag{2.3}$$

Where: p_o is the static pressure, p_v the vapor pressure of the liquid at its temperature, ρ the liquid density and v_o the uniform flow velocity a distance from the body.

The cavitation parameter is known as cavitation number in the current literature which is one important parameter in characterizing cavitation flow. Every flow has a cavitation number and increasing fluid velocity results in decreasing in the cavitation number. The cavitation inception was characterized by a cavitation cloud. From the Equation 2.3, one can note that, for a specific liquid, both static pressure and liquid velocity are parameters that influencing the cavitation number. A lower value of cavitation number results in a higher probability of cavitation occurrence or in an increase in the magnitude of cavitation [21]. Bagal [22] claimed that cavitation occurs when the cavitation number was dropped to about 1 and the best performance of cavitation was obtained at a cavitation number range between 0.1 and 1.

Cavitation inception is a complex phenomenon and is associated with many characteristics, among which cavitation nuclei is the most important one. Cavitation nuclei can be considered as weak spots of liquid, which may contain a mixture of vapour and non-condensable gases. They facilitate the development of cavitation by reducing the minimum required tensile strength of liquid. The dynamics of collapse are complex and depend on a variety of factors including surface tension, viscous effects, and non-condensable content.

Not surprisingly, cavitation number is impossible to account for all the complexities so that it alone is inappropriate to be used to determine the conditions

for cavitation inception because it is highly dependent on other physical properties. Šarc et. al. [18] observed that cavitation inception can be affected by quite a few factors such as constriction geometry, medium temperature, the density and the sizes of cavitation nuclei. Yan and Thorpe [23] reported a similar observation that the cavitation number is highly associated with the geometry. They further stated that the cavitation inception number varies between 1.7-2.4 for orifice to pipe diameter ratio from 0.4 to 0.8. Cioncolini et. al. [24] suggested that micro-orifices could have much lower cavitation number at the inception. Table 2.1 summarizes the cavitation inception numbers reported in the literature. It is seen that the cavitation number marking the inception of cavitation can greatly vary from well less than 1 to more than 3 depending on operational conditions, geometry, nuclei etc. To date, accurate prediction of cavitation inception is still a difficult task. The inception of cavitation still heavily relies on experimental observation.

Table 2.1: Cavitation numbers for the inception of cavitation

Parameters used	Cavitating device	Device details	Cavitation number	Ref.
Downstream pressure, orifice velocity	Multiple orifice	Orifice diameter 3mm Pipe diameter 3.78cm	Cavitation inception number varies between 1.7-2.4 for orifice to pipe diameter ratio from 0.4 to 0.8	Ref. [23]
Downstream pressure, orifice velocity	Multiple orifice	Orifices with diameter of 0.15mm and 0.3mm and thickness of 1.04mm, 1.06mm, 1.93mm	Cavitation inception number varies around 0.3, 0.7 and 1.1 for three orifices	Ref. [24]
Outlet static pressure, inlet flow velocity	Modelling	————	Cavitation inception number varies from 0.36 to 1	Ref. [25]
Outlet static pressure, throat velocity	Venturi tube	Throat diameter 10mm, convergent angle 45^{o}, divergent angle 12^{o}	Development tendency of cavity occurs at cavitation number around 0.51, cavitation inception number of 0.99, cavitation number independent of inlet pressures	Ref. [26]
Reference pressure,	Microfluidic	Hydraulic diameters of 75, 66.6 and 50 µm	Different upstream pressures up to 900 Psi are applied,	Ref. [27]

reference velocity	devices with rough surfaces	and length of 2 mm, roughness 5 μm	cavitation number range between 2.025 and 0.72, cavitation inception range between 0.925 and 3.266

2.2.2 Cavitation number

Equation 2.3 was first developed to determine a cavitation number based on the tests performed in an open water system, which primarily characterized cavitating flow occurred in open systems, such as hydrofoils. This dimensionless parameter has also been widely applied to orifices or Venturis of closed systems where (partial) choking of the flow expect to occur. Confusion arose when Equation 2.3 was applied to a closed system. There are a few pressures and velocities at various locations relevant to the constriction in an orifice/venturis system. Šarc et. al. [18] conducted a test and calculated the cavitation number using various combination of the pressure and velocities. For the same trials, they found that the value of cavitation number varies roughly between 1.2 and 168 by applying the pressures and velocities measured at different locations of the testing system. In the literature, inconsistences have also been observed. Some research groups directly applied the downstream pressure and velocity (that is a distance to the cavitation spot) to estimate the cavitation number. Other research groups employed, instead of downstream pressure and velocity, the pressure and velocity at the constriction in order to take choking of the flow into account. Despite the selection of pressure and velocity can greatly influence the numerical estimation of cavitation number and further affects the determination of cavitation inception. It is widely accepted that the cavitation phenomena generally occurs when cavitation number dropped to 1 and the greatest performance can be obtained for cavitation number between 0.1 and 1 [28]. Therefore, cavitation number equals to one severs as both the lower boundary of the non-cavitation regime and an important criterion to indicate the starting point of transition process from non-cavitation to cavitation regime.

2.3 Cavitation nuclei

Liquid vaporization tends to occur at free surfaces, such as gas bubbles, solid particles et al., which are known to be the source of cavitation formation and called “cavitation nuclei”. Nucleation is the accumulation of gas molecules to form micron sized bubbles. For a pure liquid that is free of pre-exist nuclei, its nucleation can only be realized through separation of the liquid molecules, at which point, new phases are created. This is termed homogeneous nucleation. Use pure deionized water at 20^{o}C as an example, cavitation cannot be initiated until the local tensile strength reaches as low as – 60 MPa [29]. However, cavitation is well observed in open water (seawater) and in tap water due to the presence of gas bubbles. The tensile strength of such waters is typically below 1 bar. The finding indicated nuclei played a key in formation of cavitation [30].

When inhomogeneities pre-exit in liquid to serve as nuclei, heterogenous nucleation takes place. In practice, heterogeneous nucleation most likely dominates the formation of cavitation. Two distinct types of nuclei have been studied in the literature. They are free-stream nuclei, which freely float in liquid media, and surface nuclei, which are attached to a surface or a wall (Figure 2.2). The surface nuclei are also known as Harvey nuclei, which can only be formed when two criteria are met. (1) The surface to which nuclei are attached should be hydrophobic. Nuclei on hydrophilic surfaces are unstable unless they are covered by organic skins. (2) The gaps with conical shapes acting as an active site for gas nucleation should exist [31]. Harvey nuclei frequently exist in porous particles and are attached to jagged particles when particles are floated in liquid. Rapid growth of surface nuclei when pressure falls below threshold pressure. It is said that the onset of cavitation is mainly associated with free-stream nuclei, and surface nuclei only play a minor role [31].

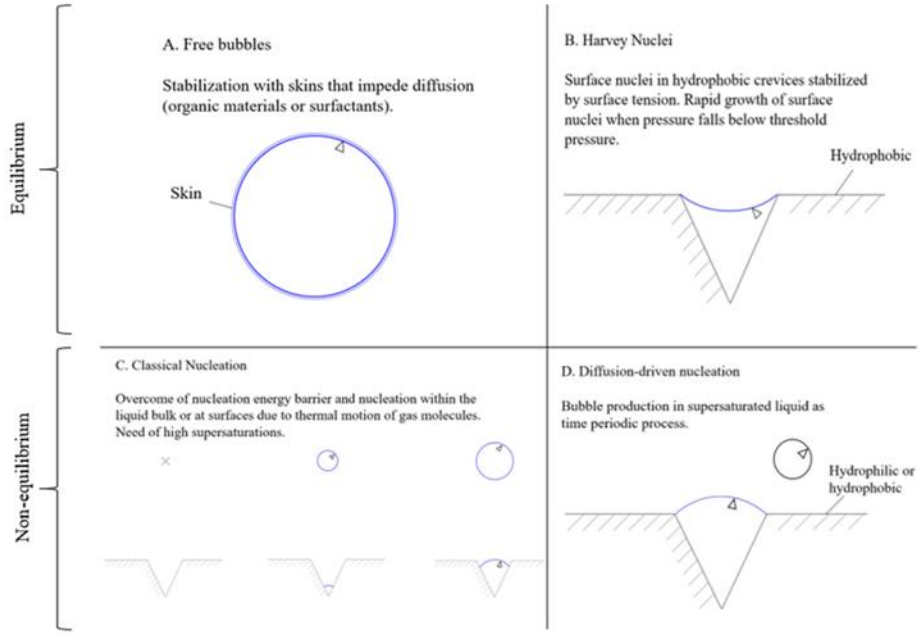

Figure 2.2: Graphical illustration of two different types of nuclei [31]. A. Free bubbles B. Harvey Nuclei C. Classical Nucleation D. Diffusion-driven nucleation

Free-stream nuclei refer to non-condensable gas bubbles entrapped in liquid. Due to the concentration gradient of the gaseous components in the liquid media, mass is expected to diffuse from the bubble surface to the bulk liquid. Equilibrium of a gas bubble in liquid is limited by the quasi-static stable balance of the far-field pressure and the Laplace pressure with the gas pressure inside the bubble.

$$Pc - Pv = \frac{-2}{3\sqrt{3}} \sqrt{\frac{\left(\frac{4S}{d}\right)^3}{\mathrm{P}\infty - \mathrm{Pv} + \frac{4S}{d}}} \tag{2.4}$$

Where S is the surface tension and d is the bubble diameter. P_c, P_v and P_∞ are the size-dependent critical pressure, vapor pressure and ambient pressure, respectively[32]. This equation indicates that gas bubbles become unstable when pressure drops below critical pressure P_c. Though microbubbles are likely to be thermodynamically instable due to gas diffusion, it is a fact that microbubble nuclei as well as their long-term stability are frequently observed in both natural

and laboratory environments. The nuclei must be stabilized one way or the other[33]. Khoo et al. has claimed that the critical pressure, P_c, was well below vapor pressure when microbubbles were smaller than 100μm diameter [32]. When gas bubbles were reduced to a few microns, Khoo et al. found that the required P_c were dropped to several atmospheres of tension and they confirmed that microbubbles could stably exist in water. The Chahine group applied Reynolds-Averaged Navier-Stokes (RANS) solver to simulate bubble nuclei populations and confirmed the important role of gas diffusion in the dynamics of microbubbles [34]. The average bubble size almost doubled, from 60 μm to 100 μm, when gas diffusion is considered. By introducing free gas bubbles that serve as cavitation nuclei, Tandiono et. al.[35] obtained intense cavitation events even before the liquid flow drops below its vapor pressure. The phenomena were recorded using a high-speed camera. The imploding cavitation bubbles are triggered by free gas bubble introduced into the liquid moving toward the constriction. The microbubbles observed were in the range of hundreds of microns.

Bubble nuclei concentrations and critical pressures were observed to be inversely correlated with system pressure but increase with increase the saturation level of dissolved gas. Russell et al.[36] evidenced that the population and size distribution of nuclei is highly associated with the pressure of the test section. Increasing pressure leads to a reduction in the number of bubble nuclei. A similar result was observed by Pascal et al. who used acoustic measurement technology [37]. When the system pressure is in negative pressure range, it was observed that reduction of pressure lead to a decreased number density of large-sized nuclei ($R > 10\ \mu m$) and an increased number density of small-sized nuclei ($R < 10\ \mu m$)[38].

The effects of gas saturation were reported by Shah et al.[39], they claimed that increasing gas solubility promoted the number of cavitation nuclei and lowered the cavitation threshold. Similar results were obtained by Edvard[40], who further stated that the impact on cavitational effects became less important when gas solubility reached very high. Venning et al.[41] confirmed the above statements by using a Cavitation Susceptibility Meter (CSM) measurement. The nuclei size

distributions were studied in an air-water system in the cavitation tunnels under laboratory conditions. They noticed that the quantity of bubble nuclei remarkably increased with the concentration of dissolved gas when the water was oversaturated. However, the impact was significantly weakened when the water was not saturated with dissolved gas. The result suggested that gaseous diffusion plays a role in the microbubble population dynamics.

2.4 Influencing factors

2.4.1 Temperature

Fluid temperature is of a determining factor that influences nuclei formation and cavitation events for many cases, including chemical reactions, hot fluid injection, and cryogenic cavitation. Theoretically, temperature functions distinctly in a cavitating flow. Increasing temperature at the same ambient pressure, on one hand, promotes liquid vaporization, resulting in a greater aptitude to cavitate; on the other hand, demotes the cavitation phenomena because of reduced vapor pressures within gas bubbles. The latent heat of evaporation of the liquid lowers the temperature around the bubbles and therefore decreases the vapor pressure within bubbles. What is worth noticing is that increasing temperature generally reduces gas solubility in liquid medium so that the number of cavitation nuclei, which is the crucial factor for cavitation initiation, is reduced. This leads to a higher threshold for cavitation initiation. Extensive research on the temperature effects were performed in the last century and it has been widely accepted that increasing temperature increases cavitation numbers, delays cavitation inception and lowers cavitation intensity [42]. Recent studies confirmed the negative impact of thermal effect on cavitation nuclei. Bogdan Niemczewski observed that the cavitation intensity was increased with decreasing temperature in water that was chemically deoxidized and was weakened as the temperature rises [43]. Similar results were reported by Torre et al. [44] who claimed that thermal effects are inversely associated with the cavitation intensity. The conclusion was derived based on the degradation performance being worsened with temperature. Li et al. [45] used dissolved oxygen and nitrogen as cavitation nuclei to study the tensile strength of water and concluded that higher gas concentrations result in

higher cavitation probability. The fact that the solubility of both oxygen and nitrogen decreases significantly at elevated temperatures is responsible for a lower cavitation probability.

The Tarantino group observed that temperature has a mixed effect when they researched the influence of water temperature on the critical cavitation number and cavitation instability onset for a turbopump inducer [46]. In the 293–333 K range, increasing temperature led to a higher cavitation number; however, when beyond the above range, a further increase temperature to 348 K results in a decrease in the cavitation number provoking the start of cavitation.

2.4.2 Pressure

Pressure is an important variable that can influence the inception of cavitation. Since vapor pressure and downstream pressure are frequently used to calculate cavitation number of a flow, inlet pressure may be worthwhile being investigated. Despite its simplicity in measurement and in control, attention was not given to inlet pressure on cavitation until recent two decades. Soyama and Hoshino [47] studied the influence of upstream and downstream pressures on cavitation intensity using a venturi tube with water as liquid medium. They observed that, when the downstream pressure is kept constant, the cavitation region increased monotonously with increasing upstream pressure, which can be visualized by Figure 2.3. As upstream pressure was kept constant, the cavitation is developed, and the intensity increases quickly with decreasing downstream pressure.

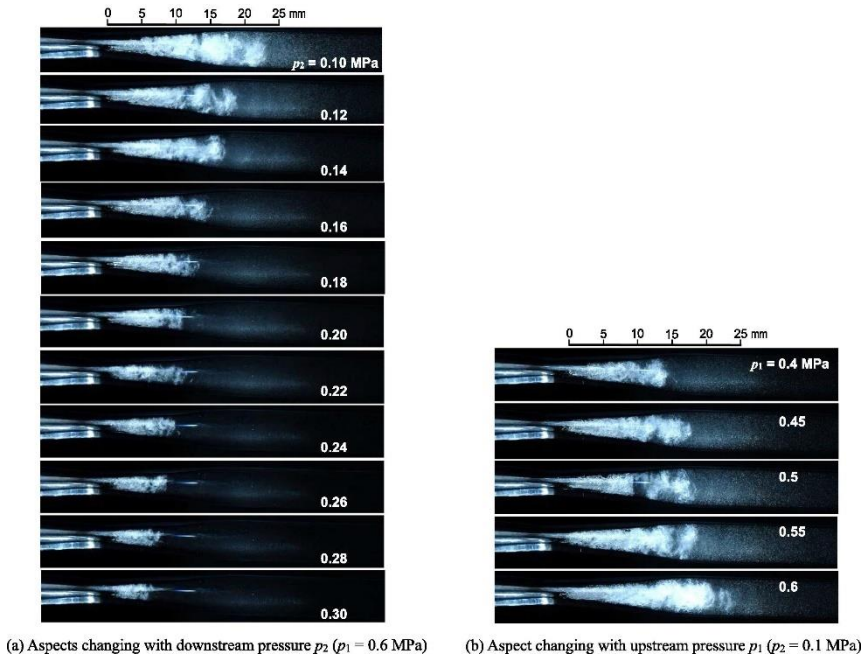

(a) Aspects changing with downstream pressure p_2 (p_1 = 0.6 MPa) (b) Aspect changing with upstream pressure p_1 (p_2 = 0.1 MPa)

Figure 2.3: Cavitation varies with upstream and downstream pressures

Ravi and Parag[48] demonstrated that dichlorvos hydrodynamic cavitation was degraded faster with increasing inlet pressures. The results indicated that increasing the inlet pressure led to an increase in both the downstream pressure and the rate of pressure recovery. Kumar and Pandit[49] reported that severe turbulent downstream flow and violent cavity collapse at higher inlet pressures, which was attributed to the large pressure drop across the orifice induced by high inlet pressure. Studied a regulating valve, Liu et. al. revealed both cavitation zone and intensity were increased with inlet pressure[50]. The enhanced cavitation phenomena caused by higher inlet pressure were further investigated by numerical simulation[51]. If an inlet pressure fluctuated following a sine wave, the cavitation process and flow structure would fluctuate accordingly. The amplitude and frequency of the fluctuation had great influence on the cavitation. There is an optimal frequency suppressing the occurrence of cavitation. However, inlet pressure corresponds to system pressure. Increased system pressure can create negative effect on the generation and intensity of cavitation.

2.4.3 Physical property of liquid medium

The physical property of liquid medium includes volatility and viscosity. There were contradictory reports on the effects of volatility of liquid medium. Atila et al.[52] observed that volatile solvents can be efficiently removed (98.4%) by a hydrodynamic cavitation reactor from wastewater even in the absence of aeration. The evaporated vapor in the liquid medium usually act as nuclei to enhance cavitation[32]. On the other hand, easy evaporation of high volatile liquid may result in difficulty in preventing vapor from escaping liquid phase so that a smaller number of cavities can be maintained in liquid phase. Bebchuk et al.[53] studied metal erosion caused by the impact of cavitation and concluded that cavitation could be promoted only when the liquid vapor pressure was in the range between 35 and 80 mm Hg for liquids like water and ethanol. This finding suggested that there existed an optimal vapor pressure and thus an optimal volatility of liquid.

Liquid viscosity could influence the formation and collapse of cavitation bubble. Although liquid with higher viscosity can be commonly seen in various industrial applications such as oils or monomers, research of viscous effects on the cavitation process remains scarce, especially for the experimental studies on cavitation. Surprisingly, almost all relevant work was only conducted at theoretical level[54]. The results suggested that a liquid must overcome its internal forces to produce cavities so that any increase in these forces will lead to an increase in the energy required to initiate cavitation. Experimental observations have confirmed the statement[55, 56]. More viscous liquid requires more energy to entrap air bubbles as nuclei and therefore tends to retard the evolutionary process of cavitation bubbles. The extent of effects exerted by liquid viscosity on cavitation is not as significant as temperature and pressure. Arndt[57] approved that the variation in cavity collapse pressure are not significant with the increasing viscosity. Later, Nazari-Mahroo et al.[58] confirmed that the bulk viscosity has a minor effect on the cavitation dynamics based on the study of a single cavitation bubble. However, the relationship between viscosity and cavitation intensity is still unclear due to the lack of experimental studies.

2.5 Hydrodynamic cavitation reactor

A hydrodynamic cavitation reactor (HCR) is designed to purposely initiate cavitation events in a controlled environment and then to utilize the energy generated by imploding cavitation bubbles for promoting a variety of physical processes or chemical transformations. These devices can be used either stand-alone unit or in combination with other industrial processes. Two main types of HCR are reported in the literature and in today's market: stationary and rotational HCRs, which are briefly introduced in the following sections.

2.5.1 Stationary cavitation reactor

Stationary HCRs employ Venturis or orifices as constrictive part to increase linear velocity of the working fluid which leads to a low-pressure region where cavitation events are induced. Due to their simple geometry, and ease of fabrication and operation, stationary HCRs have been extensively studied and widely used in laboratory-scale for the effectiveness and mechanism research of hydrodynamic cavitation technology. Owing to its considerable pressure drop of the working fluid caused by the contractive parts, a powerful pump is frequently required, which may result in a substantial cost.

2.5.1.1 Orifice plate cavitation reactor

Orifice plate is the most used pressure reducing and flow restricting device, and the borehole is designed to generate specified pressurized flow. Due to the sudden change in pipe diameter, the intensity of bubble collapse produced at an orifice is significant. The generation of bubbles occurs at the edge of the orifice. To increase the edges, multiple orifice plates are designed. Boundary layer separation occurs during the passage of liquid and huge amount of energy is lost in the form of permanent pressure drop. The magnitude of the pressure drop greatly influences the intensity of turbulence at the downstream of constriction, and the pressure drop is mainly dependent on the geometry of constriction and the flow conditions of the liquid. A typical pressure profile of an orifice plate cavitating device is shown in Figure 2.4. Where P_1 is the upstream pressure, P_2 is the recovered downstream pressure and P_v is the vapor pressure of the fluid.

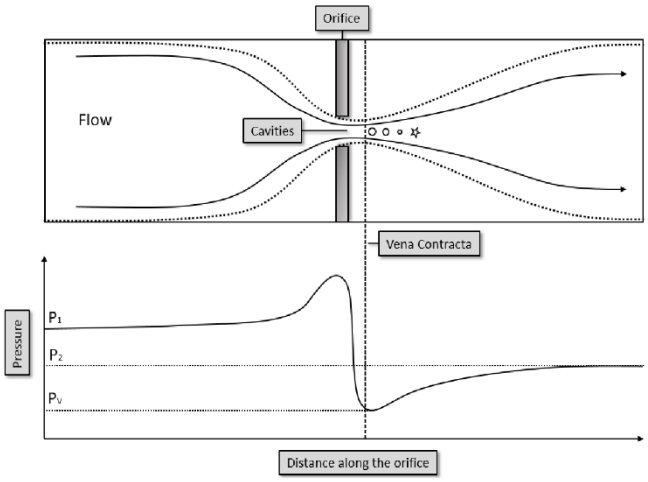

Figure 2.4: An illustration of orifice plate with pressure profile [59].

The diameter of the constriction as one of the most important factors in the orifice design can significantly affect the generation of cavitation. An example is shown in Figure 2.5. Yan et al.[23] studied both experimental and theoretical aspects of the flow regime transitions induced by cavitation where water passed through the orifice with different sizes. They observed that the cavitation number approximately linearly increased with the orifice diameter. Similar results were obtained by other research groups[7, 60-63]. The collapse pressure generated by a single cavity also increased with orifice diameter. Wan et al.[64] studied the orifice plate cavitation mechanism and its influencing factors using a numerical model. They found that the cavitation induced by orifice plate was highly related to gas nucleus distribution and the contraction ratio. The larger the contraction ratio, the higher the intensity of cavitation could produce.

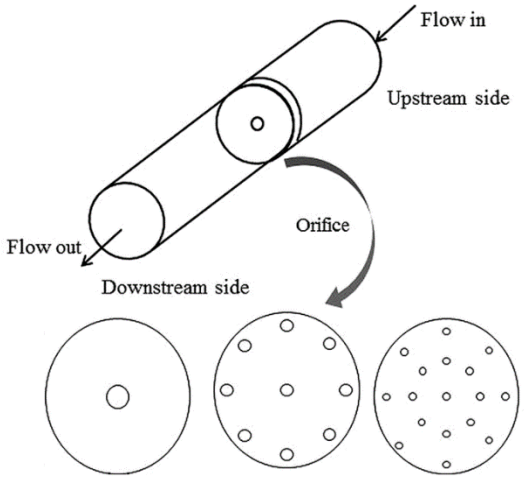

Figure 2.5: An illustration of different orifice design

2.5.1.2 Venturi cavitation reactor

Venturi tube have been extensively used and studied to produce microbubbles in the cavitation processes, and it typically consists of three sections, convergent, throat and divergence. Unlike orifice plates, fluid inside venturi contracts and expands smoothly, therefore the fluid pressure and velocity varies gradually. This gradual change in fluid condition avoids dramatic change in pressure at constriction, which is beneficial for the generation of microbubbles and its stability. Due to lower pressure loss and higher bubble generation ability, it surpasses orifice plates in industrial applications[65]. Similar to orifice plate cavitation reactor, venturis geometry can also impact the overall equipment performance (Figure 2.6).

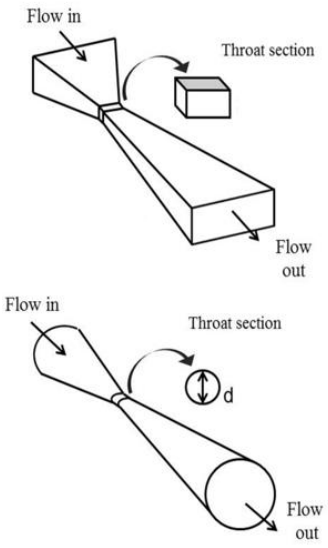

Figure 2.6: An illustration of different venturis geometries

2.5.2 Rotational cavitation reactor

Unlike the stationary HCRs, rotational hydrodynamic cavitation reactors (rotational HCR hereafter) consist of rational parts for generating cavitation. Early rotational HCRs used high-speed impellers or other sharp blades to accelerate tangential velocity of fluid so that local pressures reduce below vapor pressure and cavitation is generated. Instead of impellers, recently reported rotational HCRs used circular disks or cylinders with numerous dimples or gaps to create cavitation. The uneven surfaces (by dimples or gaps) within the rotational part create variations of the working cross-sectional area which force the liquid fluid to expand or to contract as the liquid flows through the area. Repeating pressure differentials is thus produced. In order to uniformly distribute the liquid stream, the inlet port is located at the center and the outlet port is placed at the top of the shaft for sealing and cooling purposes. Cavitation generated from this process is due to the opposite movement of two shear layers, therefore this type of cavitation is so called shear cavitation[66]. A graphic illustration of rotational cavitation reactor can be found in Figure 2.7.

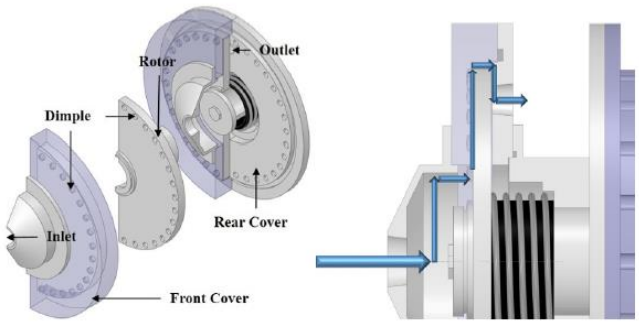

Figure 2.7: Graphic illustration of rotational cavitation reactor[67]

With different cavitation generation mechanisms, rotational HCRs eliminated the pressure fluctuations that the inherent drawbacks held by stationary HCRs. However, movable parts in rotational HCRs are expected to need frequent maintenance. For a rotational HCR, rotational speed of the rotor, liquid flow rate and pressures are of importance in determining the overall performance[68].

2.6 Applications

2.6.1 Reaction enhancement

Bubble collapse in the process of cavitation releases a large amount of energy, accompanying with extreme high local temperatures and pressures[16]. The recorded spectrum of sonoluminescence suggested a temperature of 5000 K due to the bubble collapse[69]. Qin et al. suggested that the maximum temperature could be dramatically increased with the sizes of bubbles [70]. These extreme local conditions also generate chemically active free radicals (OH•, H•), UV radiations, strong local turbulence, micro-jets and shock waves of a few thousands atmosphere pressures which special features are anticipated to significantly enhance mass and heat transfer as well as chemical reactions. Hydrodynamic cavitation has been applied to various chemical and biochemical processes as well environmental applications.

2.6.1.1 Cavitation enhanced heat transfer

It is well known that collapsing bubbles in hydrodynamic cavitation generates hot spots and violent turbulence. These phenomena have encouraged researchers to explore the applications of cavitating flow via direct harvesting the thermal energy and/or enhancing the rate of heat transfer. Russian scientists made efforts in developing hydraulic heat generators to directly collect the heat generated by hydrodynamic cavitation. Zaporozheats et al.[71] reported the experimental results on the vortex and cavitation nonuniform flows occurring in a hydraulic heat generator and demonstrated that that the heating efficiency decreases with increasing liquid temperature because of the growing saturation vapor pressure. One of the cavitation heat generator models was later tested by Scott R. Little[72] who reported 80 % efficiency was achieved. Pyun et al.[73] continued the study of cavitation-based heaters and reported a cavitation heat generator where cavitation bubbles were produced by rotating a disk at high velocity. The generation of heat energy and thermal efficiency were evaluated against several variables including inlet pressure, rotational velocity, and inlet velocity etc. Up to 94% heat efficiency was claimed. Later, the same research group applied a similar device to disinfect water[68]. Their results showed that 48.15 MJ/h of heat could be generated and thermal efficiency of 82.18% was achieved. The generated heat was directly used to heat water up to 61.9^{o}C so that *Escherichia coli* (*E. coli*) was successfully destroyed from water.

Beyond making use of the heat generated by cavitation bubbles, more research has been done in understanding the role of the collapsing bubbles in enhancing the rate of heat transfer[74]. Attention, however, has been given to the effects of acoustic cavitation on heat transfer. Relatively few studies focused on hydrodynamic cavitation enhanced heat transfer. Given the limited documentation, the effects of hydrodynamic cavitation on heat transfer mechanisms were primarily studied in microchannel systems. It was found that turbulence flow and micro-jets caused by cavitation played a key role in enhancing the rate of heat transfer both within the systems and from the wall to the systems. Schneider et al.[75] experimentally

studied the forced convection heat transfer induced by hydrodynamic cavitation in silicon channels with deionized water as the liquid medium. It concluded that convective heat transfer was the dominant heat transfer mechanism. Intensity of cavitation is a positive factor in influencing the rate of heat transfer. The maximum heat transfer coefficient was observed to increase by 67% due to the presence of cavitation phenomenon. As deionized water was replaced by refrigerant fluid R-123, as high as 84% increase in the rate of heat transfer was achieved[76, 77].

2.6.1.2 Cavitation enhanced mass transfer

As mentioned in cavitation initiation section, there are many physical and chemical effects will be generated along with cavitation, and those mechanical effects produced during the process will also reduce the resistance to mass transfer as cavitational effects enhance the contact between gases and liquids by increasing interfacial area. Cavitation also leads to the generation of local turbulence and liquid micro-circulation within the medium, enhancing transport process rates[78-80]. In order to find out the improvement of hydrodynamic cavitation on mass transport, many experiments have been done and several common evaluation standards were used including reaction rates, process yield, local mass transfer coefficient and etc.

Bubbles will be generated when the orifice pressure is reduced to a point lower than the liquid vapor pressure, and the mass transport is enhanced by those bubbles. The presence of microbubble not only extends the surface area of interaction significantly but also create concentration gradient within the mixed liquids and therefore maximizes the process output. Milton S. Plesset[81] stated that mass diffusion mostly takes place at the bubble-liquid interface and it plays an important role in the behaviour of gas bubbles, as the behaviour can eventually determine the existence or absence of bubbles in a liquid.

Many researches have been done to demonstrate the effectiveness of cavitation on improving the mass diffusion processes. Eva et al.[82] used both acoustic and hydrodynamic cavitation to enhance ozone mass transfer coefficient which is a

mathematical model proposed by Zhang et al.[83] and applied classic unsteady state methods. They found that the coefficient for hydrodynamic cavitation was around 1.6 times higher due to the increase in the mass transfer area as a result of the formation of bubbles, also the enhancement obtained from mechanical effects was lower than that from chemical effects. Kelkar et al.[84] found hydrodynamic cavitation is an efficient way (> 90% conversion) to intensify the esterification of acids for synthesis of biodiesel at ambient temperature and pressure. Milly et al.[85] used a hydrodynamic cavitation reactor to improve the mass transfer from bulk fluid to surface and proved successful in increasing the mass transfer of transparent fluid to the UV irradiated surface. Chuah et al.[86] also showed that high turbulence generated by hydrodynamic cavitation were effective in reducing the mass transfer resistance by increasing interfacial area.

2.6.2 Commercialized cavitation reactor

Due to the advantages of hydrodynamic cavitation such as low capital and operational cost, shorter production time, enhanced production efficiency and etc., it has been successfully applied to many industrial applications including oil refining, petroleum upgrading, industrial water treatment, biodiesel production, gas-liquid mixing and hydrocarbon upgrade. A few companies and their corresponding reactors which focused on cavitation technology are summarized below.

Cavitation technologies, Inc. is an innovative company which focuses on processing liquids, fluidic mixtures and emulsions and owns a patented technology named CTi Nano Neutralization process (CTi) which was a multi-stage hydrodynamic cavitation device. The reaction system is flexible in scales and can serve both large-scale and small-scale producers in the field of edible oil refining, algal oil extraction and renewable fuel production, biodiesel, alcoholic beverage enhancement, water treatment and petroleum upgrading. An illustration of their hydrodynamic cavitation-based reactor can be found in Figure 2.8 and 2.9.

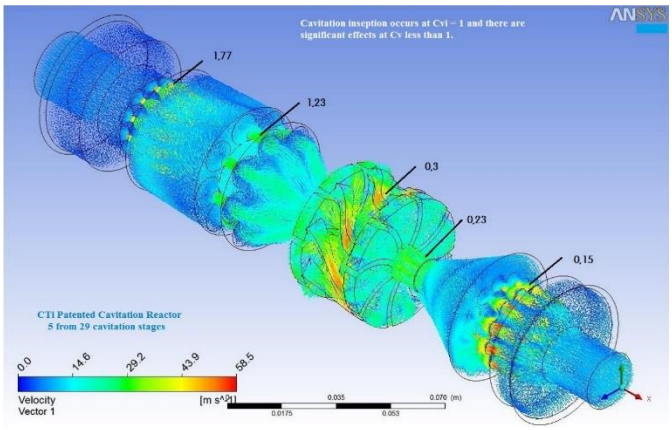

Figure 2.8: CTi patented cavitation reactor 1[87]

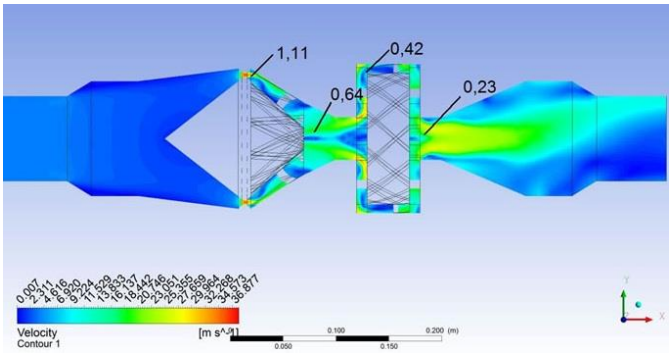

Figure 2.9: CTi patented cavitation reactor 2[87]

Hydro Dynamics, Inc. has developed a ShockWave Power Reactor which "controlled cavitation" was claimed. The core technology of the device is a specially designed rotor. The spinning action generates hydrodynamic cavitation in the rotor cavities away from the metal surfaces therefore there is no damage. It was claimed by the company that the ShockWave Power Reactor was featured by its lower capital and maintenance expenditures and improved efficiency. The reactor has been installed all over the world to fulfil the need of brewery, production of renewable fuels, mixing, extraction, emulsification, oxidation, and petroleum industries, it is also used by several Fortune 500 companies. The design of this reactor can be found in Figure 2.10 and 2.11.

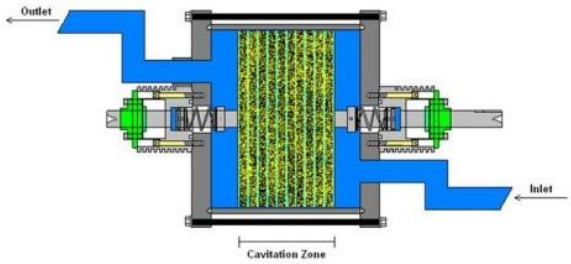

Figure 2.10: ShockWave Power Reactor 1[88]

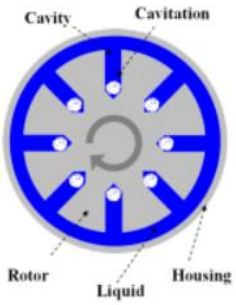

Figure 2.11: ShockWave Power Reactor 2[88]

Chapter 3

3 Experimental design

3.1 Experimental setup

The schematic of the experimental setup used in this study is shown in Figure 3.1. It consists of a transparent plexiglass cavitation unit, a water tank, a flowmeter, a pump, two pressure transducers and a high-speed camera. Deionized water was used as the working fluid and stored in a water tank. It is circulated in a closed loop configuration through plastic tubing having an inner diameter of 9.5mm and an outer diameter of 15.9mm. Water was pumped from the water tank to the cavitation unit after it flows through a liquid flowmeter, which monitors the volumetric flow rate of water in the mainline. The bypass valve was used to adjust the water flowrate and the excessive water flowed back to the water tank via the bypass line.

Visualization of cavitation phenomenon was achieved via a high-speed camera, was placed perpendicular to the cavitation unit. The pressure fluctuations across the cavitation unit were recorded by the pressure transducers which located at the upstream and downstream of the cavitation unit respectively, as shown in Figure 3.1.

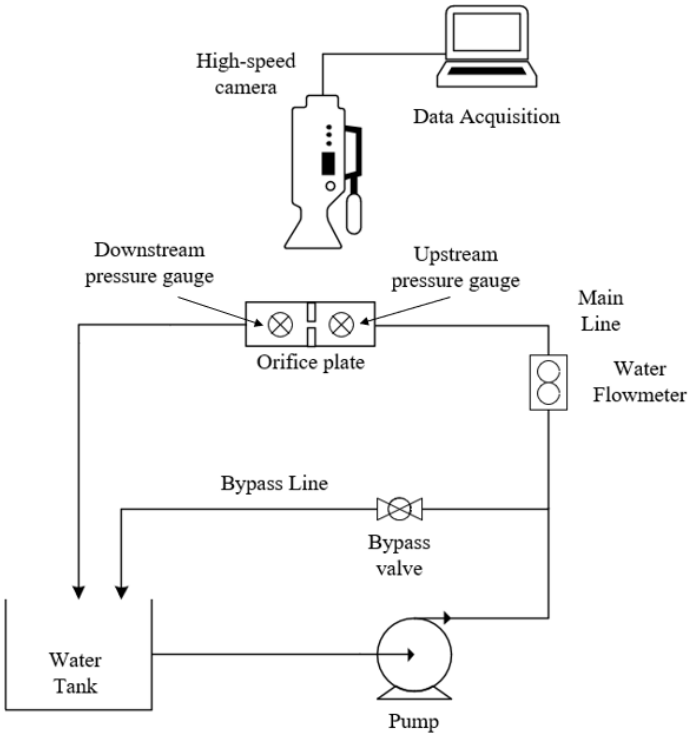

Figure 3.1: Schematic of the experimental setup

The cavitation unit is made of plexiglass consisting of two 45.7mm-in-length rectangular tubes were connected via flanges, as shown in Figure 3.2. The red dash-line framed section was enlarged and shown in Figure 3.3. Its square-shaped cross-sectional area has an inner and an outer side of 9.5 mm and 19.6 mm (Figure 3.3). Between the flanges, a perforated plate was placed. It serves as a constriction to generate cavitation. The unit had three equally spaced connecting ports located on the top of each side of the flanges. Pressure transducers were connected to these ports to measure the pressure at the corresponding location (Figure 3.3). The orifice sizes ranged from 1mm to 3mm and the number of orifices from 1 to 4. When liquid encountered the orifice plate, the water velocity at the orifice was anticipated to increase while the local pressure would be reduced. An increase in liquid flow rate would lead to a higher orifice velocity and a lower local pressure. As liquid flow rate was sufficiently high, the local pressure drop could be dropped to a pressure that is lower than the vapor pressure of the liquid. At this point cavitation was formed and accompanied with violence bubble formation and implosion.

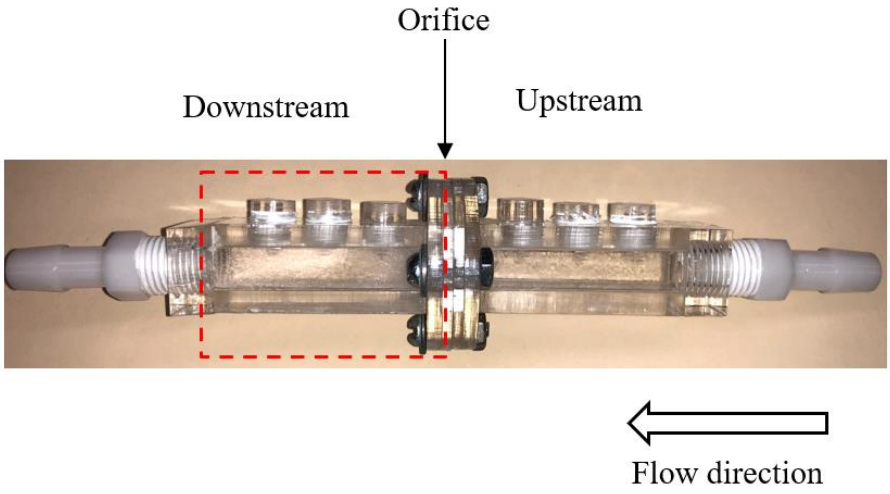

Figure 3.2: A graphic illustration of cavitation unit

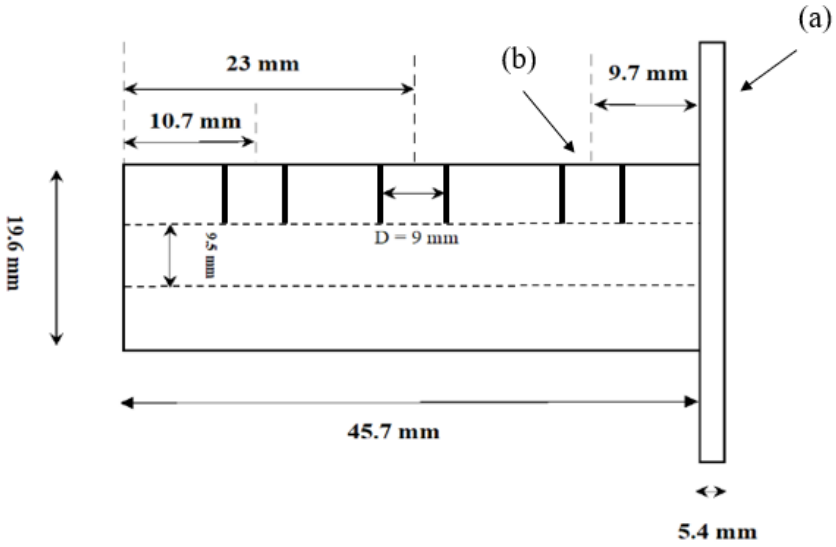

Figure 3.3: Schematic of half cavitation unit (a) Flanges (b) Connecting ports

3.2 High-speed photography

The high-speed camera, Photron FASTCAM SA5, was placed perpendicular to the cavitation unit to capture the images of bubbly flows from the side of the unit. With the help of a 7000mm camera lens and a zoom extender, the behaviors of cavitation bubble were recorded. Images were taken at a rate of 5400 frames per second for approximately

3 seconds with the resolution of 1024 x 1024 pixel and 1/35000 second shutter speed for each experiment trial. The camera was connected to a laptop computer via an Ethernet port and controlled by an image acquisition software named Photron FASTCAM Viewer. These images were then transferred to a computer from the built-in memory card of the camera not only for qualitative analysis such as regime transition but also for quantitative analysis. For example, the number of bubbles, bubble sizes and specific surface area were calculated from the collected images.

The light source, GE Everest VIT ELS-24, was employed to assist the high-speed photographing. Backlight/shadowgraphy technique was used to minimize the noise of the image and to enhance the contrast between background and generated bubbles (Figure 3.4 a). For this purpose, light source and the diffusion screen were placed behind the region of measurement which provide a uniform bright background in the images. The bright background brings clear contrast between bubbles and the liquid domain which allows for easier identification of gas bubbles. Flat lighting employs the light source at the front of the camera view and the images it produced are in a lack of depth and interest due to the even light and gradual shadows. Therefore, flat lighting was not considered in this study as it produces minimal contrast in the scene which is unfavorable for the bubble identification and further analysis (Figure 3.4 b).

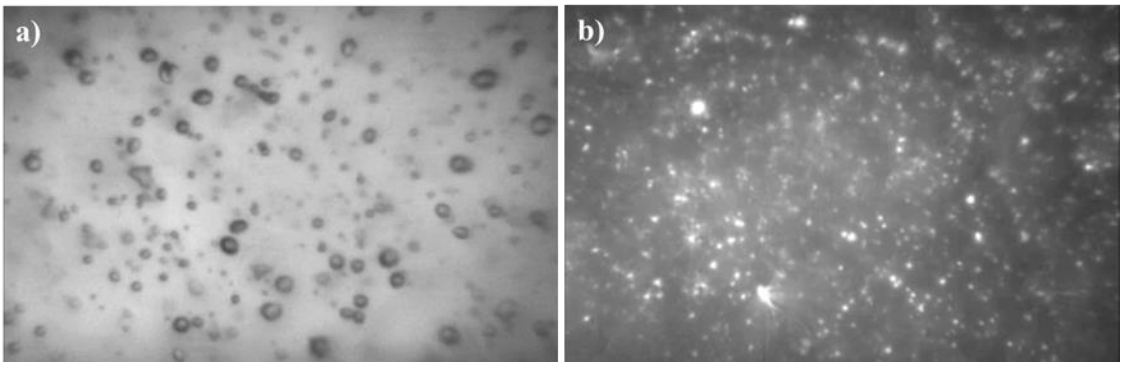

Figure 3.4: a) A picture using backlight shadowgraphy technique b) A picture using flat lighting technique

ImageJ was used to analyze the bubbles. The selected portion of the original image was firstly converted to greyscale followed by highlighting all of the bubbles within the

selected area before a further analysis was carried out. The pixel resolution used during the transformation of each image was 55pixel/mm or 0.018mm/pixel, and the source of error related to the detecting and measuring the boundary of bubbles was within ±0.5 pixel or ±0.009mm. The program counts the number of gas bubbles and computes the mean diameters, total perimeter and centroids. With the help of a built-in scale calibration tool, the measurement results can be presented in calibrated units instead of pixels. Figure 3.5(a) is a typical image recorded at orifice velocity 12m/s and cavitation number of 1.44 and (b) is the selected area of original image in (a). Once the selected portion is converted to greyscale, structures detected by the software will be highlighted automatically based on a given threshold (Figure 3.5 (c)). And then further analysis can be performed based on the processed image. Compare Figure3.5 (b) and (c), a good agreement was obtained. Twenty images were selected and analyzed in order to generate one data point in the computed results.

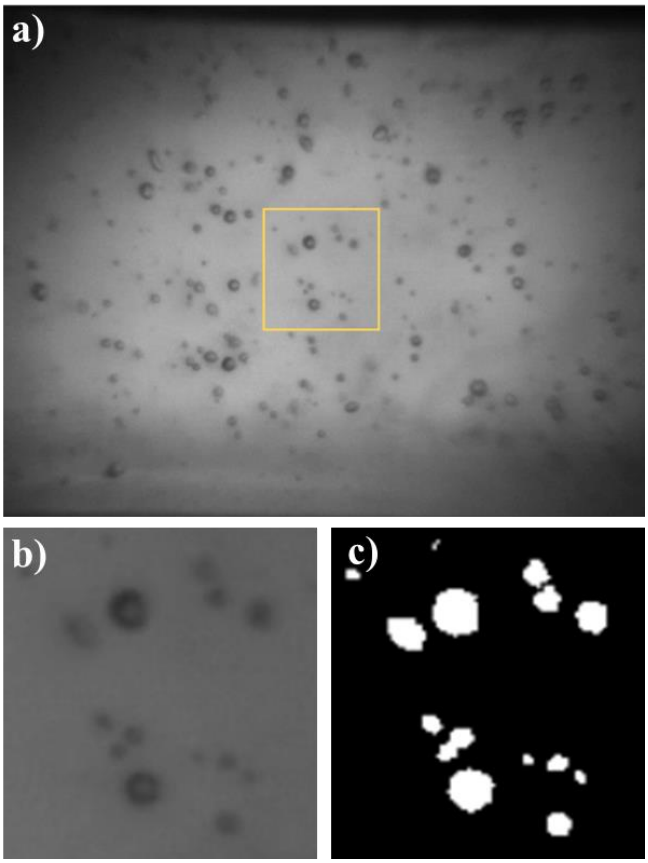

Figure 3.5: (a) An image with gas bubbles (b) Enlarged image of selected area (c) Processed image

3.3 Methodology of pressure signal processing

3.3.1 Calibration of pressure transducers

Pressure transducers (Walfront) were placed at the downstream, orifice and upstream of the cavitation unit, respectively, to measure the pressure changes at each location (see Figure 3.6). Upstream pressure was acquired by a pressure transducer with 80psi maximum range from the 2nd port. Both downstream and orifice pressure were obtained by 30psi pressure transducers from 6th and 4th ports, respectively as shown in Figure 3.6. Due to sudden changes of pressures across the orifice plate, the cavitational bubbles are expected to implode near the orifice. The pressure transducer was connected to 4th connector to record the pressure fluctuations.

Before the pressure transducers were applied to the experiments, they were calibrated using static pressures of a water column. Ten different heights of water were selected, and the corresponding pressure readings from the pressure transducers were recorded. The measured pressures were plotted against the reference pressures generated by water, as shown in Figure 3.7 and 3.8. A linear fitting line with R-square value above 0.99 was obtained for each of the pressure transducers, indicating that the pressure transducers are good for use in the experiments.

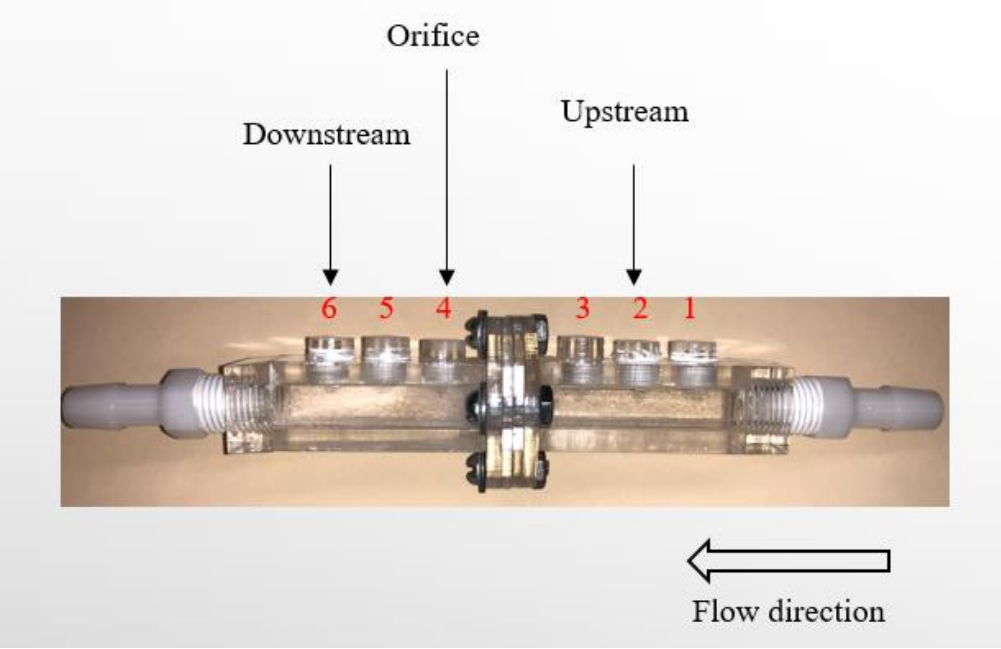

Figure 3.6: Pressure measuring port for cavitation unit

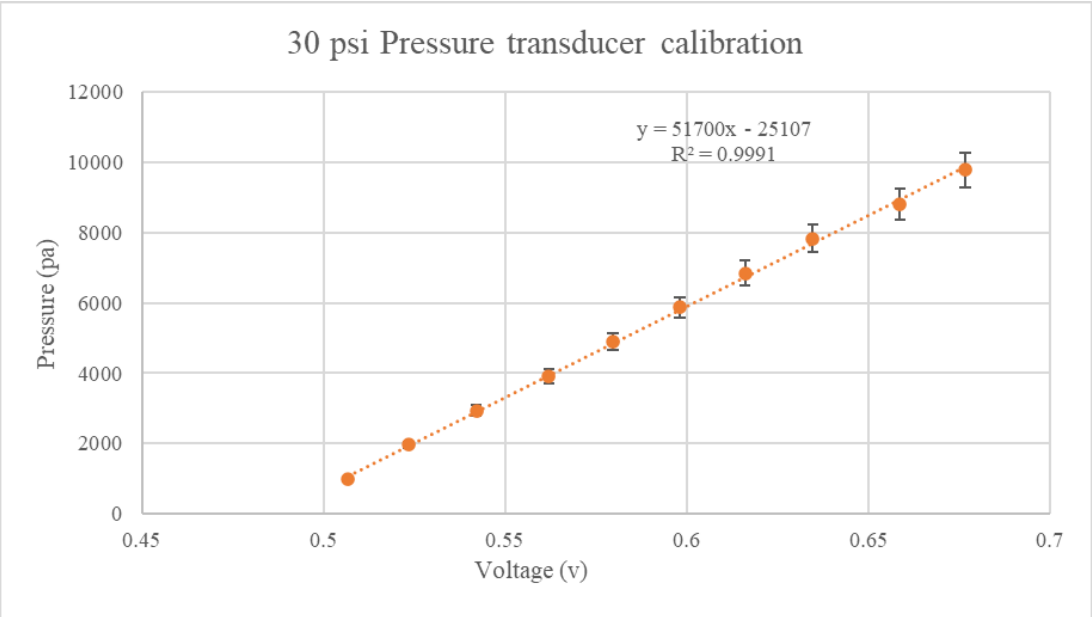

Figure 3.7: 30psi pressure transducer calibration curve

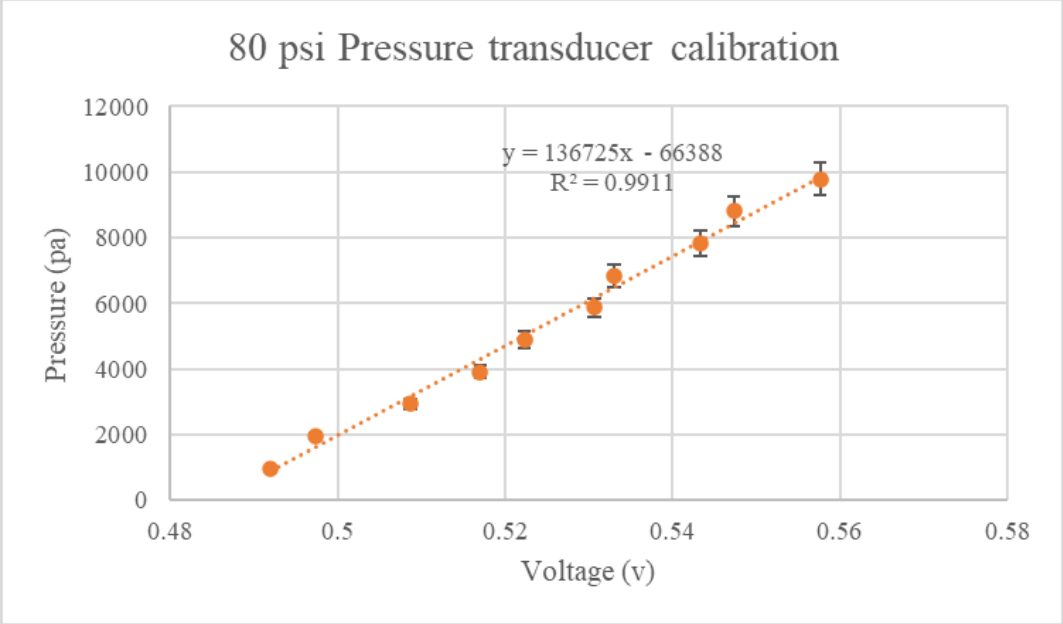

Figure 3.8: 80psi pressure transducer calibration curve

3.3.2 Analysis of pressure fluctuations

The pressure fluctuations at the above-mentioned three locations were monitored and collected by a data acquisition system (USB-6002) purchased from the National Instruments, which was connected to a PC via a USB port. LabView was used to acquire the pressure data at a rate of 25 kHz for approximately 7 seconds for each experiment trial. This sampling frequency allowed to detect all relevant events. The data acquisition was taken 3 minutes after the system reached its steady state at each operating condition.

To analyze the pressure fluctuations, standard deviation for each experimental data set was calculated.

$$\sigma = \sqrt{\frac{\sum(x_i - \mu)^2}{N}} \tag{3.1}$$

Where: σ is the population standard deviation, Pi the pressure taken at time t_i, N the number of pressure data and μ the mean pressure.
The standard deviation evaluates how intense the pressure fluctuated from the mathematical point of view. Large standard deviation indicates violent pressure fluctuations.

Spectral analysis was also applied to analyze the data collected from the pressure transducers. The method is commonly used to study the periodic phenomena in an engineering system. The power spectral density represents a frequency domain characteristic of a time-series data and has been employed to detect the frequency composition in a stochastic process [89]. There are two approaches to process time-serial pressure fluctuation signals: one is to apply the autocorrelation and power spectrum density (PSD) functions of pressure signals, followed by computation of the data using Fourier Transform procedure; The other approach is to directly perform Fast Fourier Transform procedure. In this study, Fast Fourier Transform was applied to the pressure signals and power spectrum analysis were generated in order to further investigate the possible regime transition. The Fast Fourier Transform operates by decomposing a time domain signal into N time domain signals each composed of a single data point and then

calculates their frequency spectra correspondingly. Lastly, the N spectra area synthesized into a single frequency spectrum [90].

$$X(\omega) = \int_{-\infty}^{\infty} x(t) e^{-i\omega t}\, dt \tag{3.2}$$

Time domain signals were converted into frequency domain signals using fast Fourier transforms (FFT) via an in-house MATLAB algorithm. The MATLAB code and detailed transformation process are shown in Appendix. A typical output signal of a pressure transducers is shown in Figure 3.9. The corresponding transformed power spectrum is shown in Figure 3.10. The Y-axis in the power spectrum graph represents the amplitude or the intensity of the frequency components, indicating the energy over the ranges of frequencies. The X-axis represents the frequency in Hz, and it is highly associated with the sizes of gas bubbles. Power spectrum diagram indicates how the energy of a time serial signal is distributed over the frequency. Higher frequency value means shorter period thus smaller bubble size. On the other hand, large bubbles were indicated by lower frequency value.

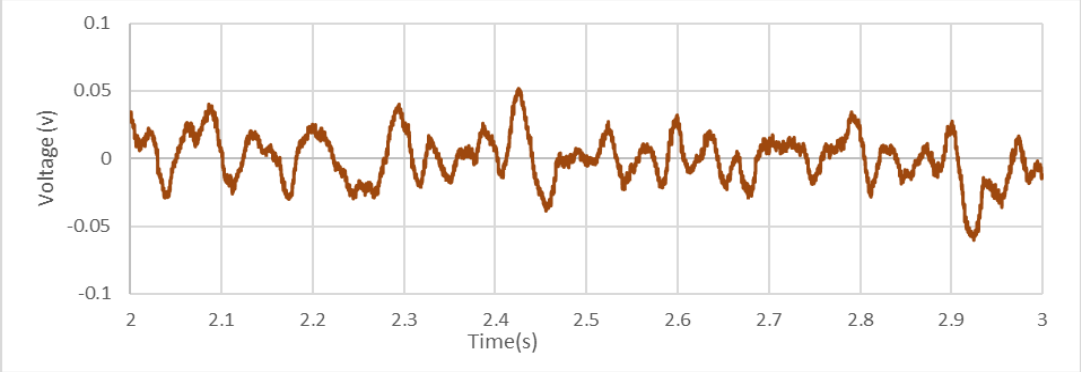

Figure 3.9: A typical time-voltage signal from pressure transducer

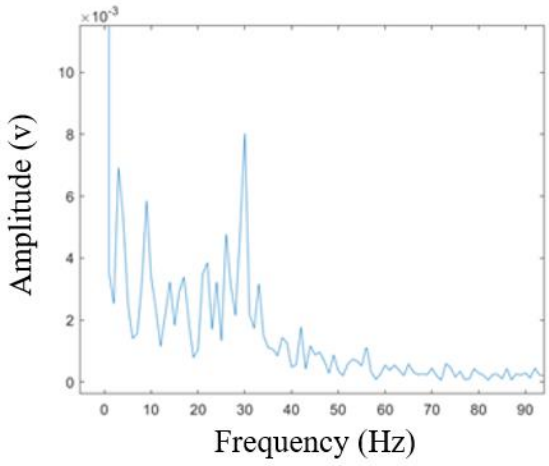

Figure 3.10: Power spectrum generated from 3mm orifice with volumetric flow rate of 4.67 l/min

3.4 Surface tension

A significant amount of chemical engineering processes are designed based on the interaction between gas and liquid phases [91]. Therefore, numerous investigations have been conducted to study the formation and stability of gas bubbles due to their wide applications [92-94]. The surface tension of liquid phase can significantly affect bubble formation and the interaction between gas bubbles and liquid flow.

An ionic surfactant, sodium dodecylbenzene sulfonate (SDBS), was used to reduce the surface tension of water. Five different concentrations of surfactant solution were prepared: 0.0026wt%, 0.0051wt%, 0.0103wt%, 0.0154wt% and 0.0206wt%. The contact angles of the solutions were measured using a Dataphysics, OCA 30. Droplets with same volume were extracted from different solutions and dripped onto the microscope slides from a dosing needle. The samples were then captured by a high-resolution optical measuring device and contact angles were computed automatically by the software. The images of the droplets of water along with five solutions and their corresponding contact angles are shown in Figure 3.11. The surface tension of the solutions was obtained from literature and they are 68mN/m, 66mN/m, 62mN/m, 60mN/m and 58mN/m[95]. Water was used as the basis for comparison, and the surface tension of water under equilibrium

conditions was found to be 72mN/m. The effect of surface tension on the cavitation inception was compared based on four different aspects: contact angle, generation of bubbles clouds, pressure fluctuation analysis and power spectrum graphs. It should be noted that this experiment was conducted using an orifice with diameter of 2mm.

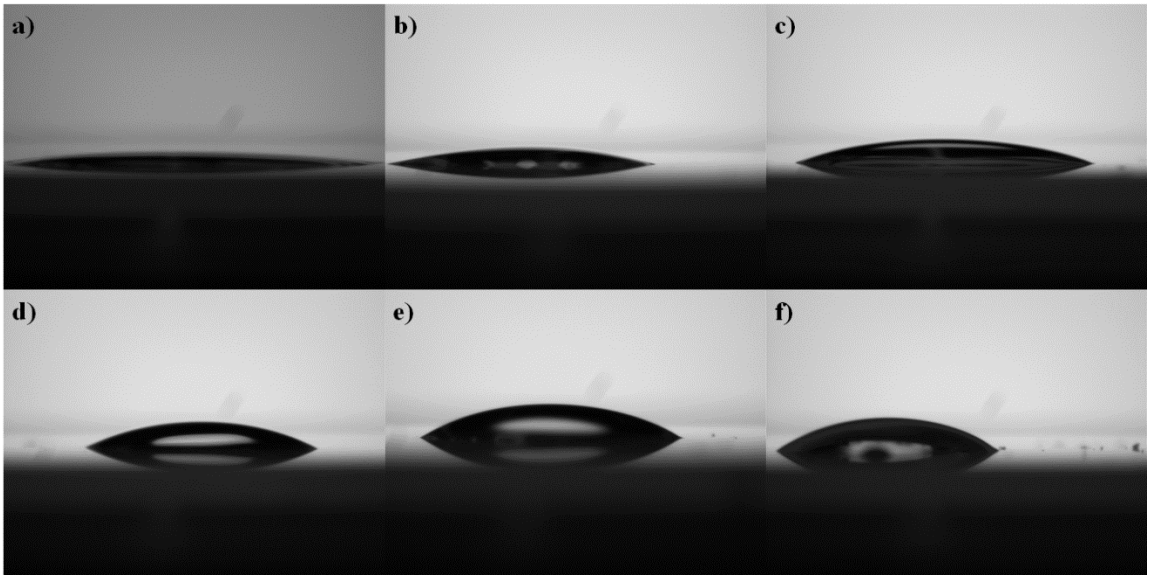

Figure 3.11: Contact angle of solutions. (a) 7.8º (b) 14.5 º (c) 20.9 º (d) 27.9 º (e) 32 º (f) 37.3 º

Chapter 4

4 Characterization of hydrodynamic cavitation

In this chapter, experimental studies were carried out to investigate the transition process from non-cavitation regime to cavitation regime when liquid flow rate was increased. The orifice plate with a single orifice of 3mm in diameter was employed as the constriction. Eight liquid flow rates (4.67, 5.09, 5.51, 5.73, 5.94, 6.36, 6.79 and 7.21 l/min) were selected. The hydrodynamic behaviors of gas bubbles, and pressure fluctuations were characterized using a high-speed camera and pressure transducers. Bubble sizes dramatically reduced when liquid velocity was increased. The occurrence of bubble clouds suggested the inception of cavitation, where the cavitation number is around 1. As the system developed from non-cavitation flow to cavitation flow, the pressure at the orifice became fluctuated violently due to implosion of gas bubbles. Three regimes, non-cavitation, transition and fully developed cavitation regime, were proposed against the pressure fluctuations. Further increased liquid velocity led to a larger bubble cloud. The effects of liquid surface tension were also studied. Reduction in liquid surface tension promoted the generation of small and stable bubbles but suppressed the transition to cavitation regime.

4.1 Overall description of the transition to cavitation regime

4.1.1 Effects of liquid flow rate

As shown in the schematics of the system (Figure 3.1), liquid was pumped from the water tank and flowed through the orifice plate that was sandwiched between the flanges of the cavitation unit. The liquid flow rate was increased from 4.67 l/min to 7.21 l/min, which led to an increase in the pressure drop across the orifice plate. The pressures recorded at the upstream and downstream of the orifice against liquid flow rates were summarized in Figure 4.1. The upstream pressure built up rapidly with volumetric liquid flow rate. The existence of the constriction is responsible for the pressure buildup. On the other hand, the downstream pressures remained unchanged with liquid flow rate and were only slightly higher than the atmospheric pressure. Thus, the pressure drop across the

constriction also increases with volumetric liquid flow rate, which suggests more kinetic energy dissipated at higher liquid flow rate.

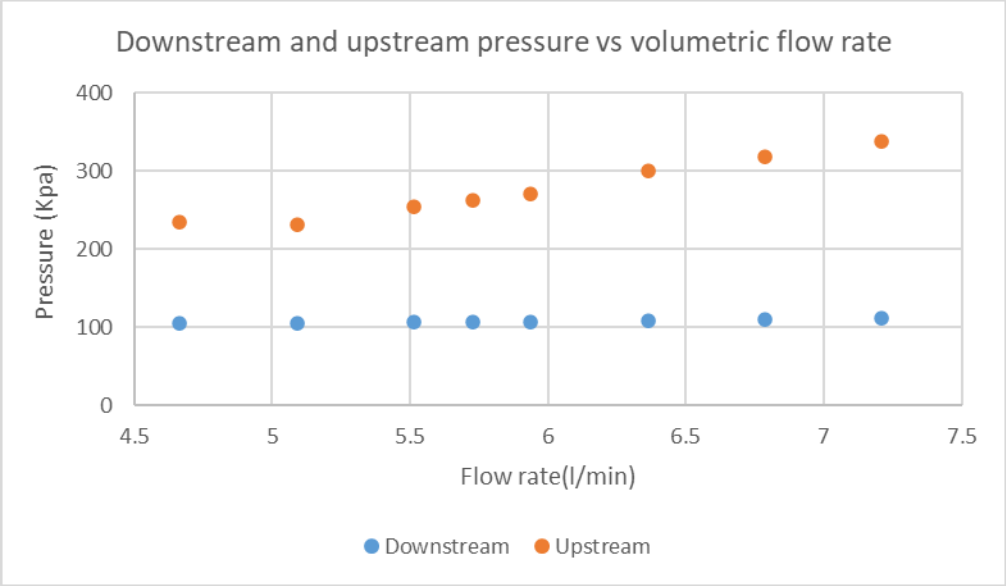

Figure 4.1: Summary of the upstream and downstream pressure at various flow rates

The orifice velocity refers to the liquid velocity passing the orifice and calculated by the equation 4.1.

$$v = \frac{V}{A} \tag{4.1}$$

Where v is the orifice velocity, V the volumetric flow rate, A the total cross-sectional area of the orifice(s). The eight liquid flow rates examined in this study had orifice velocities of 11, 12, 13, 13.5, 14, 15, 16 and 17m/s.

The cavitation number was calculated via Equation 2.3 in section 2.2.1. The cavitation number was developed based on open flow systems. Inherent issues exist when it was used for orifices or Venturies where (partial) choking of the flow[18]. Agreements have never been reached on what pressures and liquid

velocity should be employed to calculate the cavitation number as there are three potential pressures (Upstream pressure, orifice pressure and downstream pressure) and two velocities (Orifice velocity and pipe velocity) in an orifice plate or a Venturi geometry. Table 2.1 of Chapter 2 reviewed that all the three pressures and two liquid velocities in the previously published reports. The values of cavitation number for cavitation inception can vary from more than hundred to less than 1. Yan and Thorpe investigated a system using an orifice plate as constriction and suggested to apply [96] the flow velocity at the orifice and the downstream pressure of the constriction to calculate the cavitation number. In this study, the downstream pressure and the velocity at the orifice were selected to determine the cavitation numbers. And their corresponding cavitation number were calculated to be 1.71, 1.44, 1.24, 1.16, 1.08, 0.95, 0.85 and 0.76 respectively. It is seen from Figure 4.2 that the cavitation number decreases exponentially as the increasing orifice velocity and the pressure drop across orifice.

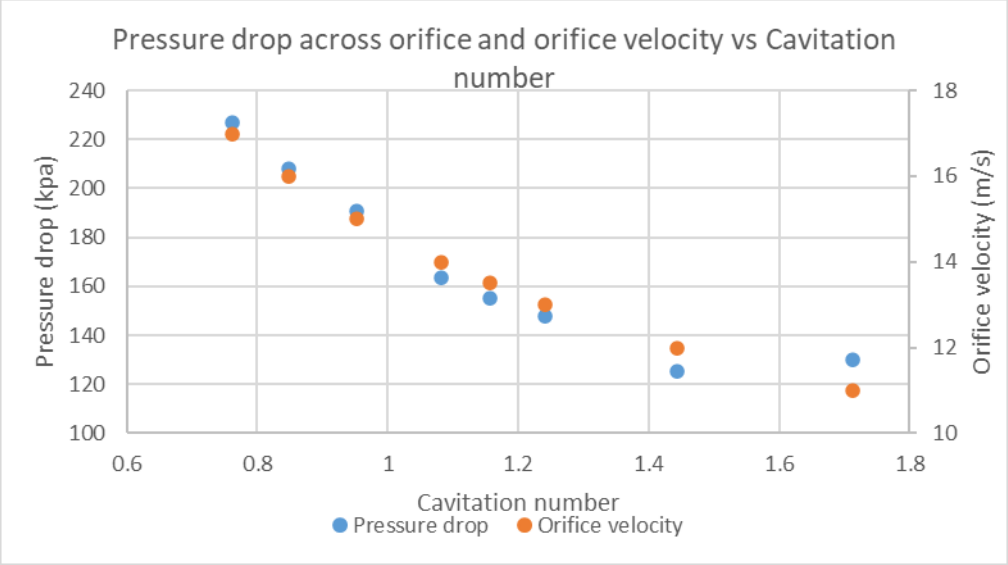

Figure 4.2: Variation of pressure drop across orifice with changing orifice velocity and cavitation number

Reynolds number was also calculated for each specific flow rate using Equation 4.2.

$$Re = \frac{uL}{\vartheta} \tag{4.2}$$

Where: Re is the orifice Reynolds number, u the orifice velocity, L the diameter of the orifice, ϑ the kinematic viscosity of the fluid.

Reynolds numbers of the cavitation unit and of the constriction was calculated using the width of the cavitation unit and the diameter of the constriction, respectively. The Reynolds number of the cavitation unit was in the range between 8,500 to 13,000. In the meantime, the Reynolds number at orifice was found to be from 34,000 to 54,000 thus turbulent flow was in the cavitation unit and at the orifice for all the trials. As the cavitation unit is not that important as the orifice, therefore only the Reynolds number at orifice was showed in Figure 4.3.

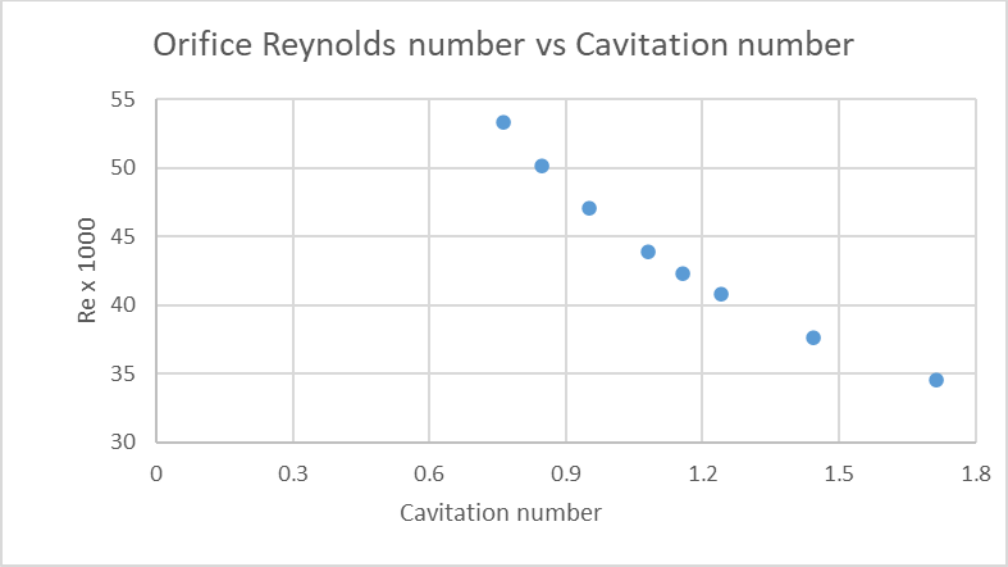

Figure 4.3: Reynolds number at orifice versus changing cavitation number

4.1.2 Cavitation and bubble clouds

Cavitation involves the creation and growth of vapor filled voids in a liquid. In this study, water was enforced to flow through a 3-mm orifice where local accelerations appear, and the local pressure drops. If the local pressures are sufficient low, a large number of air/vapor-filled bubbles, the so-called bubble clouds, are formed. These

bubbles are then carried on by the water flow to the downstream region of higher pressure, where they collapse. The point that the first occurrence of bubble cloud is considered as the actual starting point of cavitation process, the so-called cavitation inception[97]. Visual observation to determine the inception of cavitation is not always practical in engineering application. In the literature, cavitation number has also been frequently employed to describe the development of a cavitation process[98]. Significant emphasis was given on the value of the cavitation number. Many researchers claimed that cavitation occurred when cavitation number was 1[28, 99]. Lower cavitation number indicated more intensive cavitational effects. Some research groups reported the cavitation phenomena could only be observed when cavitation number is much smaller than one[100, 101]. However, cavitation phenomena were also observed at large value of cavitation numbers[102]. These controversies, summarized in Chapter 2, have suggested that cavitation number alone is not sufficient to describe the inception of cavitation. In this section, both imaging technique and pressure transducers were applied to describe the cavitation process.

The high-speed camera was employed to record the variation of bubble behaviors when liquid flowed through the constriction of the cavitation unit. All the images were captured in the area illustrated by Figure 4.4. With the help of the high-speed camera, the liquid flow and bubble behaviors were observed against liquid flowrate and are shown in Figure 4.5. The lowest liquid flowrate employed in the tests was 4.67 l/min and the orifice velocity was 11 m/s. The corresponding cavitation number is 1.71. No bubbles were observed. The liquid flow rate was then increased to 5.09 l/min, bubbles were barely observed as the liquid passed through the constriction (Figure 4.5 a). Continuous increasing the liquid flow rate led to formation of large gas bubbles. Higher the liquid velocity more gas bubbles generated (Figure 4.5 b-c).

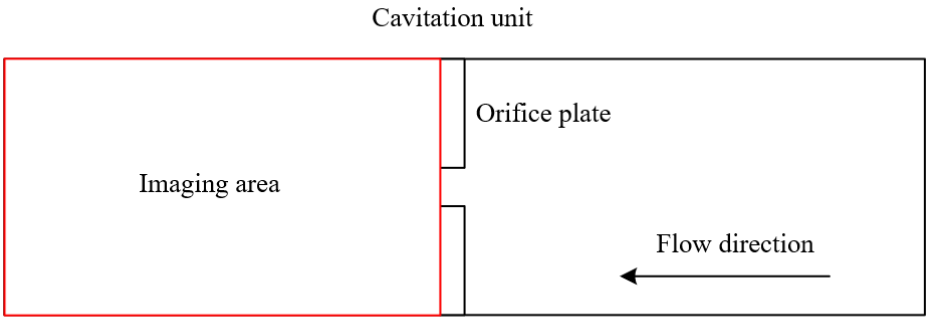

Figure 4.4: The imaging area for high-speed camera

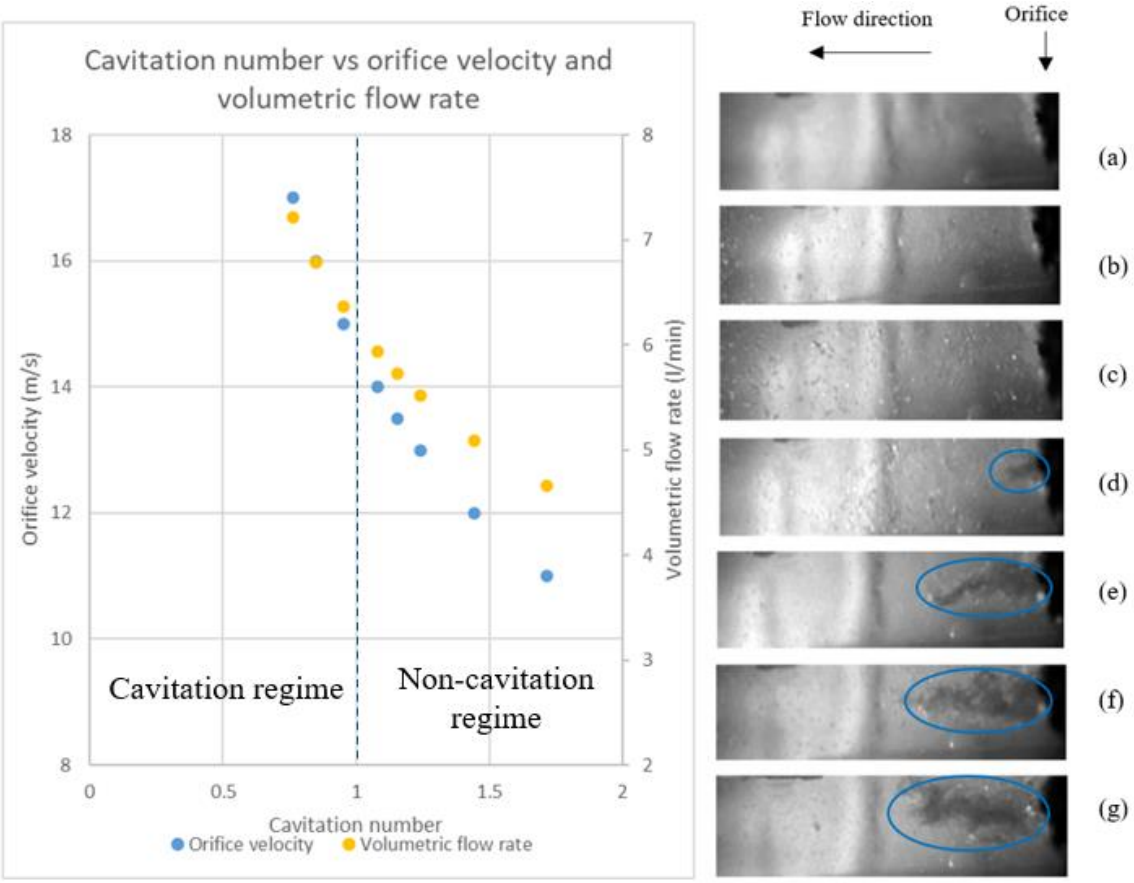

Figure 4.5: Image of bubble cloud ats different cavitation number and volumetric flow rates

A further increase in liquid flowrate/orifice velocity made the cavitation number drop to 1.08, where the very first bubble cloud was observed (Figure 4.5 d). The bubble cloud consists of huge amounts of fine gas bubbles that are normally smaller than 0.1 mm (The detailed discussion is shown in the next section.) [103]. The cavitation was initiated in the cavitation unit of this research when the cavitation number reached 1.08. The continuous increase in liquid flow rate after the inception point of cavitation, led to further reduction in the cavitation number to 0.95, 0.85 and 0.76 respectively. The bubble clouds had a significant enlarge as cavitation number drops from 1.08 to 0.95. Further reduction of cavitation number from 0.85 to 0.76, the incremental of bubble clouds became insignificant. Cavitational bubbles tends to implode in the imaging zone (Figure 4.5 e-g). Hence, for the cavitation unit tested in the experiment, the transition from non-cavitation regime to a fully developed cavitation regime took place when the cavitation number was close to 1. The intensity of cavitation was increased with increasing orifice velocity in the fully developed cavitation regime.

4.2 Photographical analysis of bubbles

4.2.1 Close-up view of bubbles at orifice

To compare the bubble behaviors from non-cavitation flow to cavitation flow, close-up images of bubbles at orifice were taken and compared. Four pictures were extracted from liquid flows with cavitation number being 1.44, 1.24, 1.08 and 0.76.

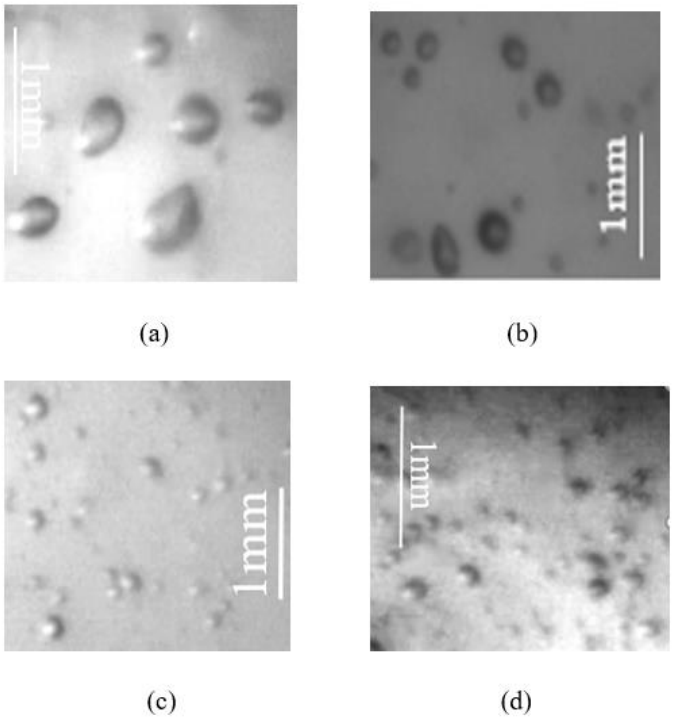

Figure 4.6: The images of bubble at four cavitation number: 1.44 (a), 1.24 (b), 1.08 (c) and 0.76 (d).

Figure 4.6 (a) was taken at orifice velocity at 12 m/s and the volumetric flow rate of 5.09 l/min, which flow has a cavitation number of 1.44. The liquid in the system was degassed and a small quantity of relatively large gas bubbles was observed in the non-cavitation regime. These bubbles were produced by the pump. Most were in the range of 0.5mm to 0.7mm, and some of them are ever larger than 0.7mm. As the orifice velocity was increased to 13m/s, Figure 4.6 (b), the number of bubbles was seen to be slightly increased to 557/cm^2, and the sizes of bubbles were reduced as well. When the cavitation number dropped to 1.08 marking the inception of cavitation, the number of bubbles were dramatically increased, reaching 802/cm^2, while the sizes of bubbles were reduced to one third of its original size in the transition from non-cavitation regime to cavitation regime. The orifice velocity was further increased to 17m/s when the cavitation regime is fully developed. (Figure 4.6 d). Both the number of bubbles and their diameter showed significant difference compared to previous three figures. Tremendous amounts of

bubbles with diameter less than 0.1mm were produced at orifice under the cavitation conditions.

The number of bubbles and their size distribution generated by the orifice can be found in Figure 4.7. As observed in the Figure, the bubble size distributions for cavitation number greater than 1.08 are quite flat with a peak bubble size between 0.6mm and 0.7mm along with a number of occurrences less than 50. This indicates that, in the non-cavitation regime, there is a good mixture of various bubble sizes. Increasing liquid velocity resulted in a decrease of bubble sizes but an increase in bubble population. In the transition from non-cavitation to cavitation, e.g., the cavitation number being 1.08, majority of the bubbles were shown between 0.2mm and 0.3mm. The bubble size distribution became narrower and reduced from 0.2-0.3mm to 0.1mm as the flow turned from the transition regime to the fully developed regime when the cavitation number decreased from 1.08 to 0.76. At the meantime, the distribution tail also extended dramatically which indicated a large number of fine bubbles with diameter around 0.1mm were produced due to the transition process from non-cavitation to fully developed cavitation state.

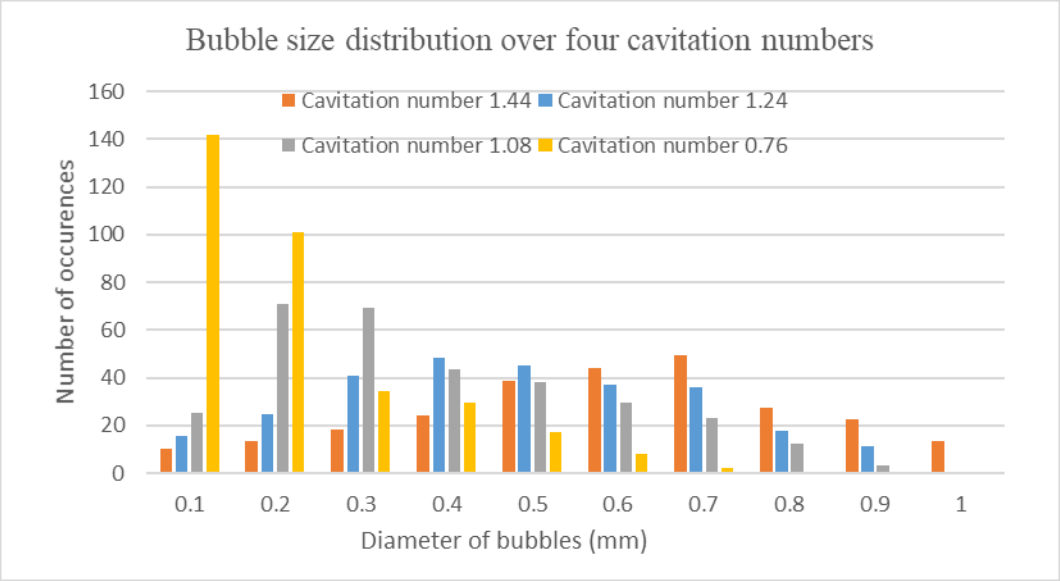

Figure 4.7: The size distribution of bubbles generated by orifice for four cavitation numbers

4.2.2 Bubble breakup and combination

As liquid flows through the orifice and reaches the downstream region, a sudden increase in pressure occurs. The gas bubbles behave violently in the downstream region that is adjacent to the orifice plate. Bubble breakup and coalition in a flow of the non-cavitation regime and the fully developed cavitation regime were recorded and compared using the high-speed camera. The shutter speed of high-speed camera further decreased to 1/41,000 second and images were taken at three selected cavitation numbers.

4.2.2.1 Bubble breakup

The behavior of bubble breakup was investigated in both the non-cavitation regime and the fully developed cavitation regime, where the cavitation numbers were 1.44 and 0.85. Figure 4.8 showed the bubble breakup process in a non-cavitational flow (Cavitation number was 1.44). Two bubbles framed in red and blue, respectively, were recorded. Use the bubble framed in blue as an example.

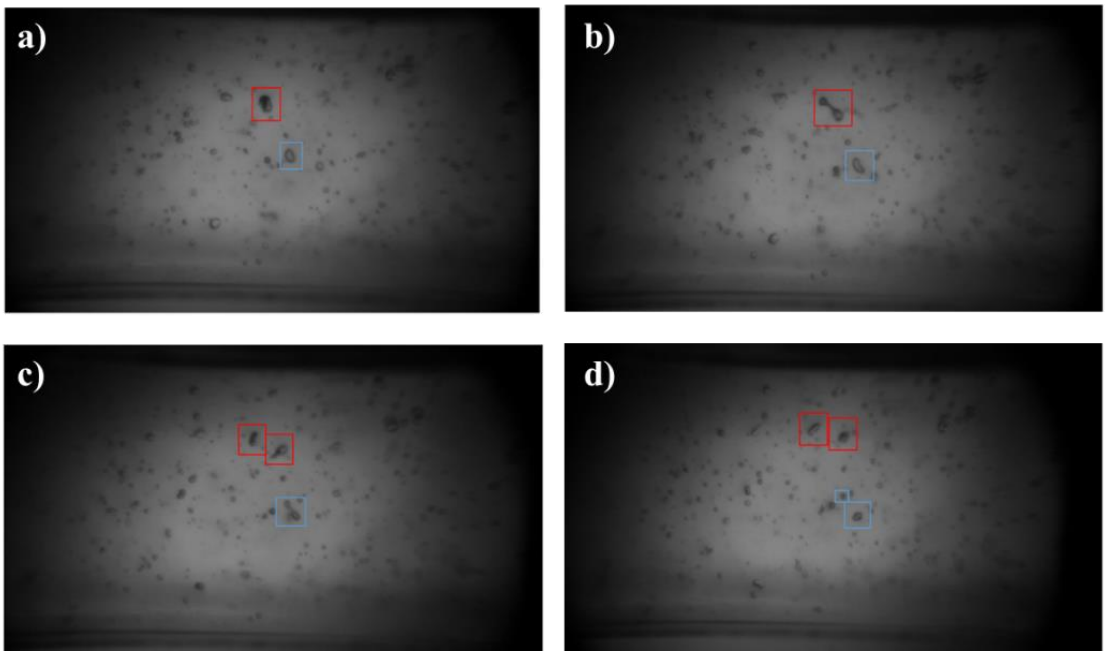

Figure 4.8: Images of bubble breakup process at non-cavitation state.

The breakup process consists of three steps: deformation, elongation and splitting. The bubble (Figure 4.8 a) was firstly deformed, becoming a non-spherical bubble (Figure 4.8

b). Then the bubble elongated (Figure 4.8 c) and finally it split into two smaller bubbles (Figure 4.8 d). In the splitting step, a pressure pulse was produced.

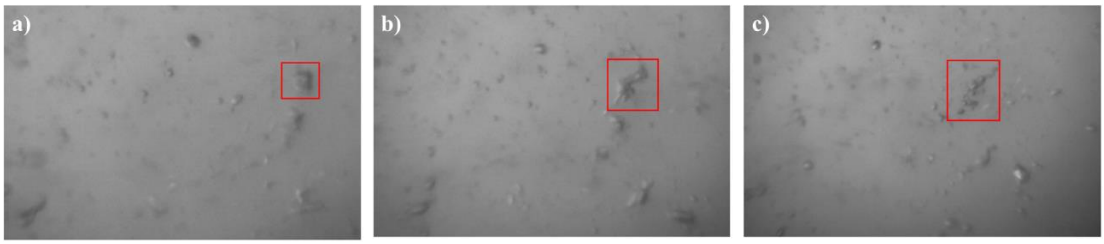

Figure 4.9: Images of bubble breakup in cavitation regime

In the fully cavitation regime with cavitation number of 0.85, the bubble breakup appeared to go through a quicker process. In this regime, gas bubbles were significantly smaller than the bubbles in a non-cavitation flow and they were in a relatively spherical shape. Without a clear deformation step recorded by the high-speed camera, the bubble showed elongation (Figure 4.9 b), quickly followed by the split step which generated multiple smaller gas bubbles (See Figure 4.9 c) instead of two bubbles as observed in the non-cavitation flow [104].

4.2.2.2 Bubble combination

Opposing to bubble breakup, combination of bubble is a physical phenomenon that two or more gas bubbles are combined to form one large bubble. It has been frequently observed in a non-cavitation flow but rarely in a fully developed cavitation flow [105]. Figure 4.10 shows the combination of bubble at orifice velocity at 12 m/s and the volumetric flow rate of 5.09 l/min, which flow has a cavitation number of 1.44. Two adjacent gas bubbles (Figure 4.10 a) continued to get closer until the clear interface between two bubbles disappeared (Figure 4.10 b). Eventually, two individual gas bubbles are merged into one larger bubble, which marked the successful completion of bubble combination (Figure c).

As liquid flow rate increased and the liquid flow gradually developed to a cavitation regime, the phenomenon of bubble combination became diminished. A cavitation flow is dominated by bubble deformation and collapse. The observation is well supported by the

previously reported results [106-108]. In the transition process from non-cavitation to fully developed cavitation, bubble formation and breakup have been observed throughout the entire selected cavitation number range. In a fully developed cavitation regime, fine gas bubbles were produced via bubble breakup. Violent bubble implosion was also observed.

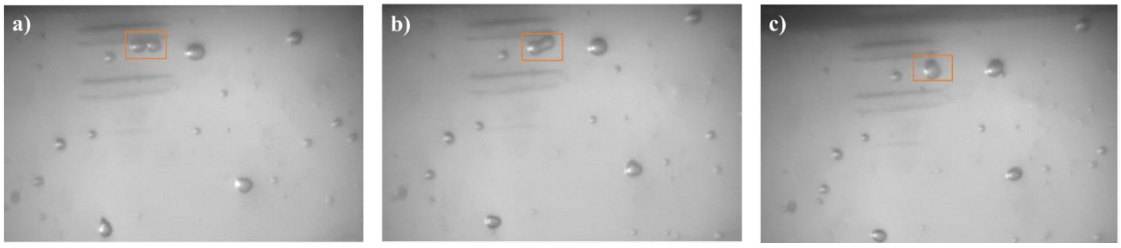

Figure 4.10: Images of bubble coalesce process in non-cavitation regime

4.3 Pressure fluctuations

Pressure fluctuation is one of the most widely employed methods in characterizing a gas-liquid two phase flow [109-112]. This technology includes pressure transducers and a data acquisition system, is inexpensive and easy to realize. The analysis of pressure fluctuation was employed in this work to study the hydrodynamics of bubbles and to characterize the flow regimes and regime transition.

A pressure transducer was connected to the 4th port (illustrated in Figure 3.6) that measures the pressure fluctuations of the flow just leaving the orifice plate. The pressure data were normalized by subtracting the average value and then divided by the average value. After normalization, all the pressure data sets were fluctuated around zero.

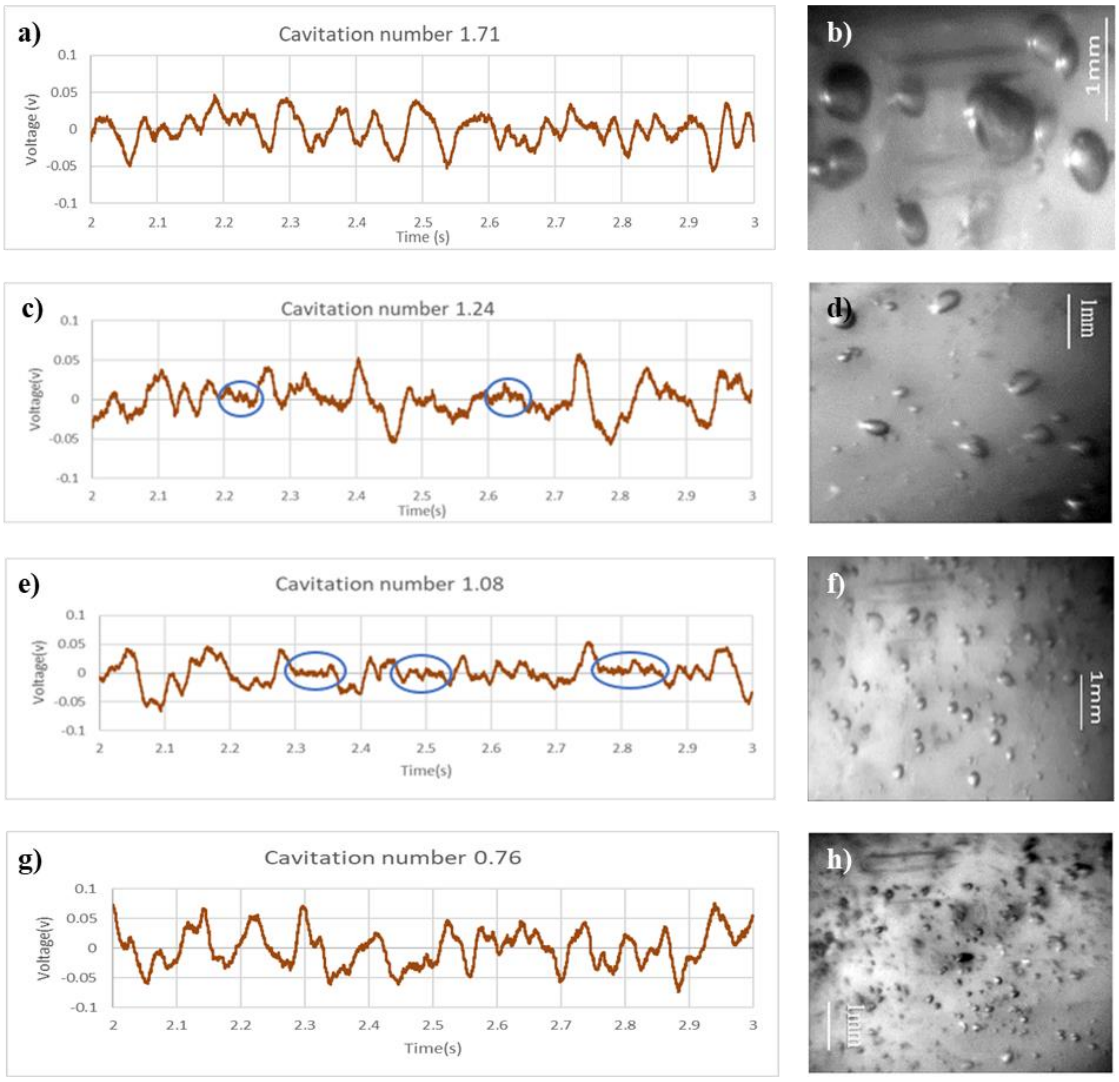

Figure 4.11: The pressure fluctuation signals at four cavitation conditions along with their corresponding close-up images.

Many sources can induce pressure fluctuations in a fluid system, including turbulence of flow, bubble coalescence and breakup, bubble formation and oscillation etc. To demonstrate the bubble dynamics and the flow regime transition, one second of pressure fluctuation signals were extracted from four liquid flows of different cavitation numbers. The pressure signal displayed in the Figure 4.11 (a) was taken when the flow has a cavitation number of 1.71, indicating it was in the non-cavitation regime. Fluctuations with wide peaks and similar amplitude were observed. This suggested that the bubbles passed through the monitoring point at a low velocity, and they were relatively large also

similar in sizes. Figure 4.11 (b) taken at the same operating condition evidenced the results extracted from the pressure signals. Johnsson et al.[109] employed pressure transducers to characterize the regime of fluidization and observed the same periodic fluctuation behavior. Small fragments of pressure fluctuation with high frequency and lower amplitude occurred when the cavitation number of the liquid flow was reduced to 1.24 (Figure 4.11 c). This was contributed by the breakup of large bubbles due to the increased shear[113]. As the cavitation number further dropped to 1.08, the flow was in the transition from non-cavitation to cavitation regime. Both bubble clouds with very fine bubbles and relatively large bubbles (Figure 4.11 f) can be observed. The mixed bubbly flow was well reflected by the pressure signals. It is seen in (Figure 4.11 e) that wide peaks with high amplitude were accompanied with low magnitude peaks with high oscillation frequency. Fully developed cavitation was presented when cavitation number dropped to 0.76 (Figure 4.11 h), tremendous number of fine bubbles with diameter around 0.1mm were formed within the liquid. Due to the continuous implosion of cavitation bubbles, violent pressure fluctuation with higher magnitude was observed from the signal[114].

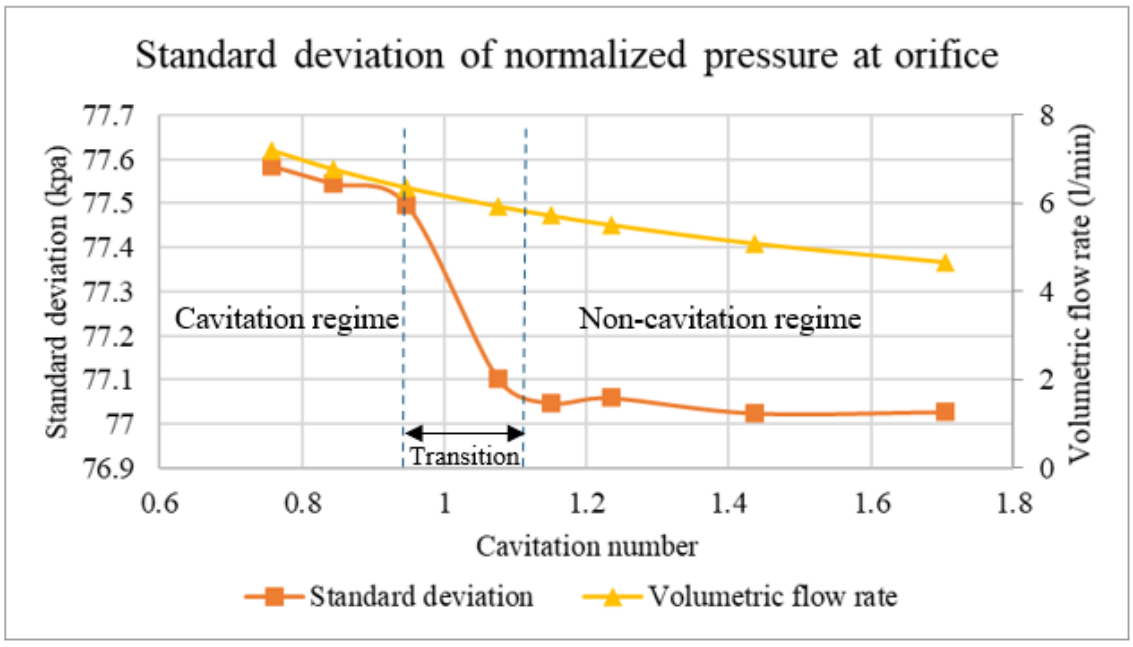

Figure 4.12: Standard deviation of pressure signals versus cavitation number

The standard deviation of pressure fluctuation signals across eight cavitation number were calculated and showed in Figure 4.12; Three regions were observed against liquid flow rate and cavitation number. It can be seen that the standard deviation of pressure signals at low liquid flow rates was maintained well at about 77kpa with the cavitation number decreased from 1.71 to 1.16. However, the standard deviation showed noticeable change from 77kpa to 77.5kpa when a cavitation number is around 1. At this cavitation number, a bubble cloud was first observed, evidenced by Figure 4.5 discussed in Section 4.1.2. It indicated that cavitation was initiated. A huge amount of fine bubbles were formed and bubble implosion became frequent due to a sudden pressure change between the orifice and the downstream of the orifice. These bubble motions induced the pressure fluctuations. Further increase liquid flowrates, even more fine bubbles were generated along with a decrease in bubble sizes which was evidenced by Figure 4.5. Implosion of these large amount small bubbles due to a sudden pressure increase is expected to elevate the fluctuation of pressure signals. The clear trend in pressure fluctuations clearly distinguished three regimes in an orifice cavitation unit, which are non-cavitation regime, transition regime and cavitation regime. Superior to visualization method, the pressure transducer technique offers an inexpensive and practical approach to in-situ monitor the status of a liquid flow in a cavitation unit.

4.4 Power spectrum analysis

Power spectral analysis based on Fourier transform has been shown to be a powerful tool to determine the transition points and also to extract regime features [115]. Drahoš et al. [116] employed this method in a bubble column reactor and investigated the various operating conditions for frequency range from 0 to 20Hz. Letzel et al. [117] applied the same approach to characterize different flow regimes and regime transition in a fluidized bed at the same frequency range. In order to obtain the accurate flow structures and their characteristics, a spectral analysis based on Fast Fourier Transform was used. The global pressure fluctuations are caused by pressure sources such as bubble formation, bubble coalescence, bubble breakup, bubble eruption, oscillations of the gas–liquid suspension and mechanical vibrations of the pump.

The local and global fluctuations are created by different pressure sources as mentioned in the previous section. These pressure fluctuations cannot be cross correlated with each other in a pressure time series and thus can be assumed independent of each other. Consequently, the product of their Fourier transforms becomes equal to zero.

The frequency of pressure pulse observed in the power spectrum graph is highly associated with bubble sizes [118]. As large gas bubble usually moves and oscillates slower. The behavior results, therefore, the frequency showed in the power spectrum graph would be lower; small bubble usually appears at higher liquid flow rate thus would appear in the higher frequency zone[119]. The amplitude of the pressure peak at any frequency in the power spectrum indicates the total energy of the gas bubbles at that frequency. High total energy of bubbles can be achieved by either high severity of bubble oscillation/interactions or large number of bubbles. Thus, large bubbles, bubble formation and widening bubble size distribution can significantly increases the intensity and width of the peaks.

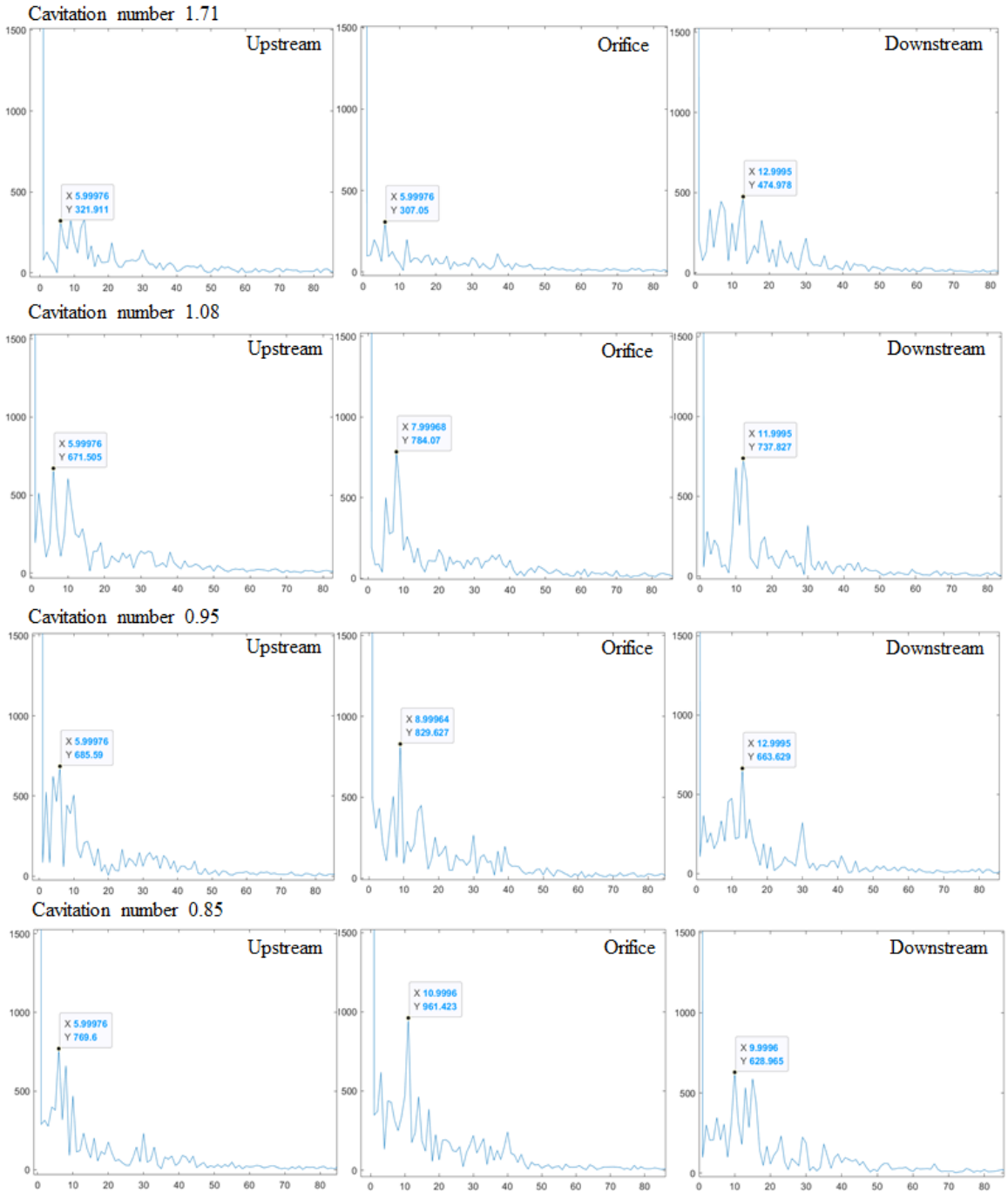

Figure 4.13: Power spectrums for four selected cavitation numbers at upstream, orifice and downstream.

Four liquid flowrates 4.67, 5.94, 6.36 and 6.79 l/min with corresponding cavitation numbers of 1.71, 1.08, 0.95 and 0.85 were selected in the discussion. The power spectrum graphs for all three positions were also listed in Figure 4.13. The upstream

pressure pulses across four cavitation numbers were found in the frequency range between 1-10 Hz. For a given liquid flow rate/cavitation number, similar high amplitudes were observed for the peaks less than 10 Hz. The spectra were expected since, in the upstream, no cavitational effects occur and a mixture of large bubbles and fine bubbles existed. Significant different bubble behaviors were revealed at the orifice position. The peaks with relatively high intensities spread out to higher frequencies. Intensive pulses were also observed between 30 and 40 Hz. The dominant frequency increased with the decreasing cavitation number indicates the reduction of bubble sizes. Secondly, the bubble sizes at transition process and developed cavitation regime were found to be slightly smaller than that at upstream and getting even smaller throughout the whole process. It should be noted that the dominant peaks were signified from 307Pa to 784Pa as the cavitation number was decreased from 1.71 to 1.08. This sudden increase in intensity was because of the occurrence of cavitation inception. The intensity of the dominant peak was further increased to 960Pa when cavitation was fully developed. Lastly, the frequency and amplitude reading for downstream was not changed significantly. It indicated that the bubble sizes and total energy at the downstream were similar for all operating conditions. The downstream was connected to the open water tank and its pressure was approximately atmospheric pressure, which is expected. Overall, it can be said that the results of power spectrum analysis also support the findings obtained from previous sections. These results agree well with the results obtained from visualization presented earlier in this chapter regarding the variation on bubble sizes and flow characteristics.

4.5 Effect of surface tension on the inception of cavitation

4.5.1 Contact angle/surface tension

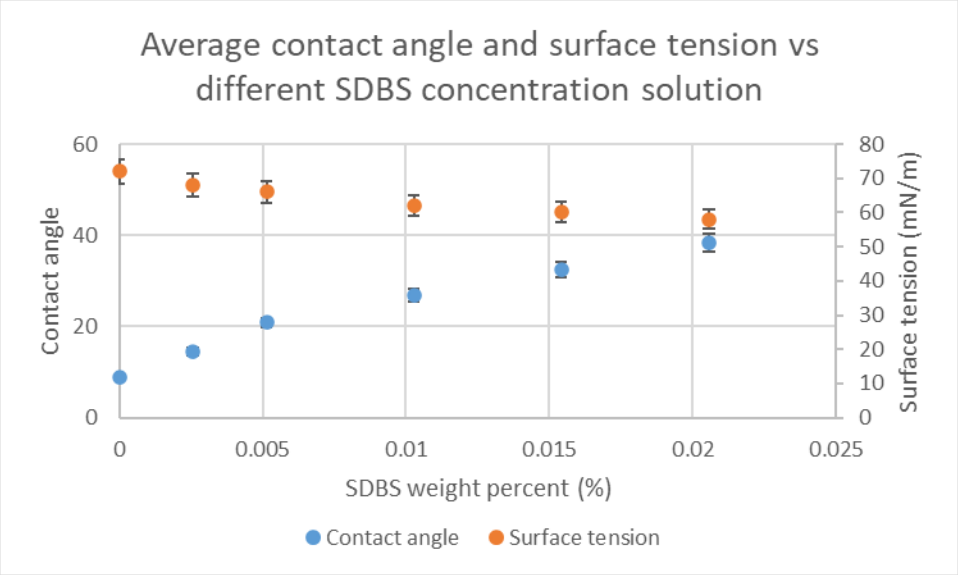

Figure 4.14: Change of surface tension and contact angle for solutions with different concentration of SDBS.

It is obvious in Figure 4.14 that with the increased concentration of surfactant, the surface tension experienced a moderate drop from 72mN/m (water) to 58mN/m. In the meantime, the contact angle of the liquid droplet increased from 8^{o} to 38^{o} due to the decreased surface tension.

4.5.2 Visualization of the effect of surface tension

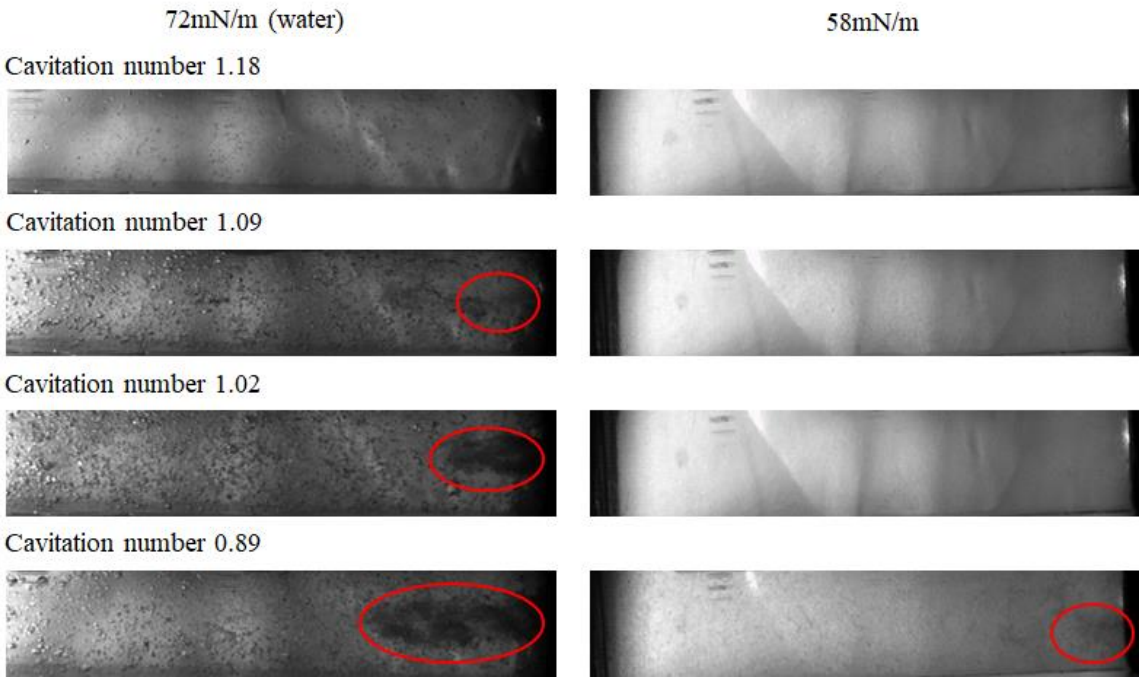

Figure 4.15: Visualization of bubble clouds for water and surfactant solution.

To study the effect of surface tension on the inception of cavitation, the recorded images were shown in Figure 4.15. When the cavitation number was 1.18 and no cavitation was formed, only a few relatively large bubbles can be observed in the pure water flow, but a huge number of tiny bubbles were formed in the surfactant containing solution(58mN/m). Reduction in surface tension can lead to easy formation of small gas bubbles, which is expected. The inception of cavitation in water (72mN/m) occurred at cavitation number of 1.09 whereas the cavitation cloud for the solution (58mN/m) was first observed only when the cavitation number dropped to 0.89. The bubble cloud was also much smaller in size. Furthermore, the number of bubbles for water increased significantly after the cavitation inception accompanied with reduced sizes. No visible change in terms of number of bubbles and bubble sizes were observed in surfactant containing solution as the cavitation was initiated. The images shown in Figure 4.16 demonstrated that surface tension delayed the inception of cavitation. The lower the surface tension that the liquid has, the lower the cavitation number required to initiate the cavitation.

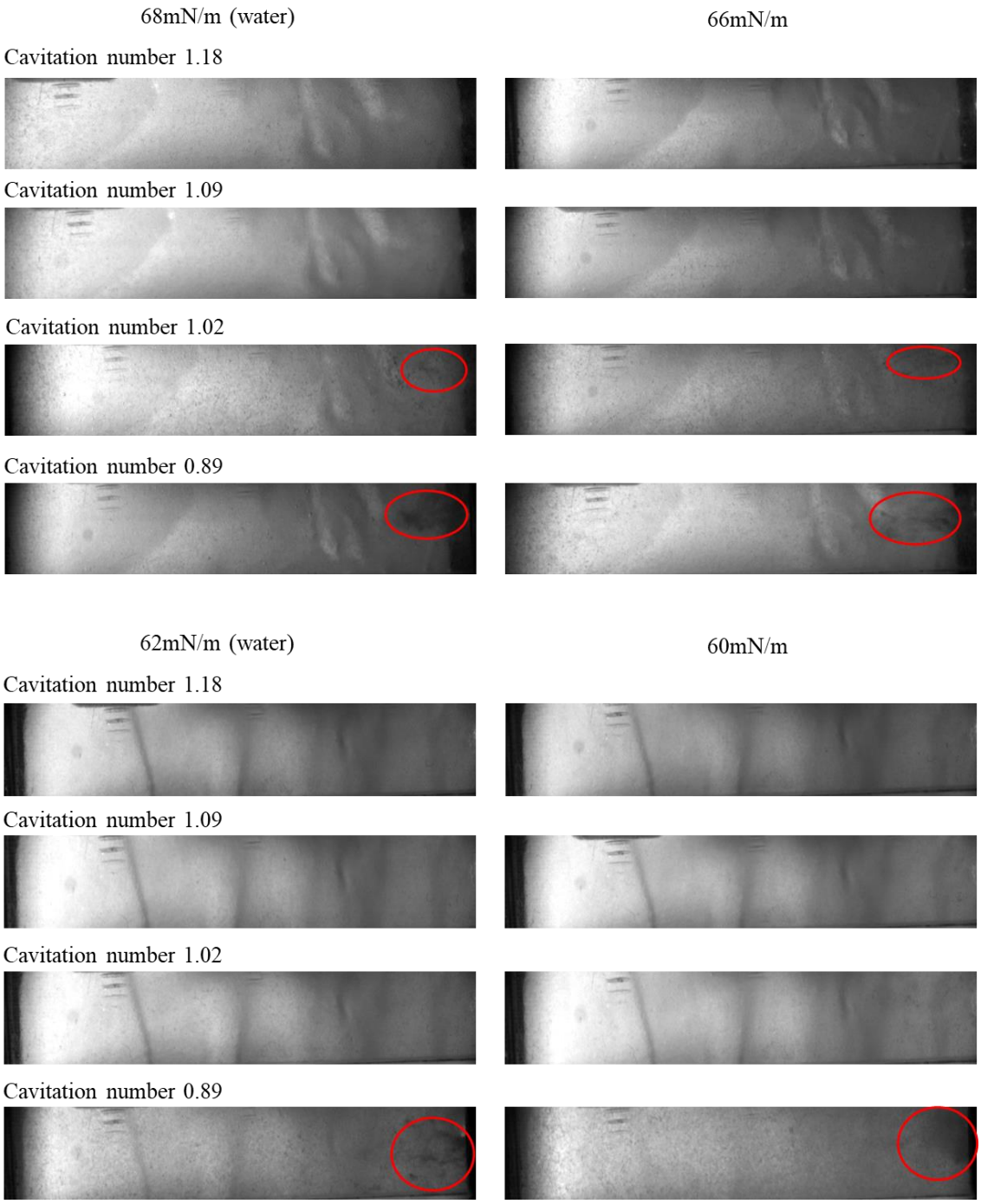

Figure 4.16: Visualization of bubble clouds for solutions with different surface tension.

4.5.3 Pressure signal analysis

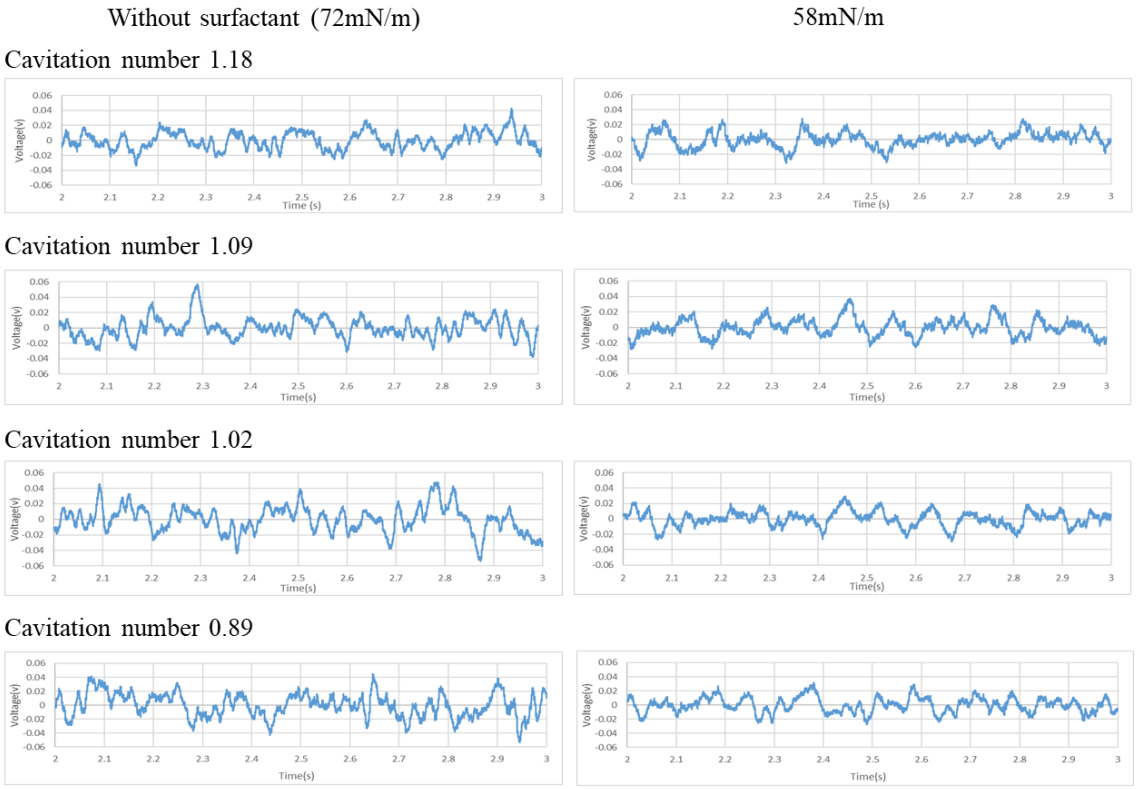

Figure 4.17: Comparison of pressure signal fluctuations between water and surfactant solution.

Pressure fluctuation data presented in Figure 4.17. It is clear that the pressure fluctuations for surfactant solution did not show visible change in either the amplitude or the frequency with the flow developed from non-cavitation to cavitation regime.

4.5.4 Power spectrum analysis

Figure 4.18 (at orifice) compared the results of the power spectrum of pressure fluctuations acquired at the orifice for pure water and surfactant containing solution with surface tension being 58mN/m. The inception of cavitation are well reflected by the occurrence of a highlighted high frequency zone in both solution's power spectrum. The frequencies and intensities of the surfactant containing solution's dominant peaks for all four cavitation numbers remain similar, thus the inception of cavitation had limited

contribution towards the flow characteristics. The findings are agreeable with the photographic analysis discussed in the previous section.

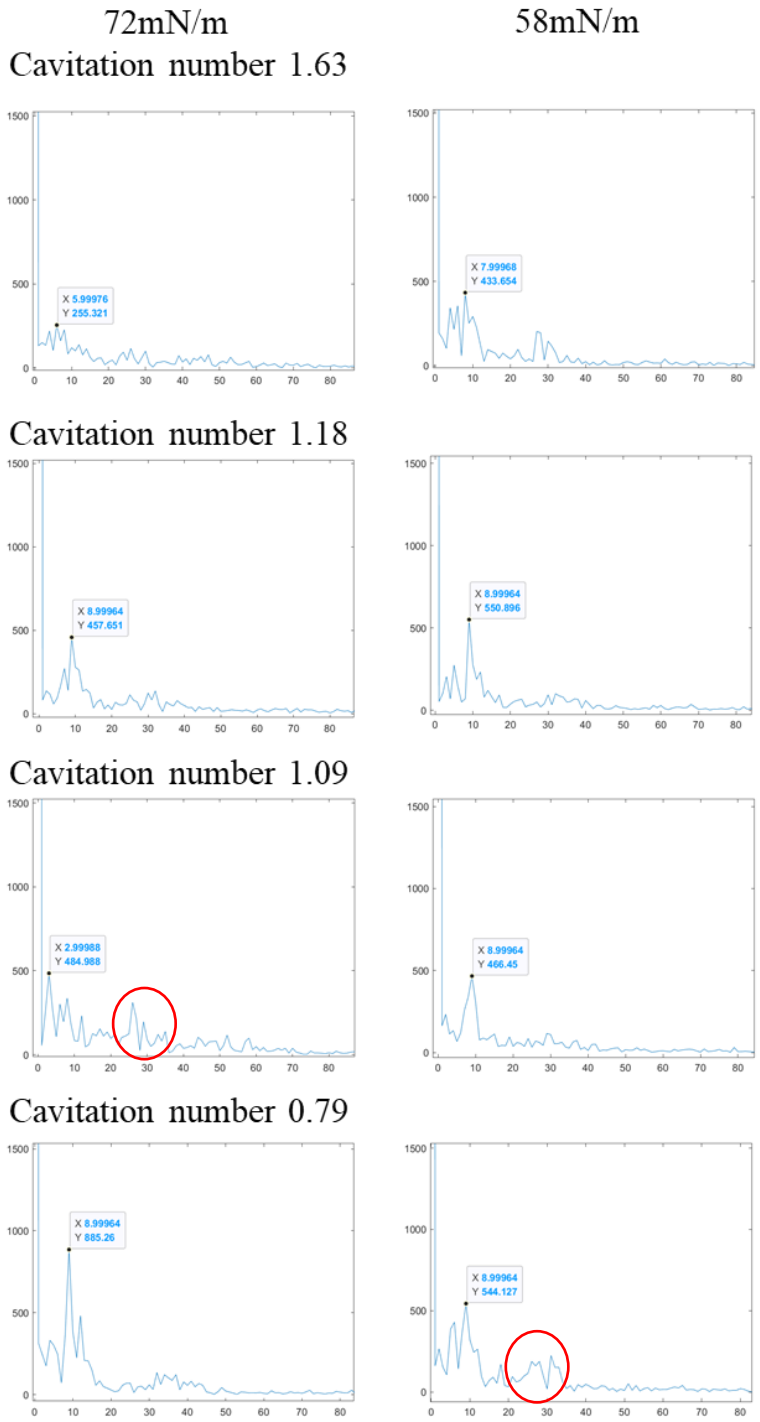

Figure 4.18: Comparison of orifice power spectrums for water and surfactant solution.

Chapter 5

5 Effects of orifice geometry on the intensity of cavitation

Orifice plate is one of the most commonly used devices for producing hydrodynamic cavitation due to its simplicity and effectiveness. Numerous studies have been conducted to investigate the orifice-induced cavitation, both experimentally and numerically. Arrojo et al. [120] studied the performance of various orifice designs in disinfection of *E.coli* and compared the results to the Venturi-generated cavitation. The performance of various orifice plates with a range of the number and sizes of holes was compared by Vichare et al. [121]. The influence of different orifice designs on the characteristics of cavitation phenomena produced were modeled and compared by Alister et al.[122]. However, the influence of geometric factors on the development process of cavitation has yet been fully understood. Therefore, the present experimental study of cavitation concerning orifice design was carried out to understand the effects of opening ratio and the length of orifice edges. Five orifice designs were studied featuring different combinations of orifice diameter and opening rates (Figure 5.1 and Table 5.1). The effects of opening ratios and orifice perimeters on the transition from the non-cavitation flow to the cavitation flow was investigated. Bubbles and bubble population were characterized. The pressure fluctuations and their power spectral analysis were presented to characterize the cavitation process.

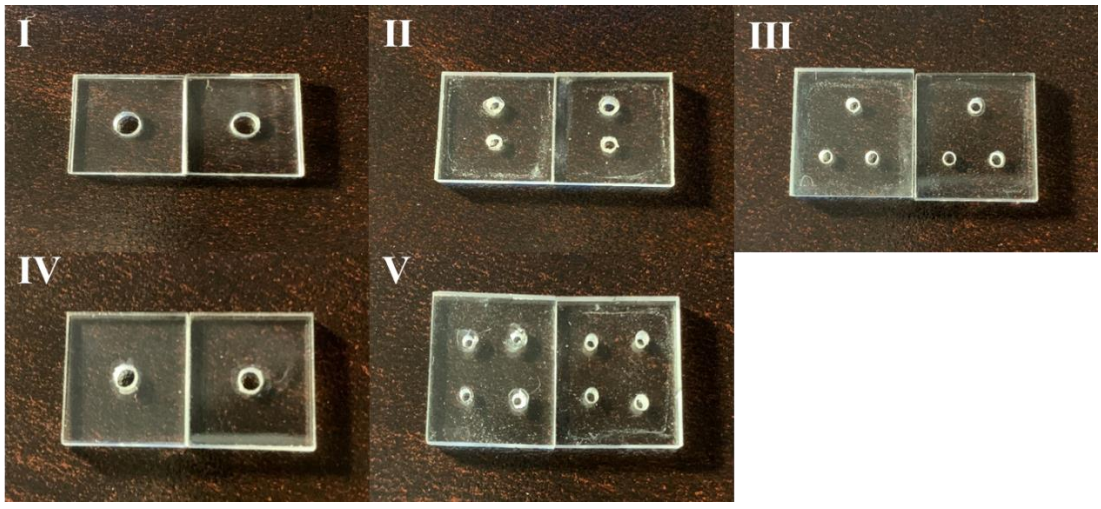

Figure 5.1: Graphic illustration of five different orifice design.

Table 5.1: Detailed information regarding five different orifice design

Plate number	Number of Orifice	Orifice diameter (mm)	Total perimeter (mm)	Total opening ratio (%)
I	1	3	3π	7.8
II	2	1.5	3π	3.9
III	3	1	3π	2.6
IV	1	2	2π	3.5
V	4	1	4π	3.5

5.1 Effect of opening rate (ratio) on cavitation transition

Three configurations of orifice plates, numbered by I, II and III (As shown in Table 5.1), were employed to investigate the effect of orifice opening ratio. The total orifice perimeters of the three plates were maintained the same (3π mm), whereas the orifice opening ratio was reduced from 7.8% to 2.6%. Eight different liquid flowrates were operated, and their corresponding orifice velocities were 11, 12, 13, 13.5, 14, 15, 16 and 17m/s. Pressures were recorded at the upstream, orifice and downstream positions.

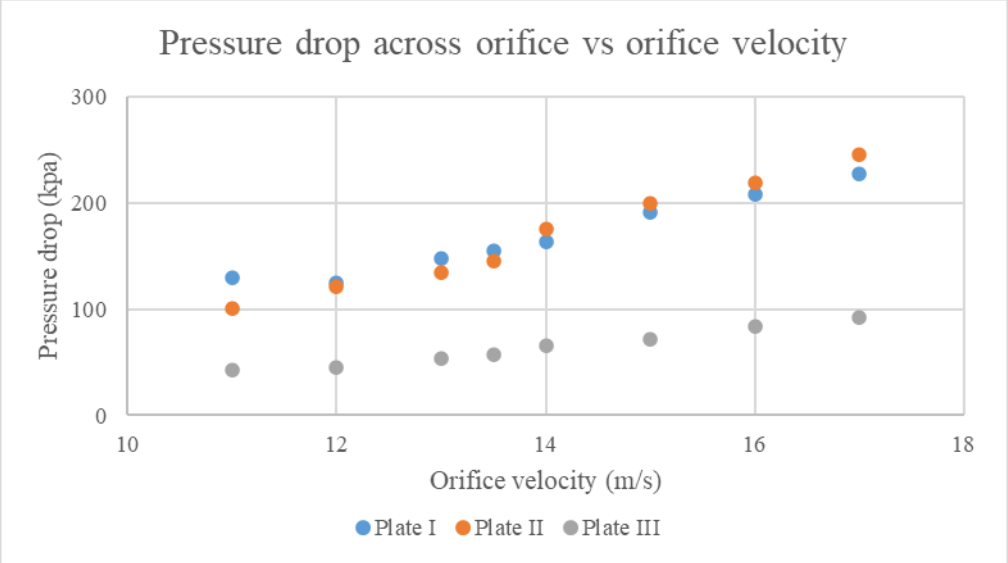

Figure 5.2: Pressure drop across orifice versus orifice velocity for plate I, II and III.

The pressure drops across the orifice plate against orifice velocity are shown in Figure 5.2. The pressure drops increased with the orifice velocity increasing from 11m/s to 17m/s. However, the pressure drops were built up slowly at Plate III with orifice velocity.

Plate I and Plate II presented a similar trend against orifice velocity, although the orifice opening ratio of Plate I was doubled that of Plate II.

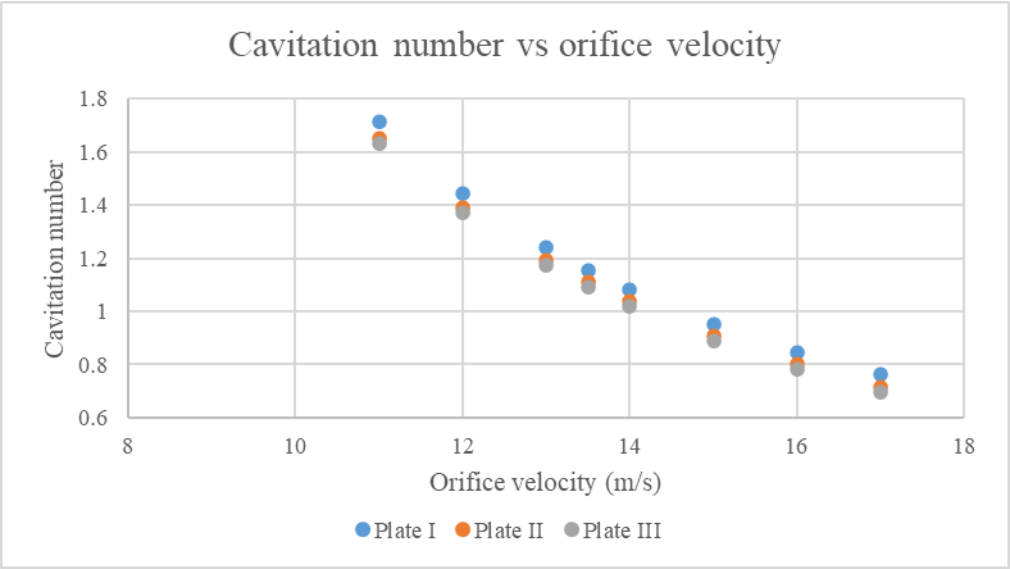

Figure 5.3: Cavitation number versus orifice velocity for plate I, II and III.

Cavitation numbers for the three orifice plates were calculated and displayed in Figure 5.3. The orifice velocity appeared to be a dominant factor in determining cavitation numbers regardless of orifice opening ratio.

The effects of orifice opening ratio were investigated with an emphasis on the bubble behaviors. As shown in the experimental design section, the numbers of bubbles were counted for a fixed area, 6 mm^2. This step was repeated three times by randomly selected different spots to minimize the error and an average number of bubbles was used for the result analysis. The average diameter of bubbles was calculated based on an assumption that all bubbles were spherical throughout the transition process.

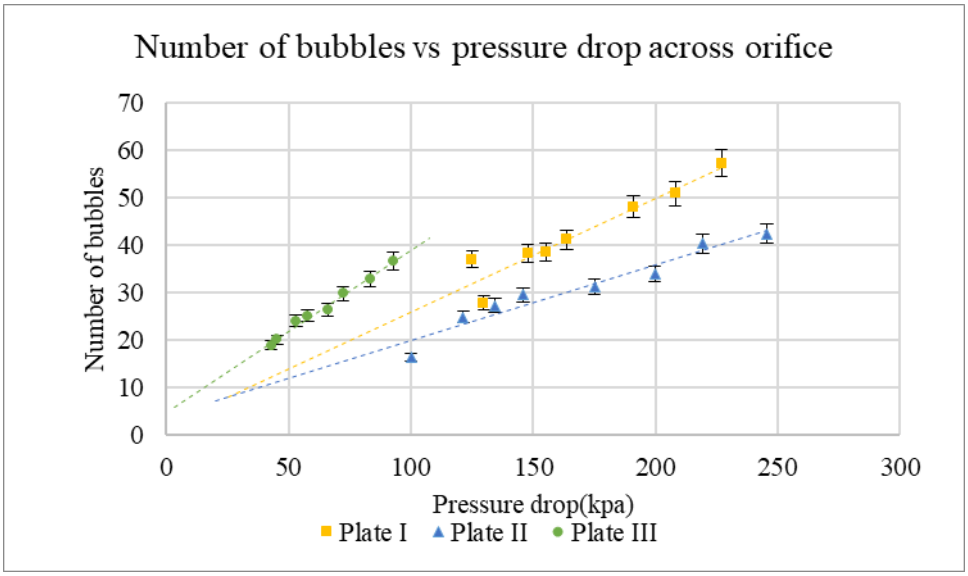

Figure 5.4: Number of bubbles produced versus pressure drop across orifice for plate I, II and III.

The number of bubbles per 6 mm^2 generated for three plates were counted and summarized in Figure 5.4. For all the three plates, an increase in orifice pressure drop can result in more bubbles generated. Large orifice opening required higher pressure drop to create the same amount of gas bubbles. For instance, about 30 gas bubbles per 6 mm^2 were generated at 125 kPa when the orifice opening is 7.8%. As the opening ratio dropped to one third, the pressure drops to create the same amount of gas bubbles was only 75 kPa. However, pressure drops can be easily built up at an orifice plate that has less opening ratio so that more gas bubbles can be produced.

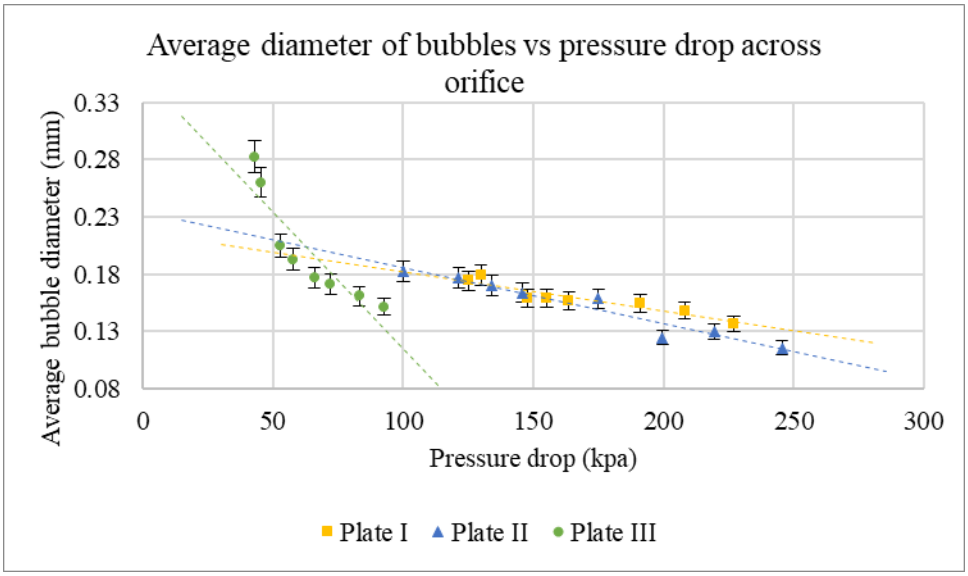

Figure 5.5: Average diameter of bubbles versus pressure drop across orifice for plate I, II and III.

Bubble sizes are also closely associated with the pressure loss across orifice. Figure 5.5 showed that higher pressure drops across the orifice resulted in smaller bubbles. Although the three plates had different orifice opening ratios, the bubble sizes generated followed a similar trend regardless the opening ratio.

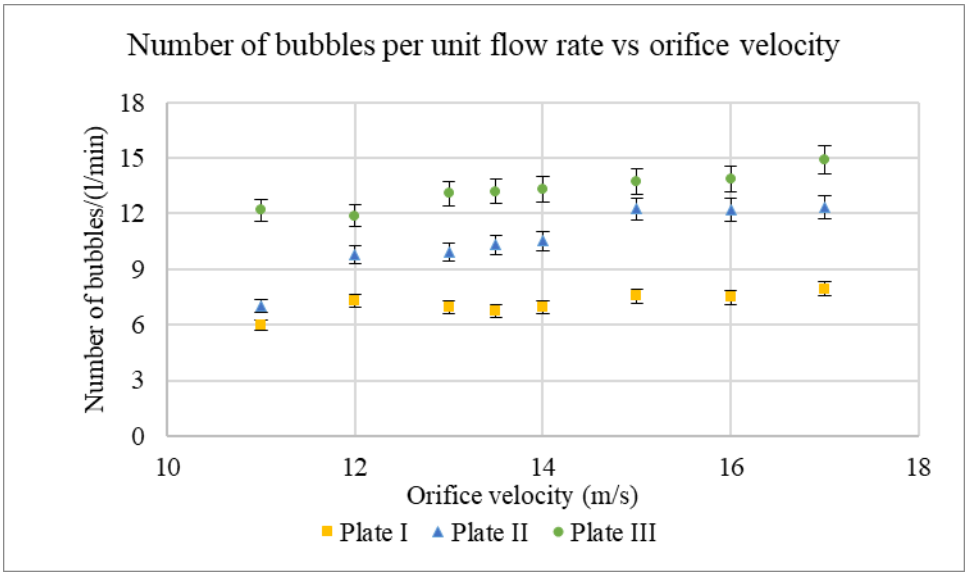

Figure 5.6: Number of bubbles produced per unit flow rate versus orifice velocity for plate I, II and III.

The number of bubbles and average bubble size were normalized by division of its corresponding liquid flow rate and compared in Figure 5.6. The numbers of bubbles produced by the three orifices increased with increasing orifice velocity and plate III had the highest bubble generation efficiency per unit flow rate. The number of bubbles produced for plate III increased from 12 to 15, in the meantime, plate I and II only reached 8 and 12 respectively under the same flow conditions, which demonstrated that the bubble generation efficiency increased with decreasing opening rate. Previously published research [122, 123] also confirmed that multiple smaller orifices produced more bubbles.

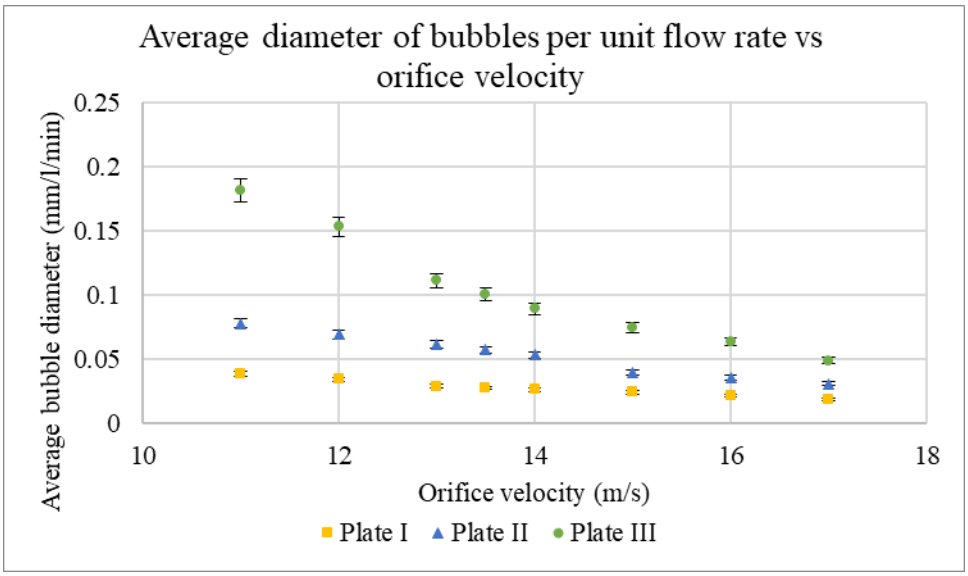

Figure 5.7: Diameter of bubbles per unit flow rate versus orifice velocity for plate I, II and III.

Figure 5.7 showed that the diameter of bubbles produced from plate I were the smallest among three plates and it only decreased marginally from 0.04 mm to 0.02mm per unit flow rate. For plate II, the variation of bubble sizes against orifice velocity became noticeable. When plate II was replaced by plate III resulting a reduction in the orifice opening from 3.9% to 2.6%, the bubble sizes were observed to decrease rapidly with increasing the orifice velocity. The bubbles produced from plate II reduced by half from 0.07mm to 0.035mm per unit flow rate and for plate III, a size reduction from 0.17mm to 0.06mm per unit flow rate was observed under the same operating conditions. As the

pressure drop across orifice is the determining factor of bubble sizes, smallest bubble diameter was achieved by plate I [124]. However, the effectiveness of bubble size reduction was found to be the plate with least opening area.

5.2 Effect of total orifice perimeter on cavitation intensity

The second group of orifice plates, numbered by II, IV and V (As shown in Table 5.1), were employed to investigate the effect of total orifice perimeter. The opening ratios of the three plates were maintained closely at 3.5% (Highlighted in blue in Table 5.1), whereas the total orifice perimeter ranged from 2π to 4π mm.

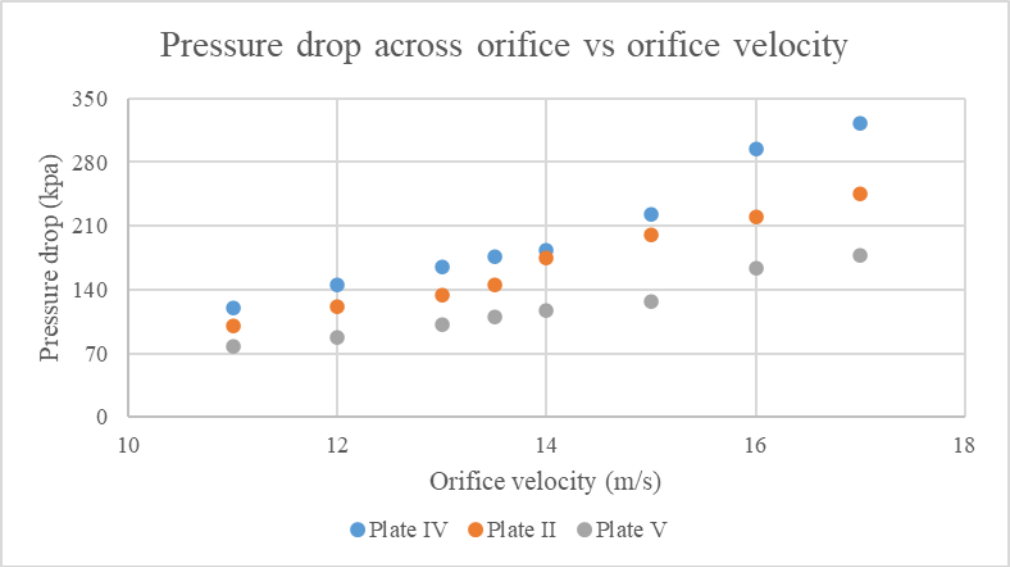

Figure 5.8: Pressure drop across orifice versus orifice velocity for plate II, IV and V.

As the orifice velocity increased from 11m/s to 17m/s, upstream pressure built up quickly while the downstream pressures were kept at atmospheric pressure because the downstream of the reactor was connected to the open water tank. As expected, high liquid velocities resulted in high pressure drop across the orifice plate. Although the three plates had the same opening ratio, the rates of pressure built up were different. The plate with least total orifice perimeter (Plate IV) generated the highest upstream pressure for a given orifice velocity. The increased orifice perimeter for the same opening rate resulted a

decreasing total energy dissipation across the orifice with increased flow rates. Thus, multi-hole plates are more effective in lowering the pressure drop across orifice.

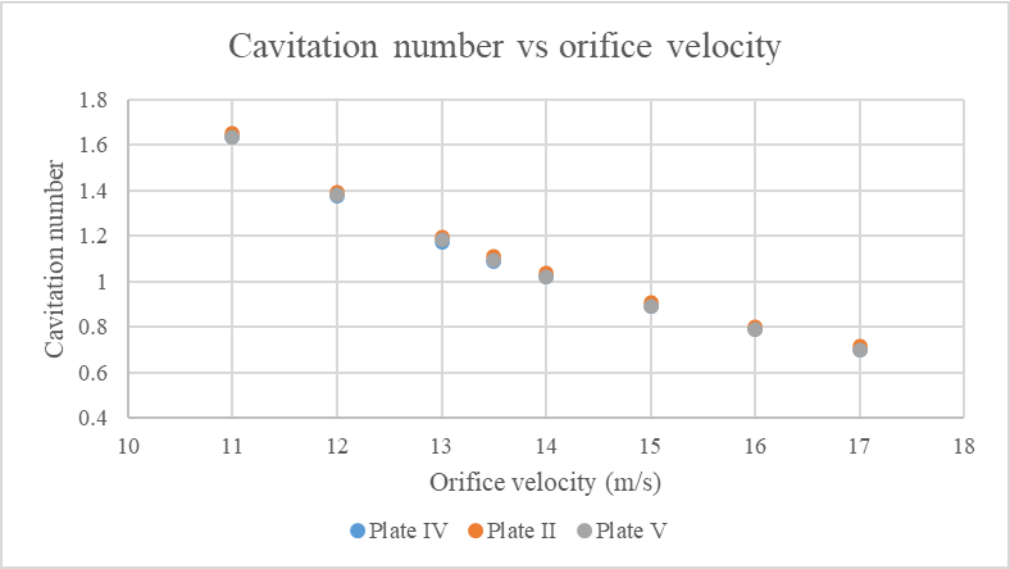

Figure 5.9: Cavitation number versus orifice velocity for plate II, IV and V.

However, the cavitation numbers for three plates are highly identical at each orifice velocity (Figure 5.9). With the same orifice velocity, sufficiently close volumetric flow rate and downstream pressure, the results calculated should be close without doubt.

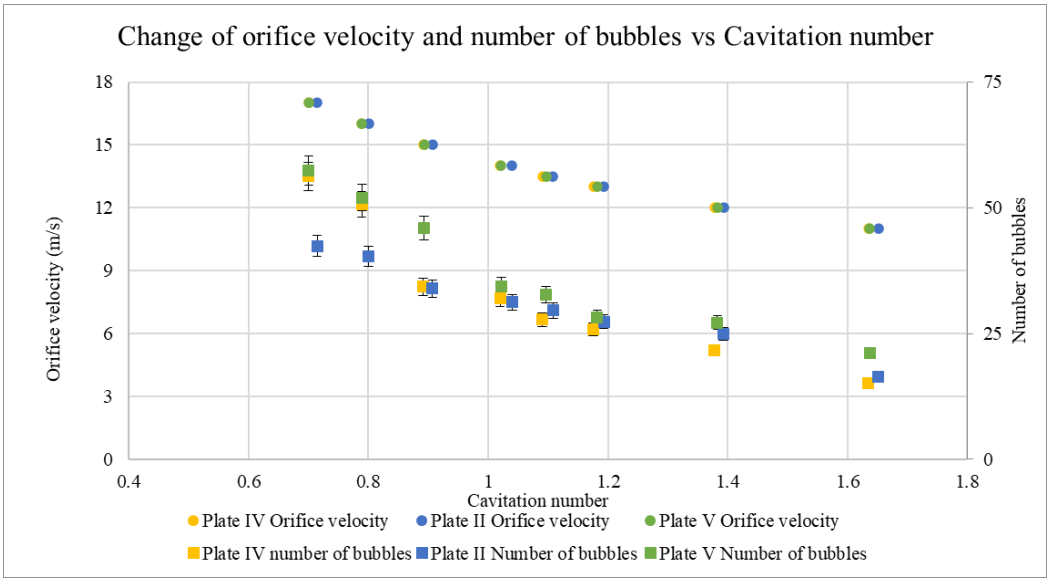

Figure 5.10: Variation of bubble population produced at different orifice velocities and cavitation number.

Figure 5.10 showed that the bubble population produced by three orifice plate follow the same trend: the number of bubbles increases with decreasing cavitation number. The perimeters of the orifice seem to have no impact on the generation of bubble quantity at relatively low orifice velocities but to produce more bubbles at higher liquid orifice velocity. When the orifice velocity was lower than or equal to 12m/s, the bubble population increases slowly with the liquid velocity. When the liquid velocity is higher than 14 m/s or the cavitation number reached about 1, bubble clouds (Images were not shown) were observed for all the three orifice plates, indicating the inception of cavitation. After the occurrence of cavitation inception, the number of bubbles increased quickly due to the generation of cavitational bubbles. In the cavitation regime, the edges for producing cavitation bubbles became important. Longer the edges, more bubbles can be produced.

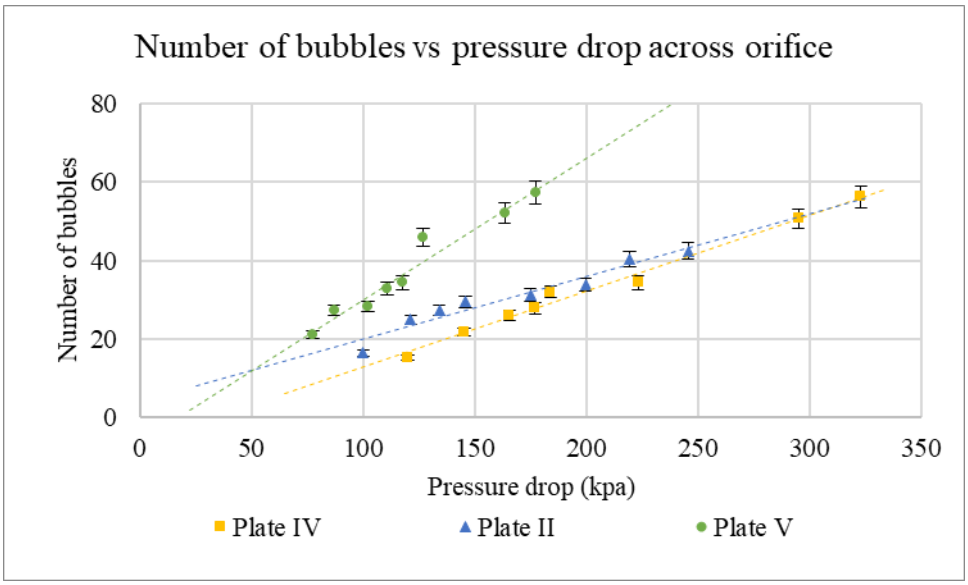

Figure 5.11: Number of bubbles produced versus pressure drop across orifice for plate II, IV and V.

Figure 5.11 showed the pressure drop across the orifice plates did play a role, so did the perimeters of orifice. For a fixed pressure drop, longer perimeters of the orifice created more bubbles. This suggests that bubbles are formed at the edges of orifice. The plate with four 1-mm orifices generated the most gas bubbles when the pressure drop is kept the same. In other words, Plate V could produce the same amounts of bubbles at much lower pressure drop to save energy.

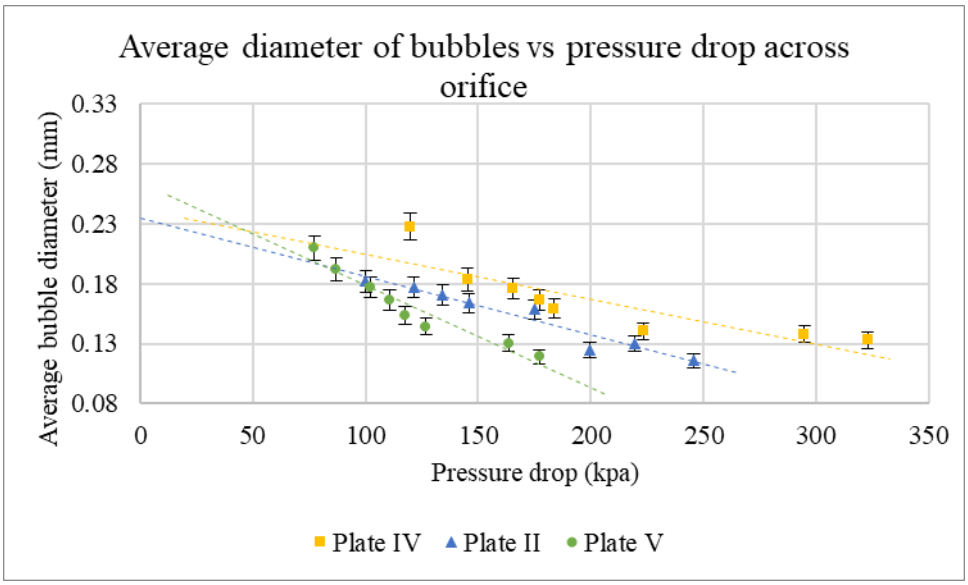

Figure 5.12: Average bubble size versus pressure drop across orifice for plate II, IV and V.

Figure 5.12 shows the effects of pressure drop on the sizes of generated bubbles. Higher pressure drop will enhance the production of small bubbles regardless. Again, for a given pressure drop, Plate V that had the longest edges of orifice created the relatively smaller bubbles. But the influence is minor.

5.3 Specific surface area

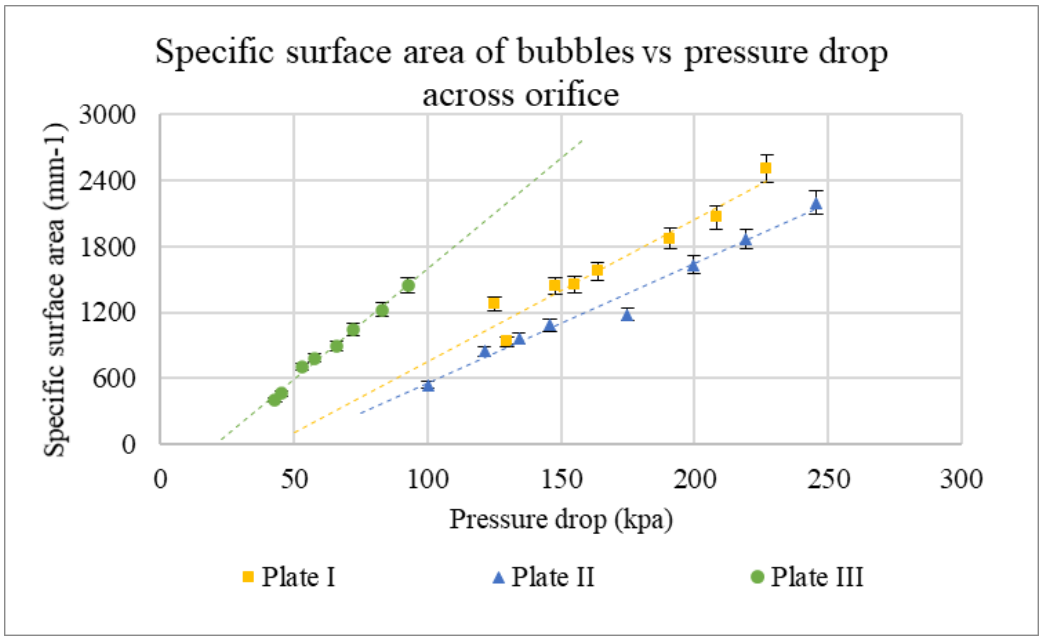

Figure 5.13: Specific surface area generated versus pressure drop across orifice for plate I, II and III.

Increased interfacial area between phases is extremely beneficial for physical and chemical processes. Total specific surface area for plates with different opening ratios was calculated and plotted in Figure 5.13. The specific surface area was found to be increased with increasing pressure drop. The plate with least opening rates had the highest interfacial area when compared at the same pressure loss across orifice.

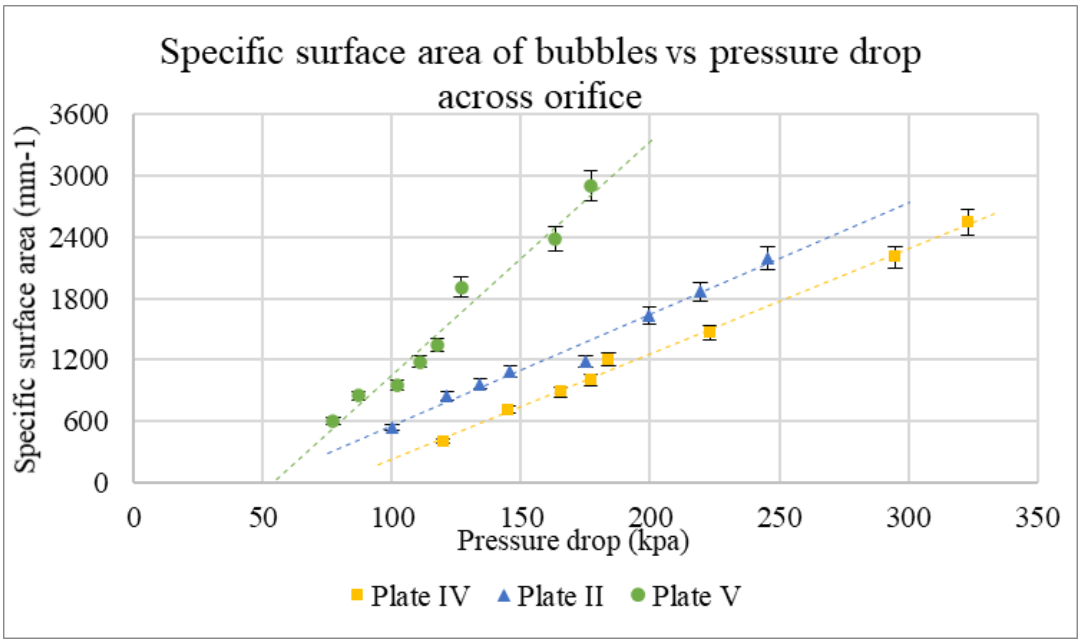

Figure 5.14: Specific surface area generated versus pressure drop across orifice for plate II, IV and V.

The pressure drops across the orifice plate with same opening rates against specific surface area are shown in Figure 5.14. For a fixed pressure drop, longer perimeters of the orifice created more fine bubbles thus higher specific surface area. In other words, Plate V could produce the same amounts of bubbles at much lower energy dissipation compared to the plates with smaller perimeter.

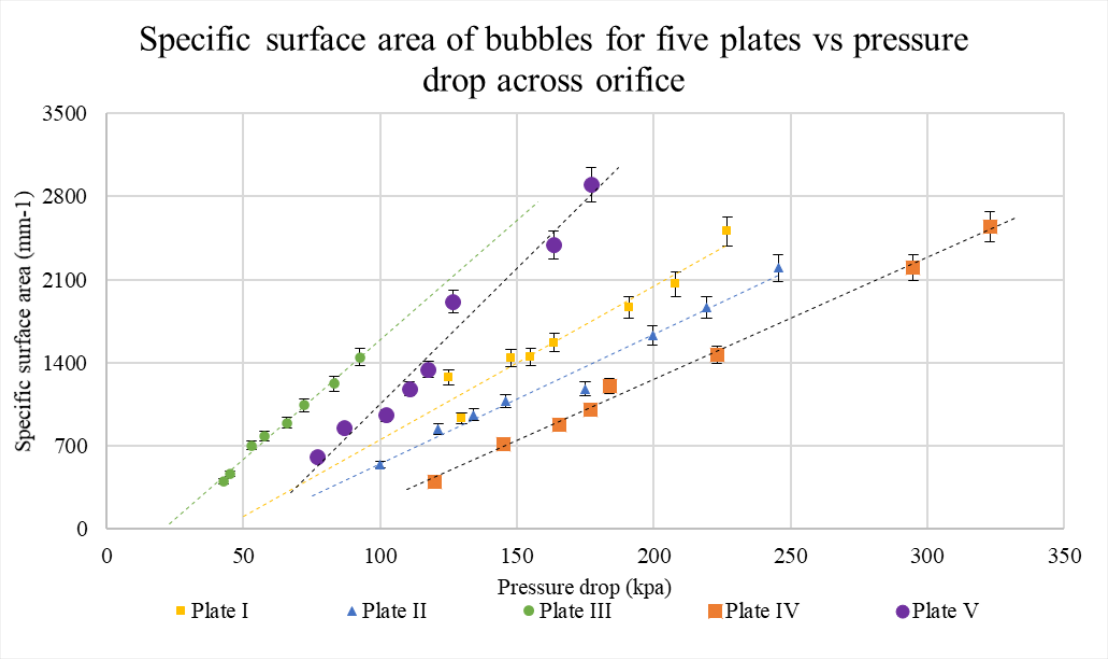

Figure 5.15: Overall comparison of specific surface area generated by five plates at different pressure drop across orifice.

The specific surface area of five different geometric designs of orifice plates featuring different combinations of orifice perimeters and orifice opening rates were summarized in Figure 5.15. Five unique trends were observed and they both increased with the pressure drop. It can be clear seen that the plate with least opening ratio (Plate III) and largest orifice perimeter (Plate V) had the highest and second highest specific surface area for the same pressure drops at all the operating conditions. The plates with higher opening ratio and shorter perimeter resulted less interfacial area at the same level of energy dissipation. It indicates that the combination effect of multi-holes and smaller opening rate are significant during the orifice design[125]. Thus, compared to a single orifice plate, an orifice plate with multiple smaller orifices can generate higher numbers of fine bubbles thus more intense cavitational effects. This finding was also confirmed by multiple published research [126-128].

Chapter 6

6 Conclusions and recommendations

6.1 Conclusion

Experimental studies were performed to characterize the development of cavitation process and transitional bubble behaviors using imaging techniques, pressure fluctuation and power spectral analysis.

The transition from non-cavitation to fully developed cavitation regime was carefully studied in a plexiglass cavitation device with a 3-mm single orifice plate with purified water as flow medium. Bubble behaviors were recorded using high speed camera at three positions: upstream, orifice and downstream. Cavitation bubble clouds were observed at orifice when the orifice velocity reached 14m/s and the cavitation number was about 1 which indicated the inception of cavitation. The bubble clouds became enlarged as liquid flowrate increased and cavitation number decreased in the fully developed cavitation regime. It demonstrated the intensity of cavitation increased with orifice velocity. The number of bubbles produced were dramatically increased from 505 to 802 per squared cm of the observation window, while the averaged diameters of bubble reduced from 0.7mm to roughly 0.2mm in the transition regime. Tremendous amounts of bubbles with diameter around 0.1mm were produced at orifice when cavitation is fully developed.

The effect of surfactant on the performance of cavitation was investigated. It was observed that the addition of surfactant can dramatically increase the number of fine bubbles (< 0.1mm). This is because of reduced surface tensions of the surfactant solutions. These fine bubbles were so stable that severe bubble implosions were not observed even at high liquid flowrates which can bring cavitation to a pure water flow. The pressure signals and corresponding power spectral analysis further evidenced enhanced production of microbubbles and delayed transition to cavitation regime as surfactant was added.

The results showed that orifice design had significant impact on the performance of hydrodynamic cavitation in terms of bubble sizes, number of bubbles produced, bubble

sizes and the interfacial area generated. Both orifice opening ratio and perimeter can affect the cavitation developing process. The orifice plates with the smallest opening ratio allow to create a desired gas-liquid interfacial area at the lowest required pressure. Formation of gas bubbles are highly associated with the length of constriction edges. A long orifice perimeter promotes the production of more fine bubbles, leading to large specific surface area. In general, an orifice plate with multiple orifices can generate higher numbers of cavities and larger interfacial area when compared to a single hole plate. Therefore, plate with multiple holes should be considered during the design of orifice-based cavitation reactor to produce higher cavitation intensity.

Pressure signals collected from pressure transducers were analyzed and power spectra analysis were also performed to study the hydrodynamics of bubbles and to characterize the flow regimes and regime transition. An in-house MATLAB algorithm was used to compute related bubble characteristics such as bubble sizes and their total energy. It is found that the results of pressure fluctuation analysis and power spectrum analysis agree well with the results obtained from visualization regarding the variation on bubble sizes and flow characteristics.

6.2 Future recommendations

The present thesis work is certainly an incremental step on the understanding of the complex bubble behavior during the transition process of hydrodynamic cavitation. However, there are still parameters which have not been considered and uncertainties that need to be further investigated:

1. The investigation of geometric factors on the performance of hydrodynamic cavitation can be further expanded, e.g., plate thickness, orifice opening angle.
2. Computational Fluid Dynamics (CFD) simulations can be performed to model the nature of cavitating flows.
3. Reactions can be employed to testify the enhancement of cavitation-based reactor on the transport processes.

References

[1] K.S. Suslick, Sonochemistry, Science, 247 (1990) 1439.

[2] Y. Tao, J. Cai, X. Huai, B. Liu, Z. Guo, Application of Hydrodynamic Cavitation to Wastewater Treatment, Chemical Engineering & Technology, 39 (2016) 1363-1376.

[3] N. Asaithambi, P. Singha, M. Dwivedi, S.K. Singh, Hydrodynamic cavitation and its application in food and beverage industry: A review, Journal of Food Process Engineering, 42 (2019) e13144.

[4] M. Wan, Y. Feng, G. ter Haar, Cavitation in biomedicine, Principles and Techniques, 23 (2015) 1-503.

[5] P.J. Milly, R.T. Toledo, M.A. Harrison, D. Armstead, Inactivation of food spoilage microorganisms by hydrodynamic cavitation to achieve pasteurization and sterilization of fluid foods, J Food Sci, 72 (2007) M414-422.

[6] A.B. Pandit, J.B. Joshi, hydrolysis of fatty oils: effect of cavitation, Chemical Engineering Science, 48 (1993) 3440-3442.

[7] S. Arrojo, Y. Benito, A theoretical study of hydrodynamic cavitation, Ultrasonics Sonochemistry, 15 (2008) 203-211.

[8] C. Mishra, Y. Peles, An experimental investigation of hydrodynamic cavitation in micro-Venturis, Physics of Fluids, 18 (2006) 103603.

[9] P.R. Gogate, A.B. Pandit, HYDRODYNAMIC CAVITATION REACTORS: A STATE OF THE ART REVIEW, Reviews in Chemical Engineering, 17 (2001) 1-85.

[10] W. Lauterborn, Cavitation and Coherent Optics, in: W. Lauterborn (Ed.) Cavitation and Inhomogeneities in Underwater Acoustics, Springer Berlin Heidelberg, Berlin, Heidelberg, 1980, pp. 3-12.

[11] W. Lauterborn, H. Bolle, Experimental investigations of cavitation-bubble collapse in the neighbourhood of a solid boundary, Journal of Fluid Mechanics, 72 (1975) 391-399.

[12] Y.T. Shah, A.B. Pandit, V.S. Moholkar, Cavitation reaction engineering / Y.T. Shah, and A.B. Pandit, and V.S. Moholkar, Kluwer Academic/Plenum Publishers, New York, 1999.

[13] V.S. Moholkar, P. Senthil Kumar, A.B. Pandit, Hydrodynamic cavitation for sonochemical effects, Ultrasonics Sonochemistry, 6 (1999) 53-65.

[14] P. Gogate, Greener processing routes for reactions and separations based on use of ultrasound and hydrodynamic cavitation, in, 2016, pp. 126-160.

[15] C.R. Holkar, A.J. Jadhav, D.V. Pinjari, A.B. Pandit, Cavitationally Driven Transformations: A Technique of Process Intensification, Industrial & Engineering Chemistry Research, 58 (2019) 5797-5819.

[16] S. Li, C. Brennen, Y. Matsumoto, Introduction for amazing (cavitation) bubbles, Interface Focus, 5 (2015) 20150059.

[17] P.R. Gogate, Cavitational reactors for process intensification of chemical processing applications: A critical review, Chemical Engineering and Processing: Process Intensification, 47 (2008) 515-527.

[18] A. Šarc, T. Stepišnik-Perdih, M. Petkovšek, M. Dular, The issue of cavitation number value in studies of water treatment by hydrodynamic cavitation, Ultrasonics sonochemistry, 34 (2017) 51-59.

[19] T. D., Kavitation und Korrosion, Hydraulische Probleme, (1926).

[20] M.S. Plesset, The dynamics of cavitation bubbles, Journal of applied mechanics, 16 (1949) 277-282.

[21] M. Petkovšek, M. Zupanc, M. Dular, T. Kosjek, E. Heath, B. Kompare, B. Širok, Rotation generator of hydrodynamic cavitation for water treatment, Separation and Purification Technology, 118 (2013) 415-423.

[22] M.V. Bagal, P.R. Gogate, Wastewater treatment using hybrid treatment schemes based on cavitation and Fenton chemistry: A review, Ultrasonics Sonochemistry, 21 (2014) 1-14.

[23] Y. Yan, R.B. Thorpe, Flow regime transitions due to cavitation in the flow through an orifice, International Journal of Multiphase Flow, 16 (1990) 1023-1045.

[24] A. Cioncolini, F. Scenini, J. Duff, M. Szolcek, M. Curioni, Choked cavitation in micro-orifices: An experimental study, Experimental Thermal and Fluid Science, 74 (2016) 49-57.

[25] X. Cheng, X. Shao, L. Zhang, The characteristics of unsteady cavitation around a sphere, Physics of Fluids, 31 (2019) 042103.

[26] X. Long, J. Zhang, J. Wang, M. Xu, Q. Lyu, B. Ji, Experimental investigation of the global cavitation dynamic behavior in a venturi tube with special emphasis on the cavity length variation, International Journal of Multiphase Flow, 89 (2017) 290-298.

[27] M. Ghorbani, A.K. Sadaghiani, L.G. Villanueva, A. Koşar, Hydrodynamic cavitation in microfluidic devices with roughened surfaces, Journal of Micromechanics and Microengineering, 28 (2018) 075016.

[28] P.R. Gogate, Cavitation: an auxiliary technique in wastewater treatment schemes, Advances in Environmental Research, 6 (2002) 335-358.

[29] K. Ando, A.-Q. Liu, C.-D. Ohl, Homogeneous Nucleation in Water in Microfluidic Channels, Physical Review Letters, 109 (2012) 044501.

[30] K.A. Mørch, Cavitation inception from bubble nuclei, Interface Focus, 5 (2015) 20150006.

[31] T.F. Groß, P.F. Pelz, Diffusion-driven nucleation from surface nuclei in hydrodynamic cavitation, Journal of Fluid Mechanics, 830 (2017) 138-164.

[32] M.T. Khoo, J.A. Venning, B.W. Pearce, K. Takahashi, T. Mori, P.A. Brandner, Natural nuclei population dynamics in cavitation tunnels, Experiments in Fluids, 61 (2020) 34.

[33] F.E. Fox, K. Herzfeld, Gas Bubbles with Organic Skin as Cavitation Nuclei, Journal of the Acoustical Society of America, 26 (1954) 984-989.

[34] C.-T. Hsiao, G.L. Chahine, Effect of a propeller and gas diffusion on bubble nuclei distribution in a liquid, Journal of Hydrodynamics, Ser. B, 24 (2012) 809-822.

[35] T. Tandiono, C.W. Kang, X. Lu, C.K. Turangan, M. Tan, H.B. Osman, F. Lim, An experimental study of gas nuclei-assisted hydrodynamic cavitation for aquaculture water treatment, Journal of Visualization, 23 (2020) 863-872.

[36] P.S. Russell, L. Barbaca, J.A. Venning, B.W. Pearce, P.A. Brandner, Measurement of nuclei seeding in hydrodynamic test facilities, Experiments in Fluids, 61 (2020) 79.

[37] R.W. Pascal, M.J. Yelland, M.A. Srokosz, B.I. Moat, E.M. Waugh, D.H. Comben, A.G. Cansdale, M.C. Hartman, D.G.H. Coles, P. Chang Hsueh, T.G. Leighton, A Spar Buoy for High-Frequency Wave Measurements and Detection of Wave Breaking in the Open Ocean, Journal of Atmospheric and Oceanic Technology, 28 (2011) 590-605.

[38] X. Yao, Z. Li, L. Sun, H. Lu, A study on bubble nuclei population dynamics under reduced pressure, Physics of Fluids, 32 (2020) 112019.

[39] Y.T. Shah, A.B. Pandit, V.S. Moholkar, Cavitation reaction engineering, Kluwer Academic/Plenum Publishers, New York, 1999.

[40] E.A. Hemmingsen, Cavitation in gas−supersaturated solutions, Journal of Applied Physics, 46 (1975) 213-218.

[41] J.A. Venning, M.T. Khoo, B.W. Pearce, P.A. Brandner, Background nuclei measurements and implications for cavitation inception in hydrodynamic test facilities, Experiments in Fluids, 59 (2018) 71.

[42] J. Kim, S.J. Song, Measurement of Temperature Effects on Cavitation in a Turbopump Inducer, Journal of Fluids Engineering, 138 (2015).

[43] B. Niemczewski, Observations of water cavitation intensity under practical ultrasonic cleaning conditions, Ultrasonics Sonochemistry, 14 (2007) 13-18.

[44] L. Torre, A. Cervone, A. Pasini, L. d'Agostino, Experimental Characterization of Thermal Cavitation Effects on Space Rocket Axial Inducers, Journal of Fluids Engineering, 133 (2011).

[45] B. Li, Y. Gu, M. Chen, An experimental study on the cavitation of water with dissolved gases, Experiments in Fluids, 58 (2017) 164.

[46] M.G. De Giorgi, A. Ficarella, M. Tarantino, Evaluating cavitation regimes in an internal orifice at different temperatures using frequency analysis and visualization, International Journal of Heat and Fluid Flow, 39 (2013) 160-172.

[47] H. Soyama, Luminescence intensity of vortex cavitation in a Venturi tube changing with cavitation number, Ultrasonics Sonochemistry, 71 (2021) 105389.

[48] R.K. Joshi, P.R. Gogate, Degradation of dichlorvos using hydrodynamic cavitation based treatment strategies, Ultrasonics Sonochemistry, 19 (2012) 532-539.

[49] P.S. Kumar, A.B. Pandit, Modeling Hydrodynamic Cavitation, Chemical Engineering & Technology, 22 (1999) 1017-1027.

[50] X. Liu, Z. Wu, B. Li, J. Zhao, J. He, W. Li, C. Zhang, F. Xie, Influence of inlet pressure on cavitation characteristics in regulating valve, Engineering Applications of Computational Fluid Mechanics, 14 (2020) 299-310.

[51] J. Liang, X. Luo, Y. Liu, X. Li, T. Shi, A numerical investigation in effects of inlet pressure fluctuations on the flow and cavitation characteristics inside water hydraulic poppet valves, International Journal of Heat and Mass Transfer, 103 (2016) 684-700.

[52] A. Taşdemir, İ. Cengiz, E. Yildiz, Y.K. Bayhan, Investigation of ammonia stripping with a hydrodynamic cavitation reactor, Ultrasonics Sonochemistry, 60 (2020) 104741.

[53] H. Flynn, Physics of acoustic cavitation in liquids, Physical acoustics, 1 (1964) 57-172.

[54] S.J. Kim, K.H. Lim, C. Kim, Deformation characteristics of spherical bubble collapse in Newtonian fluids near the wall using the Finite Element Method with ALE formulation, Korea Australia Rheology Journal, 18 (2006) 109-118.

[55] Q. Deng, A.V. Anilkumar, T.G. Wang, The role of viscosity and surface tension in bubble entrapment during drop impact onto a deep liquid pool, Journal of Fluid Mechanics, 578 (2007) 119-138.

[56] J. Luo, W. Xu, Y. Zhai, Q. Zhang, Experimental study on the mesoscale causes of the influence of viscosity on material erosion in a cavitation field, Ultrasonics Sonochemistry, 59 (2019) 104699.

[57] R.E.A. Arndt, Cavitation in Fluid Machinery and Hydraulic Structures, Annual Review of Fluid Mechanics, 13 (1981) 273-326.

[58] H. Nazari-Mahroo, K. Pasandideh, H.A. Navid, R. Sadighi-Bonabi, How important is the liquid bulk viscosity effect on the dynamics of a single cavitation bubble?, Ultrasonics Sonochemistry, 49 (2018) 47-52.

[59] J. Lunnbäck, Hydrodynamic cavitation applied to anaerobic degradation of fats, oils and greases (FOGs), in, 2016, pp. 53.

[60] P.R. Gogate, A.B. Pandit, Engineering design methods for cavitation reactors II: Hydrodynamic cavitation, AIChE Journal, 46 (2000) 1641-1649.

[61] A. Sharma, P.R. Gogate, A. Mahulkar, A.B. Pandit, Modeling of hydrodynamic cavitation reactors based on orifice plates considering hydrodynamics and chemical reactions occurring in bubble, Chemical Engineering Journal, 143 (2008) 201-209.

[62] N.P. Vichare, P.R. Gogate, A.B. Pandit, Optimization of Hydrodynamic Cavitation Using a Model Reaction, Chemical Engineering & Technology, 23 (2000) 683-690.

[63] B. Balasundaram, S.T.L. Harrison, Disruption of Brewers' yeast by hydrodynamic cavitation: Process variables and their influence on selective release, Biotechnology and Bioengineering, 94 (2006) 303-311.

[64] W.-z. Ai, T.-m. Ding, Orifice plate cavitation mechanism and its influencing factors, Water Science and Engineering, 3 (2010) 321-330.

[65] V.K. Saharan, M.A. Rizwani, A.A. Malani, A.B. Pandit, Effect of geometry of hydrodynamically cavitating device on degradation of orange-G, Ultrasonics Sonochemistry, 20 (2013) 345-353.

[66] J.-P. Franc, J.-M. Michel, Fundamentals of Cavitation [electronic resource] / by Jean-Pierre Franc, Jean-Marie Michel, 1st ed. 2005. ed., Springer Netherlands, Dordrecht, 2005.

[67] H. Kim, B. Koo, S. Lee, J.Y. Yoon, Experimental study of cavitation intensity using a novel hydrodynamic cavitation reactor, Journal of Mechanical Science and Technology, 33 (2019) 4303-4310.

[68] X. Sun, J.J. Park, H.S. Kim, S.H. Lee, S.J. Seong, A.S. Om, J.Y. Yoon, Experimental investigation of the thermal and disinfection performances of a novel hydrodynamic cavitation reactor, Ultrasonics Sonochemistry, 49 (2018) 13-23.

[69] E.B. Flint, K.S. Suslick, The temperature of cavitation, Science (New York, N.Y.), 253 (1991) 1397-1399.

[70] Z. Qin, H. Alehossein, Heat transfer during cavitation bubble collapse, Applied Thermal Engineering, 105 (2016) 1067-1075.

[71] E.P. Zaporozhets, L.P. Kholpanov, G.K. Zibert, A.V. Artemov, Vortex and Cavitation Flows in Hydraulic Systems, Theoretical Foundations of Chemical Engineering, 38 (2004) 225-234.

[72] S. Little, Null Tests of Breakthrough Energy Claims, in: 42nd AIAA/ASME/SAE/ASEE Joint Propulsion Conference & Exhibit, Sacramento, California, July 2006.

[73] K.B. Pyun, W.C. Kwon, K.T. Oh, J.Y. Yoon, Investigation of the Performance for a Heat Generator Using Hydrodynamic Cavitation, in: ASME-JSME-KSME 2011 Joint Fluids Engineering Conference, Hamamatsu, Japan, July, 2011.

[74] Y. Song, C.-w. Gu, Development and Validation of a Three-Dimensional Computational Fluid Dynamics Analysis for Journal Bearings Considering Cavitation and Conjugate Heat Transfer, Journal of Engineering for Gas Turbines and Power, 137 (2015).

[75] B. Schneider, A. Koşar, Y. Peles, Hydrodynamic cavitation and boiling in refrigerant (R-123) flow inside microchannels, International Journal of Heat and Mass Transfer, 50 (2007) 2838-2854.

[76] M. Ghorbani, H. Chen, L.G. Villanueva, D. Grishenkov, A. Koşar, Intensifying cavitating flows in microfluidic devices with poly(vinyl alcohol) (PVA) microbubbles, Physics of Fluids, 30 (2018) 102001.

[77] M. Ghorbani, G. Deprem, E. Ozdemir, A.R. Motezakker, L.G. Villanueva, A. Koşar, On “Cavitation on Chip” in Microfluidic Devices With Surface and Sidewall Roughness Elements, Journal of Microelectromechanical Systems, 28 (2019) 890-899.

[78] T. Mason, J. Lorimer, Applied Sonochemistry: The Uses of Power Ultrasound in Chemistry and Processing, 2002.

[79] P.R. Gogate, A.M. Kabadi, A review of applications of cavitation in biochemical engineering/biotechnology, Biochemical Engineering Journal, 44 (2009) 60-72.

[80] P.R. Gogate, V.S. Sutkar, A.B. Pandit, Sonochemical reactors: Important design and scale up considerations with a special emphasis on heterogeneous systems, Chemical Engineering Journal, 166 (2011) 1066-1082.

[81] M.S. Plesset, A. Prosperetti, Bubble dynamics and cavitation, Annual review of fluid mechanics, 9 (1977) 145-185.

[82] E.F. Karamah, S. Bismo, W.W. Purwanto, Significance of Acoustic and Hydrodynamic Cavitations in Enhancing Ozone Mass Transfer, Ozone: Science & Engineering, 35 (2013) 482-488.

[83] H. Zhang, L. Duan, D. Zhang, Absorption kinetics of ozone in water with ultrasonic radiation, Ultrasonics Sonochemistry, 14 (2007) 552-556.

[84] M.A. Kelkar, P.R. Gogate, A.B. Pandit, Intensification of esterification of acids for synthesis of biodiesel using acoustic and hydrodynamic cavitation, Ultrasonics Sonochemistry, 15 (2008) 188-194.

[85] P.J. Milly, R.T. Toledo, J. Chen, B. Kazem, Hydrodynamic Cavitation to Improve Bulk Fluid to Surface Mass Transfer in a Nonimmersed Ultraviolet System for Minimal Processing of Opaque and Transparent Fluid Foods, Journal of Food Science, 72 (2007) M407-M413.

[86] L.F. Chuah, S. Yusup, A.R. Abd Aziz, A. Bokhari, M.Z. Abdullah, Cleaner production of methyl ester using waste cooking oil derived from palm olein using a hydrodynamic cavitation reactor, Journal of Cleaner Production, 112 (2016) 4505-4514.

[87] C. Technologies, Technology Overview, in, 2021.

[88] H. Dynamics, Technology, in, Hydro Dynamics, Inc., 2020.

[89] W.T. Medjiade, A.R. Alvaro, A. Schumpe, Flow regime transitions in a bubble column, Chemical Engineering Science, 170 (2017) 263-269.

[90] S.W. Smith, The scientist and engineer's guide to digital signal processing, (1997).

[91] K. Loubière, G. Hébrard, Influence of liquid surface tension (surfactants) on bubble formation at rigid and flexible orifices, Chemical Engineering and Processing: Process Intensification, 43 (2004) 1361-1369.

[92] J. Eastoe, J. Dalton, Dynamic surface tension and adsorption mechanisms of surfactants at the air–water interface, Advances in colloid and interface science, 85 (2000) 103-144.

[93] V. Fainerman, R. Miller, P. Joos, The measurement of dynamic surface tension by the maximum bubble pressure method, Colloid and Polymer Science, 272 (1994) 731-739.

[94] Q. Xu, M. Nakajima, S. Ichikawa, N. Nakamura, P. Roy, H. Okadome, T. Shiina, Effects of surfactant and electrolyte concentrations on bubble formation and stabilization, Journal of Colloid and Interface science, 332 (2009) 208-214.

[95] P. Amani, R. Miller, S. Ata, S. Hurter, V. Rudolph, M. Firouzi, Dynamics of interfacial layers for sodium dodecylbenzene sulfonate solutions at different salinities, Journal of Industrial and Engineering Chemistry, 92 (2020) 174-183.

[96] Y. Yan, R. Thorpe, Flow regime transitions due to cavitation in the flow through an orifice, International journal of multiphase flow, 16 (1990) 1023-1045.

[97] V.H. Arakeri, Cavitation inception, Proceedings of the Indian Academy of Sciences Section C: Engineering Sciences, 2 (1979) 149-177.

[98] F. Avellan, Introduction to cavitation in hydraulic machinery, in, Politehnica University of Timișoara, 2004.

[99] Z. Li, Criteria for jet cavitation and cavitation jet drilling, International Journal of Rock Mechanics and Mining Sciences, 71 (2014) 204-207.

[100] S. Raut-Jadhav, V.K. Saharan, D. Pinjari, S. Sonawane, D. Saini, A. Pandit, Synergetic effect of combination of AOP's (hydrodynamic cavitation and H2O2) on the degradation of neonicotinoid class of insecticide, Journal of hazardous materials, 261 (2013) 139-147.

[101] Z. Wu, H. Shen, B. Ondruschka, Y. Zhang, W. Wang, D.H. Bremner, Removal of blue-green algae using the hybrid method of hydrodynamic cavitation and ozonation, Journal of hazardous materials, 235 (2012) 152-158.

[102] M. Dular, B. Bachert, B. Stoffel, B. Širok, Relationship between cavitation structures and cavitation damage, Wear, 257 (2004) 1176-1184.

[103] P.S. Kumar, A. Pandit, Modeling hydrodynamic cavitation, Chemical Engineering & Technology: Industrial Chemistry-Plant Equipment-Process Engineering-Biotechnology, 22 (1999) 1017-1027.

[104] G.L. Chahine, Nuclei effects on cavitation inception and noise, in: 25th Symposium on naval hydrodynamic, 2004.

[105] O. Keplinger, N. Shevchenko, S. Eckert, Visualization of bubble coalescence in bubble chains rising in a liquid metal, International Journal of Multiphase Flow, 105 (2018) 159-169.

[106] S. Dabiri, W.A. Sirignano, D.D. Joseph, Interaction between a cavitation bubble and shear flow, Journal of fluid mechanics, 651 (2010) 93-116.

[107] A.-m. Zhang, B.-y. Ni, B.-y. Song, X.-l. Yao, Numerical simulation of bubble breakup phenomena in a narrow flow field, Applied Mathematics and Mechanics, 31 (2010) 449-460.

[108] A. Fujiwara, K. Okamoto, K. Hashiguchi, J. Peixinho, S. Takagi, Y. Matsumoto, Bubble breakup phenomena in a venturi tube, in: Fluids Engineering Division Summer Meeting, 2007, pp. 553-560.

[109] F. Johnsson, R. Zijerveld, J.v. Schouten, C. Van den Bleek, B. Leckner, Characterization of fluidization regimes by time-series analysis of pressure fluctuations, International journal of multiphase flow, 26 (2000) 663-715.

[110] B. Gourich, C. Vial, A.H. Essadki, F. Allam, M.B. Soulami, M. Ziyad, Identification of flow regimes and transition points in a bubble column through analysis of differential pressure signal—influence of the coalescence behavior of the liquid phase, Chemical Engineering and Processing: Process Intensification, 45 (2006) 214-223.

[111] C. Vial, S. Poncin, G. Wild, N. Midoux, A simple method for regime identification and flow characterisation in bubble columns and airlift reactors, Chemical Engineering and Processing: Process Intensification, 40 (2001) 135-151.

[112] M.E. Díaz, F.J. Montes, M.A. Galán, Experimental study of the transition between unsteady flow regimes in a partially aerated two-dimensional bubble column, Chemical Engineering and Processing: Process Intensification, 47 (2008) 1867-1876.

[113] S.-H. Yang, S.-Y. Jaw, K.-C. Yeh, Single cavitation bubble generation and observation of the bubble collapse flow induced by a pressure wave, Experiments in fluids, 47 (2009) 343-355.

[114] L. Zhang, G. Zhang, M. Ge, O. Coutier-Delgosha, Experimental study of pressure and velocity fluctuations induced by cavitation in a small Venturi channel, Energies, 13 (2020) 6478.

[115] C. Vial, E. Camarasa, S. Poncin, G. Wild, N. Midoux, J. Bouillard, Study of hydrodynamic behaviour in bubble columns and external loop airlift reactors through analysis of pressure fluctuations, Chemical engineering science, 55 (2000) 2957-2973.

[116] J. Drahoš, J. Zahradnik, M. Punčochář, M. Fialova, F. Bradka, Effect of operating conditions on the characteristics of pressure fluctuations in a bubble column, Chemical Engineering and Processing: Process Intensification, 29 (1991) 107-115.

[117] H. Letzel, J. Schouten, R. Krishna, C. Van den Bleek, Characterization of regimes and regime transitions in bubble columns by chaos analysis of pressure signals, Chemical engineering science, 52 (1997) 4447-4459.

[118] A. Ajbar, W. Al-Masry, E. Ali, Prediction of flow regimes transitions in bubble columns using passive acoustic measurements, Chemical Engineering and Processing: Process Intensification, 48 (2009) 101-110.

[119] J. van der Schaaf, J. Schouten, F. Johnsson, C. Van den Bleek, Non-intrusive determination of bubble and slug length scales in fluidized beds by decomposition of the power spectral density of pressure time series, International Journal of Multiphase Flow, 28 (2002) 865-880.

[120] S. Arrojo, Y. Benito, A.M. Tarifa, A parametrical study of disinfection with hydrodynamic cavitation, Ultrasonics Sonochemistry, 15 (2008) 903-908.

[121] N.P. Vichare, P.R. Gogate, A.B. Pandit, Optimization of hydrodynamic cavitation using a model reaction, Chemical Engineering & Technology: Industrial Chemistry-Plant Equipment-Process Engineering-Biotechnology, 23 (2000) 683-690.

[122] A. Simpson, V.V. Ranade, Modelling of hydrodynamic cavitation with orifice: Influence of different orifice designs, Chemical Engineering Research and Design, 136 (2018) 698-711.

[123] D. Ghayal, A.B. Pandit, V.K. Rathod, Optimization of biodiesel production in a hydrodynamic cavitation reactor using used frying oil, Ultrasonics sonochemistry, 20 (2013) 322-328.

[124] H. Unno, I. Inoue, Size reduction of bubbles by orifice mixer, Chemical Engineering Science, 35 (1980) 1571-1579.

[125] V. Bagade, P. Suryawanshi, S. Nalavade, A review of multi-hole orifice plate, Int. J. Res. Appl. Sci. Eng. Technol, 7 (2019) 3197-3208.

[126] M. Sivakumar, A.B. Pandit, Wastewater treatment: a novel energy efficient hydrodynamic cavitational technique, Ultrasonics sonochemistry, 9 (2002) 123-131.

[127] P. Rudolf, D. Kubina, M. Hudec, J. Kozák, B. Maršálek, E. Maršálková, F. Pochylý, Experimental investigation of hydrodynamic cavitation through orifices of different geometries, in: EPJ Web of Conferences, EDP Sciences, 2017, pp. 02098.

[128] P.S. Kumar, M.S. Kumar, A. Pandit, Experimental quantification of chemical effects of hydrodynamic cavitation, Chemical Engineering Science, 55 (2000) 1633-1639.

Appendix

MATLAB algorithm used for Fast Fourier Transform:

```
N = 25001;

Fs = 25000;

Df = Fs/N;

F = 0:Df:Df*N-Df;

Y = fft(data);

Y=abs(Y)*2/N;

Plot(F,Y)
```

Curriculum Vitae

Name: Haoxuan Zheng

Post-secondary Education and Degrees:
University of New Brunswick
Fredericton, New Brunswick, Canada
2014-2019 B.Sc.Eng

The University of Western Ontario
London, Ontario, Canada
2019-present M.E.Sc

Honours and Awards:
Western Graduate Research Scholarship

Related Work Experience
Teaching Assistant
The University of Western Ontario
2019-2021

Publications:
H. Zheng, Y. Zheng, and J. Zhu, Recent developments in hydrodynamic cavitation and the application in radical-induced multiphase reactions, Engineering. (Under review)